5-10-1963

Self-Diffusion in Single-Crystal Tungsten and Diffusion of Rhenium Tracer in Single-Crystal Tungsten

Robert L. Andelin

Recommended Citation

Andelin, Robert L.. "Self-Diffusion in Single-Crystal Tungsten and Diffusion of Rhenium Tracer in Single-Crystal Tungsten." (1963). https://digitalrepository.unm.edu/chem_etds/96

SELF-DIFFUSION
IN
SINGLE-CRYSTAL
TUNGSTEN

ANDELIN

SELF-DIFFUSION IN SINGLE-CRYSTAL TUNGSTEN
AND
DIFFUSION OF RHENIUM TRACER IN SINGLE-CRYSTAL TUNGSTEN

by

Robert L. Andelin

A Dissertation
Submitted in Partial Fulfillment of the
Requirements for the Degree of
Doctor of Philosophy in Chemistry

The University of New Mexico

1963

This dissertation, directed and approved by the candidate's committee, has been accepted by the Graduate Committee of The University of New Mexico in partial fulfillment of the requirements for the degree of

DOCTOR OF PHILOSOPHY

Wm J Parish
DEAN

May 10, 1963
DATE

SELF-DIFFUSION IN SINGLE-CRYSTAL TUNGSTEN
AND
DIFFUSION OF RHENIUM TRACER IN SINGLE-CRYSTAL TUNGSTEN

by

Robert L. Andelin

Committee

Milton Kahn

Jere D. Knight
CHAIRMAN

J. L. Riebsomer

Guido H. Daub

S. A. Cooley

ABSTRACT

Self-diffusion in single-crystal tungsten and diffusion of rhenium tracer in single-crystal tungsten have been measured over the temperature range 2660 °C to 3230 °C by the direct sectioning technique. The initial radioactive layer of tungsten and rhenium tracers was produced on the diffusion samples by bombardment with 9.0-MeV deuterons. It was shown that the initial radioactive layer satisfactorily approximated the boundary-condition requirements of the one-dimensional diffusion equation. The tracers observed in determining the diffusion coefficients were W^{185}, Re^{183}, and Re^{184}.

Diffusion heating of the samples in high vacuum was accomplished by an induction-heating arrangement which included an eddy-current concentrator. Temperatures were measured by optical pyrometry, and the system was calibrated by reference to the melting points of tantalum (2996 °C), molybdenum (2620 °C), niobium (2468 °C), and rhodium (1966 °C).

Sectioning of the diffusion-heated samples was done with a precision surface grinding machine, and the particles from the layers ground off were radiochemically analyzed.

Radiochemical procedures were developed for separating pure fractions of tungsten and rhenium from one another and from the grinding wheel particles collected from each layer. The tungsten fraction was mounted as the 8-hydroxyquinoline derivative of tungsten for beta counting. The final form of the rhenium fraction for gamma counting was tetraphenylarsonium perrhenate.

The temperature dependence of the diffusion coefficients in the two systems, obtained by least-squares analyses of the data, is well represented by the equations

$$D(W) = (42.8 \pm 4.8)\, e^{-(153,100 \pm 600)/RT}\ \mathrm{cm^2/sec},$$

and

$$D(Re) = (275 \pm 110)\, e^{-(162,800 \pm 2,500)/RT}\ \mathrm{cm^2/sec}.$$

These data have been compared with the predictions of the current models of the diffusion process. The results are consistent with a ring mechanism as the fundamental step in tungsten self-diffusion. The theory of impurity diffusion in metals has not advanced sufficiently to establish a mechanism for diffusion of rhenium tracer in tungsten. However, the high activation energy indicates that there are no easy diffusion paths for rhenium atoms; and since rhenium atoms have nearly the same charge and size as tungsten atoms, it is reasonable to conjecture that rhenium tracer may diffuse through a tungsten lattice by a similar mechanism.

In the process of determining an optimum deuteron energy for activation of the diffusion samples, total cross sections as a function of deuteron energy were measured for the reactions, $W^{184}(d,p)W^{185}$, $W^{186}(d,p)W^{187}$, and $W^{184}(d,2n)$ 34-day Re^{184}, by the stacked-foil technique. Cross-section values for the reactions leading to the production of both W^{185} and W^{187} increased from about 3 mb at 6 MeV to a fairly broad maximum of 300 mb between 11 and 13 MeV. Cross sections for production of 34-day Re^{184} range from about 3 to 380 mb for deuterons with energies ranging from 7 to 14 MeV. Deuteron energies employed (14 MeV maximum) were not high enough to indicate the position of the maximum for the $W^{184}(d,2n)$ 34-day Re^{184} excitation function.

The decay of W^{185} was observed over a period of about 9 half-lives, and a new half-life value of 75.14 ± 0.63 days, with the uncertainty expressed to 3 σ, was obtained. The half-life value obtained for W^{187} was 23.72 ± 0.06 hours.

ACKNOWLEDGEMENTS

The author wishes to express his appreciation to Professor Milton Kahn and to Dr. Jere D. Knight for expert guidance and counsel during the course of this research. The author is particularly indebted to Dr. Knight for many helpful discussions on all phases of this research, and he hopes he has captured some of Dr. Knight's enthusiasm for the exploration of basic phenomena of nature.

The author is greatly indebted to Dr. B. Kent Harrison for helpful discussions on the mathematics of diffusion, and for his mathematical analyses of the diffusion process as applied to this research.

It is a pleasure to thank Dr. Melvin G. Bowman, Mr. N. H. Krikorian, and other members of Group CMB-3 for generous use of induction heating equipment, and for suggestions and assistance in conducting the high temperature diffusion runs.

This research was jointly sponsored by the University of New Mexico and the Los Alamos Scientific Laboratory under an Advanced Study Program. The author wishes to express his appreciation to Drs. David B. Hall, R. Philip Hammond, and L. Dale Kirkbride for approving this research, and for making available the facilities and equipment of K Division of the Los Alamos Scientific Laboratory.

The author's sincere thanks are expressed to many members of the Los Alamos Scientific Laboratory staff for general assistance during the course

f this research. In particular, he wishes to acknowledge the following:

Mr. John O'Rourk for x-ray analysis of tungsten crystals.

Dr. Donald R. F. Cochran and Mr. Kenneth D. Wells for assistance n the deuteron bombardment of the tungsten foil stack and the tungsten diffusion amples.

Dr. Glenn R. Waterbury and the staff of Group CMB-1 for many careil tungsten analyses.

Dr. George A. Cowan and the staff of Group J-11 for generous use of ounting facilities.

Mr. Kenneth J. Schowalter for instruction in the use of the surface rinding machine, and for the excellent machining of many apparatus parts, everal of which were machined from tungsten.

Dr. Robert B. Gibney and many members of Group CMF-13 for helpful scussions and assistance throughout the course of this research.

Dr. R. Keith Zeigler for valuable assistance in the use of the IBM-704 ad the IBM-7090 computers.

Mrs. Marjorie H. Gardiner for her cheerful, efficient secretarial ervice.

TABLE OF CONTENTS

TABLE OF CONTENTS (Continued)

TABLE OF CONTENTS (Continued)

TABLES

FIGURES

FIGURES (Continued)

Chapter 1

INTRODUCTION

1.1 General

Interest in refractory metals for high temperature applications has increased tremendously in recent years, due in large part to material demands of the nuclear and space industries. In advancing refractory metal technology, diffusion data are important because diffusion is rate-controlling in many metallurgical reactions.[1] For example, diffusion is important in the formation of metallurgical bonds, in the growth and dissolution of phases, and in homogenization and densification of powder compacts.[2] In addition, diffusion plays an important role in the theories of oxidation,[3] sintering,[4] creep,[5] relaxation and other phenomena in metals.[6] Self-diffusion (diffusion of like atoms) is the simplest type of diffusion and, therefore, most amenable to theoretical interpretation. In recent years, theoretical treatments of self-diffusion data have helped provide insight into the atomistic nature of mass transport phenomena in metals.[7-11] (For other references on the theory of self-diffusion, and on the application of self-diffusion to other phenomena in metals, see the annotated bibliography compiled by the author and L. E. Godfrey.[12])

Although a considerable body of experimental information has been accumulated on self-diffusion in solids, the major part of the detailed work has thus far dealt with relatively low-melting systems. Diffusion studies on the high-melting elements niobium, molybdenum, tantalum, and tungsten have been limited to polycrystalline material, for which data interpretation and theoretical

CHAPTER 1

INTRODUCTION

1.1 Objectives

Interest in refractory metals for both [illegible] applications has increased tremendously in recent years, due in part to potential requirements of the nuclear and space industries. [illegible] refractory metal technology, diffusion data are important because diffusion is rate-controlling in many [illegible] metallurgical reactions. For example, diffusion is important in the formation of metallurgical bonds, in the growth and dissolution of phases, and in homogenization and densification of powder compacts. In addition, diffusion plays an important role in the theories of [illegible] and other phenomena at [illegible]. Self-diffusion (diffusion of like atoms) [illegible] is a basic type of diffusion [illegible] theoretical [illegible] tion. In recent years [illegible] of self-diffusion have helped provide insight into the atomistic nature of these transport phenomena in metals.

For other references on the theory of self-diffusion, and on the application of self-diffusion to other [illegible] and the associated bibliography compiled by the author and [illegible].

Although a considerable body of experimental information has been accumulated on self-diffusion in metals, the major part of the detailed work thus far deals with relatively low-melting systems. Diffusion studies on the high-melting elements [illegible] have been limited to polycrystalline material, for which the interpretation and theoretical analysis are difficult. The present work was undertaken to obtain fundamental information on a high-melting element in single-crystal form, at temperatures approaching the melting point. The element chosen was tungsten, and the reasons for the choice were the following:

1. Tungsten is a metal of special interest at Los Alamos. It is currently being considered for application in a number of systems, including nuclear rocket engines, thermionic electric power generators, and high-temperature fast-neutron power reactors.
2. Tungsten has cubic symmetry (b. c. c.) and single-crystal specimens of suitable size were available.
3. Tungsten has the highest melting point of the metals (3410 °C),[13] and apparatus was available for prolonged heating of large diffusion samples at temperatures approaching the melting point.

1.2 Prior Work

Only one direct measurement of self-diffusion in tungsten prior to this research has been found in the literature.[7] In this work, reported in 1956 by Russian investigators Vasil'ev and Chernomorchenko,[14] the diffusion of tracer W^{185} into polycrystalline tungsten was deduced from measurements of the mass absorption of its beta radiation. The radioactive layer was applied to tungsten discs by coating them with a mixture of an organic binder and tungsten trioxide powder containing W^{185}. The samples were dried and fired in a hydrogen furnace for 15-20 minutes at 960-1100 °C. The decrease in surface activity of the discs was then measured as a function of time at constant temperature. The diffusion coefficients they obtained over the temperature range 1287 to 1453 °C fit the usual Arrhenius relationship

$$D = D_0 \, e^{-Q/RT}, \qquad 1.2.1$$

where D is the diffusion coefficient in cm^2/sec, D_0 is the frequency factor in cm^2/sec, Q is the activation energy in calories per mole, R is the universal

gas constant in cal/mole-°K, and T is the temperature in degrees Kelvin. Their values for D_0 and Q were 6.3×10^7 cm^2/sec and 135,800 cal/mole, respectively. They estimate an uncertainty in D of 25-30%. Although the activation energy appears to be of the right order of magnitude, the D_0 value is several orders of magnitude too high in comparison with D_0 values reported for self-diffusion in other metals.[12] At temperatures as low as the ones used in this investigation (only about 40% of the melting point of the metal instead of the usual 75% and above), it is expected that considerable grain-boundary diffusion would occur.

Several indirect measurements of self-diffusion in polycrystalline tungsten have been reported in the literature. Van Liempt[15] (1945) determined an approximate activation energy and frequency factor for self-diffusion in tungsten by measuring the iron loss in iron-containing (~ 0.04%) tungsten wires during incandescence in vacuum. He attempted to show that self-diffusion in tungsten occurred at approximately the same rate as diffusion of iron in tungsten. Van Liempt's expression for the temperature dependence of tungsten self-diffusion is

$$D = 11.5\, e^{-142,000/RT} \text{ cm}^2/\text{sec}.$$

In 1959, two investigators reported activation energies for self-diffusion in tungsten. From high temperature creep measurements on 1/2-inch commercial tungsten rod, Green[16] estimated the activation energy to be 160,000 cal/mole. Schnitzel[17] obtained a value of 125,000 cal/mole from internal friction measurements (damping) of 20-mil tungsten wires. He also reported an activation energy for self-diffusion in rhenium of 140,000 cal/mole.

While the present work was in progress Danneberg[18] investigated self-diffusion in 0.2-mm W^{185}-coated polycrystalline tungsten wires over the temperature range 2000°C to 2700°C. The W^{185} activity was applied to the surface of the wires by electrophoresis of tungsten trioxide suspended in alcohol with calcium chloride as conducting salt. The tungsten trioxide was then reduced to tungsten, although reduction conditions are not mentioned in the report. Lateral layers 1 to 5 microns thick were removed electrolytically from the wire and the activity

of the resulting solution was measured with a scintillation counter. His results fit the equation

$$D = 0.54\ e^{-120,500/RT}\ \text{cm}^2/\text{sec}.$$

Danneberg also obtained self-diffusion coefficients by creep measurements on tungsten wires at 2600 °K and 2700 °K. His values for diffusion coefficients at these temperatures (of the order of 10^{-11} cm^2/sec) agree to within about 55% with those obtained using radioactivity.

The author is not aware of any experimental determination of self-diffusion in rhenium, other than the indirect measurement of activation energy mentioned above, or of impurity diffusion of rhenium in tungsten.

1.3 Objectives and Approach

The objectives of this research were to (1) measure self-diffusion in single-crystal tungsten at temperatures greater than 75% of the melting point of tungsten, (2) measure diffusion of rhenium tracer in single-crystal tungsten at these temperatures, (3) determine the temperature dependence of the diffusion coefficients in these systems and thus the activation energy and frequency factor for diffusion in each system, and (4) analyze the activation energy and frequency factor for self-diffusion in tungsten in the light of current models of the diffusion process. In the course of accomplishing these objectives, the excitation functions for the reactions $W^{184}(d,p)W^{185}$, $W^{186}(d,p)W^{187}$, and $W^{184}(d,2n)Re^{184}$ were measured; and new half-life values for W^{185} and W^{187} were determined.

To avoid the effects of grain-boundary diffusion, single-crystal tungsten rather than polycrystalline tungsten was used in this research. The sectioning method, which is generally considered most accurate for diffusion work,[19, 20] was used with 75-day W^{185} (0.43-MeV β) as tracer. The radioactive layer was produced on the diffusion samples directly by cyclotron bombardment with deuterons. This technique, which has been reported previously in the literature,[21, 22] has the advantage of the tracer atoms being born in the crystal lattice. With

other techniques of forming the radioactive layer, such as electroplating (tungsten is not readily electroplated) or condensing radioactive tungsten vapor on the diffusion samples, there is always the possibility of an oxide or other type chemical film being interposed between the tracer layer and the bulk material, thus presenting a possible barrier to the diffusing atoms. Although the thin radioactive "layer" of W^{185} formed by deuterons varied approximately exponentially with depth, it was shown that diffusion equation boundary conditions were satisfactorily met.

In addition to the (d, p) reactions that take place when tungsten is bombarded with deuterons, competing (d, xn) reactions also occur, producing radioactive rhenium isotopes. Thus, it was possible to measure impurity diffusion of rhenium tracer in tungsten as well as self-diffusion in tungsten on the same diffusion samples. (It is noteworthy that tungsten crystal structure is body-centered cubic whereas rhenium has a hexagonal close-packed lattice.) Rates for impurity diffusion in metals have been reported[23] to be either faster, slower or the same as for self-diffusion.

To determine the optimum deuteron energy to be used in activating the tungsten diffusion samples, cross sections as a function of deuteron energy were experimentally determined for the $W^{184}(d,p)W^{185}$, $W^{186}(d,p)W^{187}$ and $W^{184}(d,2n)Re^{184}$ reactions. The stacked-foil technique was used with an initial deuteron energy of 14 MeV. Also, the half-lives of W^{185} and W^{187} were determined by observing the decay of these isotopes for several months.

Heating of diffusion samples in the temperature range 2660 °C to 3230 °C was accomplished in a 25-kW induction heating furnace with an eddy-current concentrator. Temperatures were measured by optical pyrometry, and the system was calibrated by reference to the melting points of pure metals. Temperature gradients on the surface and within the diffusion samples were also measured.

Because of its unusual machining characteristics, tungsten cannot be sectioned by the more conventional techniques involving use of a microtome or precision lathe. Sectioning therefore was accomplished by grinding. Although

a grinding machine similar to the one developed at the University of Illinois[24] and now becoming popular in diffusion research[25] would perhaps have been suitable, a somewhat novel technique of sectioning with a precision surface grinder was developed. In this technique, a sample is mounted in a V-block and placed on a magnetic chuck for grinding of successive layers. The ground particles from each layer are collected on a piece of moist filter paper placed a few inches from the grinding wheel. Since a high percentage of particles "fly off" tangent to the wheel, a radioactive spot, which may be analyzed, collects on the filter paper. Quantitative recovery is not necessary since specific activity is all that is required. Cross contamination of activity from one ground layer to the next is not significant when proper precautions are taken. Layers as thin as 0.2 mil may be ground off and collected with this technique, which has the added advantage of insuring that each layer ground off is parallel to each succeeding layer since the sample is not removed from its mounting during the entire sectioning process. The thickness of sections is determined by measuring the sample with a precision micrometer before and after a layer is ground off.

Radiochemical procedures were developed for separating tungsten and rhenium from grinding wheel abrasive. The 8-hydroxyquinoline derivative of tungsten was mounted for beta counting. Tetraphenylarsonium perrhenate was mounted for gamma counting.

Temperature dependence equations for self-diffusion in tungsten and for diffusion of rhenium tracer in tungsten were determined according to the Arrhenius relationship $D = D_0\, e^{-Q/RT}\ \mathrm{cm^2/sec}$. The activation energy and frequency factor for self-diffusion in tungsten were compared with predicted theoretical values, and were analyzed in the light of current models of the diffusion process. Computer methods were used in obtaining the best least-squares fit of all data.

Chapter 2

EXCITATION FUNCTIONS FOR THE REACTIONS $W^{184}(d,p)W^{185}$, $W^{186}(d,p)W^{187}$, AND $W^{184}(d,2n)Re^{184}$

The purpose in measuring excitation functions for (d,p) reactions on natural tungsten was to determine the optimum deuteron energy to use for production of a thin layer of radioactive tungsten tracer on tungsten diffusion samples. In addition, it was of interest to know the extent of competing (d,xn) reactions which would produce a thin layer of rhenium tracer on the tungsten diffusion samples.

2.1 Experimental

The stacked-foil technique was used to measure total cross sections for the reactions $W^{184}(d,p)W^{185}$, $W^{186}(d,p)W^{187}$, and $W^{184}(d,2n)Re^{184}$.

2.1.1 Target Material

Tungsten foil for the foil stack was obtained from H. Cross Co., Union City, New Jersey. The foil was 0.34 ±0.01 mil thick, and was relatively pin-hole free and of high purity. Results of a spectrochemical analysis of the foil, performed by Group CMB-1 of this Laboratory, are presented in Table 2.1.

The foil was cut into disks 1.000 ± 0.005 in. in diameter for deuteron bombardment. The average foil thickness obtained by weighing was 16.75 mg/cm^2. The foil stack contained 17 foils, each of which was washed with trichloroethylene, acetone, and ethanol prior to bombardment.

TABLE 2.1

SPECTROCHEMICAL ANALYSIS OF TUNGSTEN FOIL

Element	Concentration (ppm)	Element	Concentration (ppm)
Ag	< 3	Mn	< 10
Al	< 30	Mo	<100
B	< 10	Na	< 30
Ba	< 10	Nb	<100
Be	< 3	Ni	< 10
Ca	< 30	Si	< 50
Co	< 30	Sn	< 10
Cr	< 10	Sr	< 30
Cu	< 3	Ta	<100
Fe	50	Ti	< 30
K	< 30	V	< 30
Li	< 10	Zn	<100
Mg	5	Zr	< 30

2.1.2 Deuteron Bombardment

The foil stack was bombarded with 14.01 ± 0.05-MeV deuterons at the Los Alamos variable-energy cyclotron, with an experimental arrangement similar to the one described by Cochran and Knight.[26] The foil stack was held in a combination target holder and Faraday cup (Fig. 2.1) mounted at the end of a 24-ft tube extending from the beam extraction port of the cyclotron. The deuteron beam was magnetically and electrostatically focused and collimated so as to strike an area approximately 1/2 in. in diameter on the foil stack. The target assembly was water cooled during bombardment. Beam current during bombardment was approximately 2 μamps, and the integrated flux was 3,041 μC, which represented a total of 1.899×10^{16} deuterons incident on the foil stack.

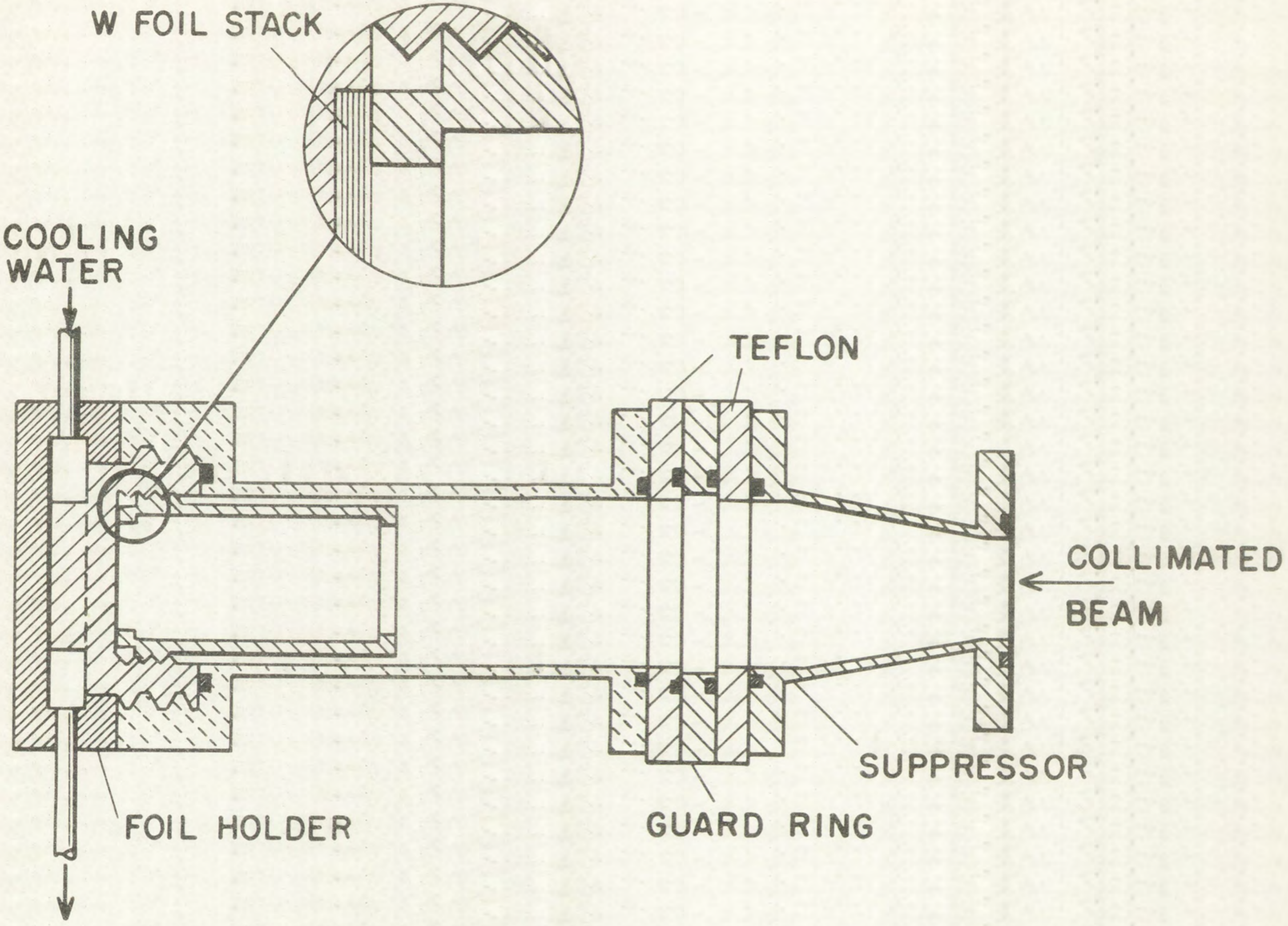

Fig. 2.1 Target Arrangement for Deuteron Bombardment of Tungsten Foil Stack

2.1.3 Radiochemistry

After bombardment, the tungsten foils were dissolved in a mixture of hydrofluoric and nitric acids, rhenium carrier was added, and pure fractions of the tungsten and rhenium activities were separated and mounted for counting. The radiochemical procedures used were essentially those presented in Chapter 7, with the omission of the silicon separations. The tungsten was mounted for counting as the 8-hydroxyquinoline derivative, and the rhenium fraction was mounted as rhenium sulfide (Re_2S_7).

2.1.4 Beta Counting Equipment and Procedures

The radioactive isotopes produced by (d, p) reactions on natural tungsten were mainly 23.7-hour W^{187} (0.63-MeV β), and 75-day W^{185} (0.43-MeV β). Only trace amounts of 130-day W^{181} and 65-day W^{188} were produced.

The tungsten samples were counted on the first shelf of a propane-flow proportional counter which was operated at atmospheric pressure at about 4200 volts. The electronic components were a Los Alamos Model PA-6 pulse amplifier and a Los Alamos Model SC-10-A decade scaler.

Beginning two days after the irradiation, the samples were counted three times daily for a period of five days. Thereafter, the samples were counted twice daily for three days, and daily for a period of 34 to 36 days.

The zero-time (time at the end of irradiation) activities (W^{185} and W^{187}) for each sample were obtained from a least-squares analysis of the data, performed on an IBM 704 Electronic Data Processing Machine. The FORTRAN Code used, called "Skitzo", resolves zero-time activities or half-lives or both from the decay data of multi-component systems. This code was an early version of a general least-squares code prepared by Moore and Zeigler,[27] and included corrections for counter dead time and for decay during the counting period. The standard error in determining zero-time activities for W^{185} and W^{187} was less than 0.3% for each of seventeen samples. Half-life values used were 23.72 hours for W^{187}, and 72.92 days for W^{185}.

The zero-time activities obtained were corrected for chemical yield, and, in the case of W^{187}, for decay during the bombardment. Absolute disintegration rates were computed from the beta counts by the method of Bayhurst and Prestwood,[28] and were estimated to be accurate to within 3%. The counting efficiency curves used, which include corrections for self-absorption, scattering, etc., are presented in Fig. 2.2, and the zero-time distintegration rates for W^{185} and W^{187} in each of the samples are given in Table 2.2.

TABLE 2.2

ZERO-TIME DISINTEGRATION RATES OF W^{185} AND W^{187}

Foil No.	W^{185} Decay (d/m)	W^{187} Decay (d/m)
1	5.46×10^5	3.66×10^7
2	6.11×10^5	4.15×10^7
3	5.87×10^5	4.03×10^7
4	5.78×10^5	4.07×10^7
5	5.79×10^5	4.07×10^7
6	5.82×10^5	4.17×10^7
7	5.40×10^5	3.96×10^7
8	6.72×10^5	5.10×10^7
9	4.39×10^5	3.30×10^7
10	4.28×10^5	2.96×10^7
11	3.66×10^5	2.50×10^7
12	2.48×10^5	1.97×10^7
13	1.63×10^5	1.31×10^7
14	9.38×10^4	7.45×10^6
15	4.51×10^4	3.66×10^6
16	1.55×10^4	1.24×10^6
17	4.96×10^3	3.77×10^5

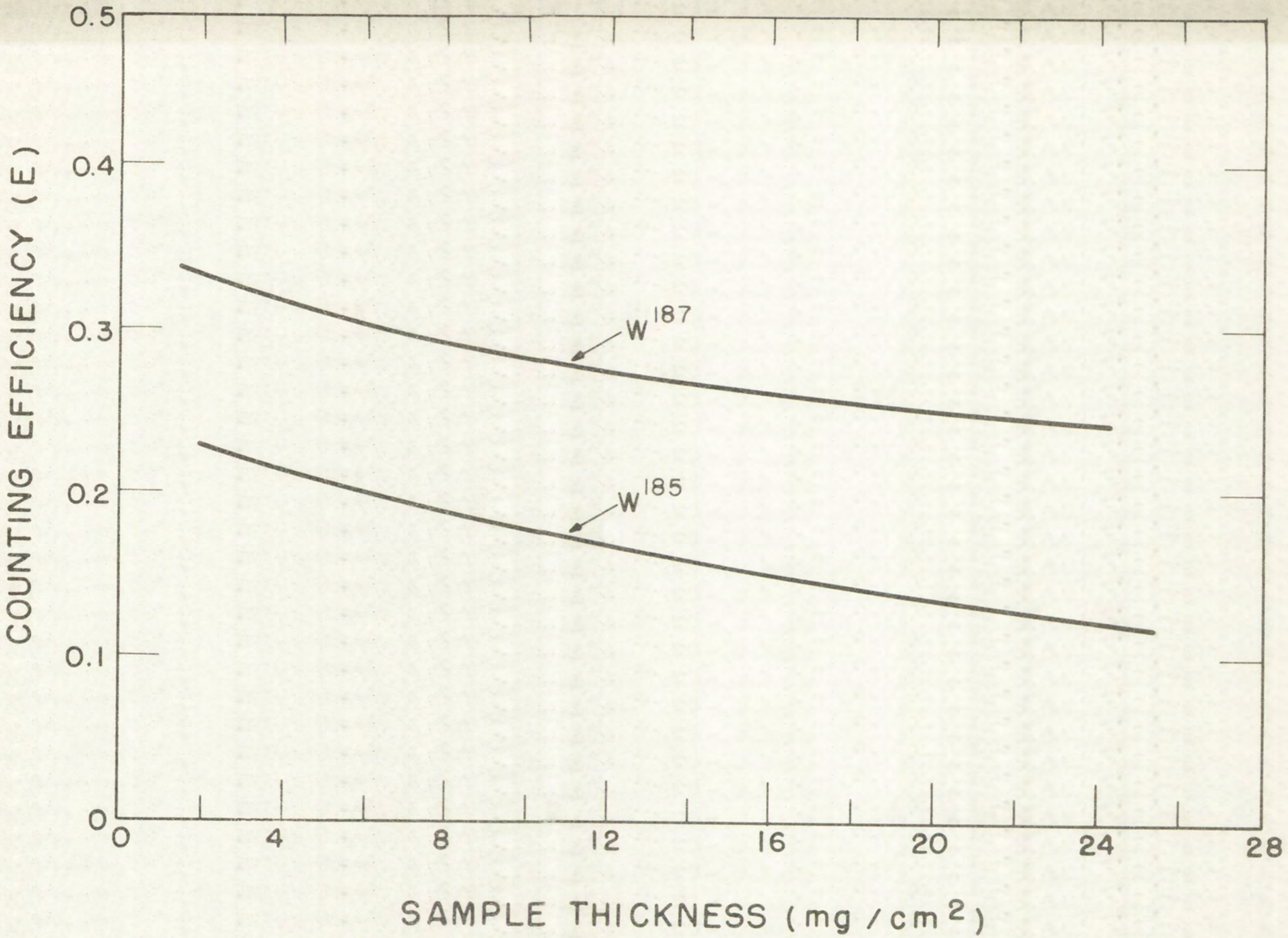

Fig. 2. 2 Counting Efficiency Curves of W^{185} and W^{187} as a Function of Sample Thickness

2.1.5 Gamma Counting Equipment and Procedures

Rhenium isotopes from mass number 180 through 187 were produced by (d, xn) reactions on natural tungsten. The reactions occurring were mainly (d, n) and (d, 2n). The gamma spectrum from a rhenium sample obtained three days after the irradiation indicated the presence of 20-hr Re^{181}, 13-hr and 64-hr Re^{182}, 68-day Re^{183}, 34-day Re^{184}, and 90-hr Re^{186}. Many of these isotopes have complicated γ-ray spectra with energies near 1.0 MeV, and thus it was not possible to obtain absolute disintegration rates for most of them. However, after 50 days decay time, an examination of the γ-spectrum indicated a reasonably pure photopeak of Re^{184} (0.895- and 0.904-MeV γ's), and absolute disintegration rates at zero time were obtained for this isotope.

The rhenium samples were measured with a γ-scintillation spectrometer system consisting of shielded 3 in. x 3 in. NaI (Tl) scintillator coupled to a 5-in. DuMont 6364 photomultiplier tube, a Los Alamos Model 260 amplifier, and a Los Alamos Model II-A 100-channel pulse-height analyzer. The rhenium γ-ray spectra, observed at a source-to-crystal distance of 1 cm, were obtained for fifteen of the seventeen samples; the last two samples were too weak to give useful photopeaks. The high-energy portion of a typical scintillation spectrum, showing the Re^{184} photopeaks at 0.793 MeV and at 0.895 and 0.904 MeV (0.902 MeV is the weighted average of the 0.895 and 0.904 MeV γ-rays), is shown in Fig. 2.3.

The absolute disintegration rate of Re^{184} in each of the samples was computed from the area under the 0.902-MeV hybrid photopeak by dividing the area (in counts/min) by the photopeak efficiency and by the number of γ-rays per disintegration. Since the low-energy portion of the 0.902-MeV photopeak overlapped the high-energy portion of the 0.793-MeV photopeak, the correct shape of the former was established by comparison with a "pure" standard of 0.885 MeV. The standard was obtained by subtracting a 1.119-MeV photopeak and the associated Compton spectrum (Zn^{65} scintillation spectrum) from a spectrum with photopeaks at 1.119 and 0.885 MeV (Sc^{46}). The Re^{184}, Zn^{65}, and Sc^{46} spectra used in this comparison were all recorded under identical conditions,

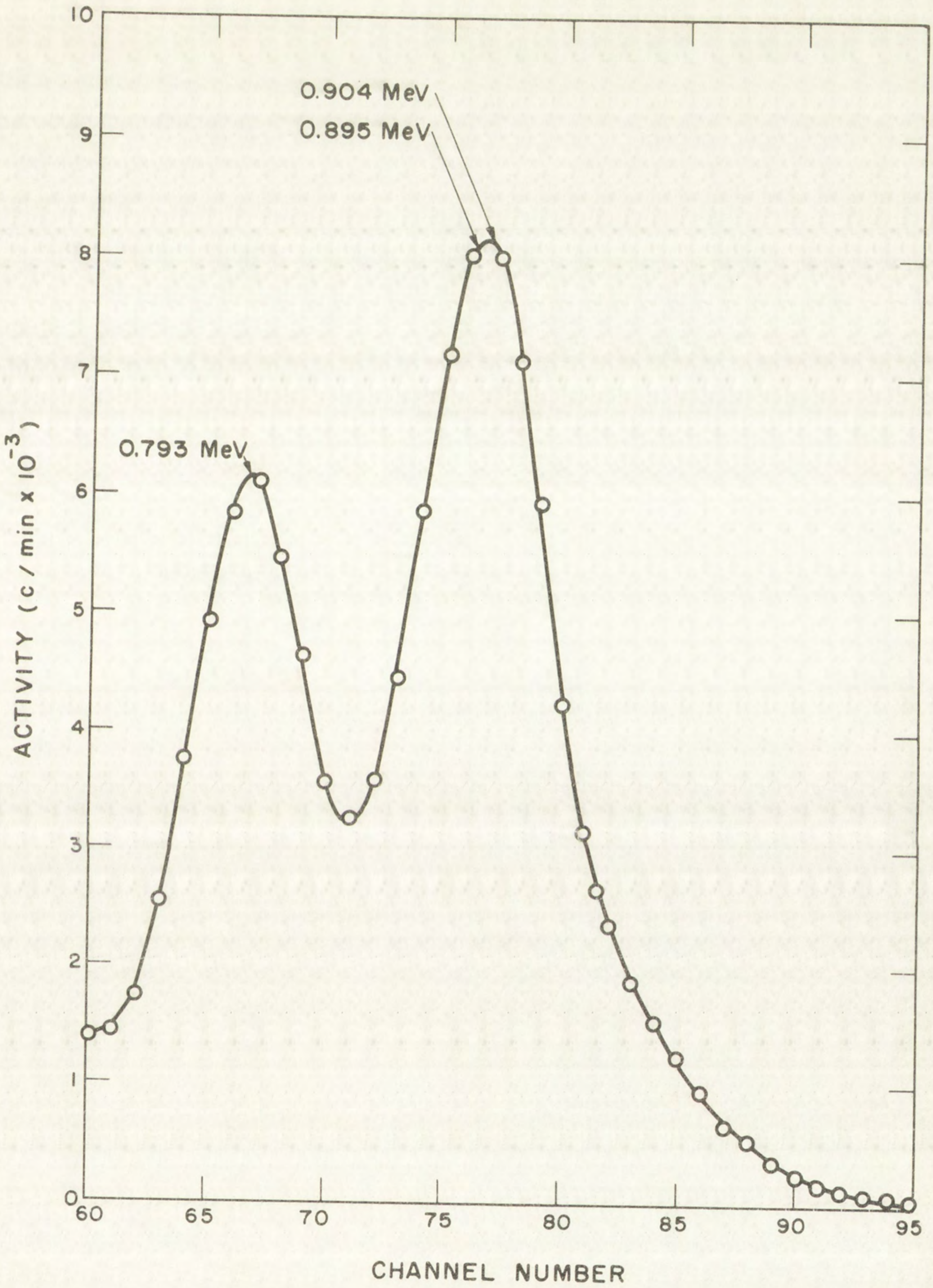

Fig. 2.3 High Energy γ-Ray Photopeaks of Re^{184}

2.1.6 Range of Deuterons in Tungsten

Before experimental cross sections could be determined from zero-time disintegration rates of W^{185}, W^{187}, and Re^{184}, it was necessary to determine, from range-energy relationships, the energy of the deuterons at the midpoint of each of the seventeen foils in the foil stack. The ranges of 1 MeV to 20 MeV deuterons in tungsten were calculated from the following expression given by Friedlander and Kennedy,[31]

$$R = R_a \left(2.935 - 0.5764 \log \frac{E}{2}\right) - 0.74, \qquad 2.1.6.1$$

where R is the range of deuterons in tungsten in mg/cm^2, R_a is the range, expressed in mg/cm^2, of deuterons in air at 15 °C and 760 mm Hg, and E is the initial deuteron energy in MeV. Friedlander and Kennedy state that this equation is valid to within a few percent for deuterons with energies ranging from 1 to 100 MeV. The ranges of deuterons in air (R_a) were taken from the data of Rich and Madey.[32] Figure 2.4 is a plot of the calculated range-energy function from which deuteron energies at the midpoint of each foil were obtained. The 14 MeV incident deuterons degraded to about 6 MeV in the foil stack.

2.2 Results and Discussion

2.2.1 Experimental Cross Sections for the Reaction $W^{184}(d,2n)Re^{184}$

At the time the present work on excitation functions was undertaken, the 2.2-day and 50-day half-life values reported by Wilkinson and Hicks[33] for Re^{184} isomers were the generally accepted ones. It was on the basis of the 50-day Re^{184} isomer that the excitation function was calculated, since it was assumed that little of the 2.2-day Re^{184}, which was thought to decay by electron capture and isomeric transition, would be formed and contribute to 50-day Re^{184}. At

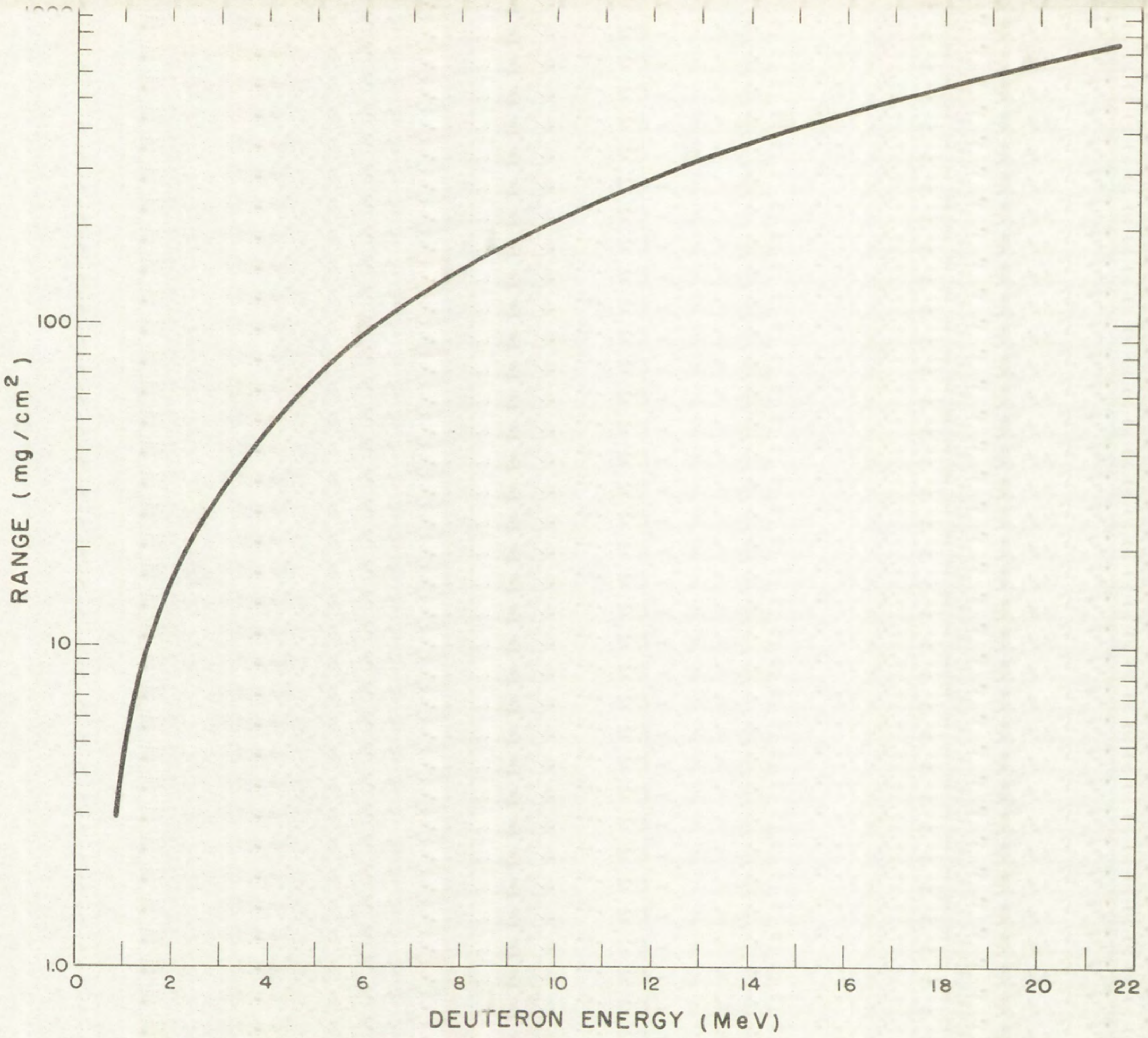

Fig. 2.4 Deuteron Range in Tungsten as a Function of Deuteron Energy

the time the counting had commenced, the 2.2-day Re^{184} activity was to have been negligible because of decay.

After the excitation function work was complete, Johnson[34] reported half-life values of 165 ± 8 days and 34 ± 5 days for Re^{184} isomers. The 165-day isomer, the upper transition state, decayed by γ-emission to the 34-day Re^{184} isomer which in turn decayed by electron capture to excited levels of W^{184} ($Re^{184m} \xrightarrow{\text{I. T. (165 days)}} Re^{184} \xrightarrow{\text{E. C. (34 days)}} W^{184}$). Bodenstedt, et al.,[35] reported a half-life of 38 ± 1 days for Re^{184}, but their value is probably too high because they were apparently unaware of the 165-day Re^{184} isomer forming some of the 34-day Re^{184} isomer which they were counting. At any rate, the 50-day half-life was no longer valid, and it was necessary to make some corrections to the data.

The most active sample (Foil No. 1) which was counted 58.924 days after zero time and which gave 5.10×10^5 d/m at that time, was, fortunately, counted under identical conditions at 190.198 days from zero time. The decay rate at the latter time was 6.16×10^4 d/m. Using half-life values of 165 days and 34 days for the Re^{184} isomers, the number of atoms of each isomer present at zero time was calculated with the aid of the general equations governing decay and growth of parent-daughter transformations. The calculations indicated that 86% of the total Re^{184} atoms present at zero time were those of the 34-day isomer. Cross sections for each isomer were then calculated on the basis of 30.6% abundance of W^{184} in natural tungsten. (The total number of deuterons, as indicated in Section 2.1.2, was 1.899×10^{16}.) The cross sections for formation of 34-day Re^{184} and 165-day Re^{184} by bombardment of natural tungsten with 13.80-MeV deuterons were calculated to be 352 mb and 57 mb, respectively.

The cross sections for formation of 34-day Re^{184} at lower deuteron energies were calculated on the basis of the same ratio of 34-day isomer to 165-day isomer being formed as was found for 13.80-MeV deuterons. This assumption is not likely to be very much in error, since a slightly greater percentage of the 34-day isomer was probably produced at lower deuteron energies than was produced at 13.80 MeV. The lower the deuteron energy, the less

angular momentum is brought into the compound nucleus (in this case Re^{186}), and the greater is the probability of forming the low-spin nuclear isomer, 34-day Re^{184}. The disintegration rates originally observed in the remaining fourteen samples were corrected for decay (using the apparent half-life of 42 days) to the time of measurement (58.924 days) of the sample from Foil No. 1. The correction was never for more than 3.215 days. The cross sections for formation of the 34-day Re^{184} isomer in the remaining samples were then calculated from the relationship,

$$\sigma(\text{mb}) = 6.91 \times 10^{-4} A_0 , \qquad 2.2.1.1$$

where A_0 is the absolute disintegrations per minute corrected for decay as described above. The corrected values of A_0, along with the experimentally determined cross sections for the reaction $W^{184}(d,2n)$ 34-day Re^{184} as calculated from Eq. 2.2.1.1, are presented in Table 2.4. Figure 2.5 is a plot of the data.

In principle it would have been possible to measure the Re^{184} activity at a later time (provided sufficient activity was present) in each of the remaining fourteen samples, as was done with the first one, and then calculate the number of atoms of each isomer present at zero time from the equations governing parent-daughter transformations, and hence the cross sections for each isomer as a function of deuteron energy. However, little would have been gained in accuracy because of a previously unmentioned uncertainty which will now be discussed.

Actually, two reactions can contribute to Re^{184} production from deuteron bombardment of tungsten. These are the previously considered $W^{184}(d,2n)Re^{184}$ reaction with an estimated Q value of - 4.6 MeV, and the reaction $W^{183}(d,n)Re^{184}$ with an estimated Q value of + 2.85 MeV. The isotopic abundances of W^{183} and W^{184} in natural tungsten are 14.4% and 30.6%, respectively. To know precisely how much Re^{184} is produced from each of these reactions would require a separate bombardment experiment on isotopically pure W^{183} or W^{184}. However, an estimate of the contribution of each reaction was obtained by comparison of

TABLE 2.4

EXPERIMENTAL VALUES OF THE CROSS SECTIONS FOR THE W^{184}(d, 2n) 34-DAY Re^{184} REACTION AT VARIOUS DEUTERON ENERGIES

Foil No.	A_0 (d/m)	Deuteron Energy at Midpoint of Foil (MeV)	Cross Section (mb)
1	5.10×10^5	13.8	352
2	3.55×10^5	13.4	246
3	3.25×10^5	13.0	225
4	2.78×10^5	12.6	192
5	1.84×10^5	12.1	127
6	1.95×10^5	11.7	135
7	1.00×10^5	11.3	69
8	8.88×10^4	10.8	61
9	6.67×10^4	10.4	46
10	6.10×10^4	9.9	42
11	3.50×10^4	9.4	24
12	2.78×10^4	8.9	19
13	1.96×10^4	8.4	14
14	8.68×10^3	7.8	6
15	5.86×10^3	7.2	4

the present data with the data of Ramler, et al.,[36] for (d, n) and d, 2n) reactions on the comparatively heavy isotope Bi^{209}. Ramler's data indicate that the (d, n) reaction cross sections are consistently less than 10% of the (d, 2n) reaction cross sections for deuterons with energies between 9 and 18 MeV. Because of this fact, and considering the relative abundances of W^{183} and W^{184}, it is estimated that 95% of the Re^{184} activity was produced by the reaction, W^{184}(d, 2n)Re^{184}, at deuteron energies above about 9 MeV.

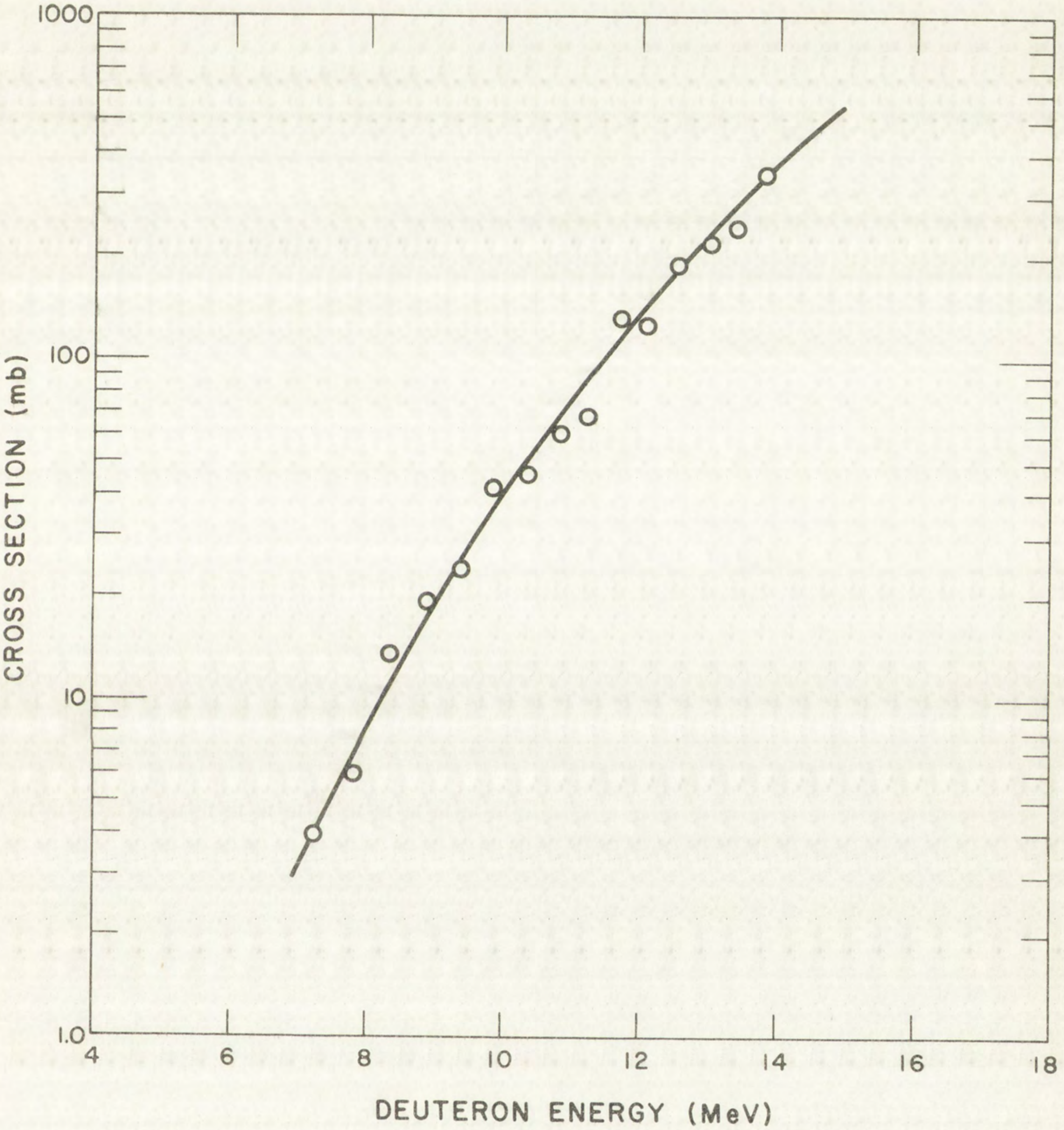

Fig. 2.5 Experimental Cross Sections for the Reaction W^{184}(d, 2n) 34-day Re^{184} as a Function of Deuteron Energy. Approximately 5% of the cross section values at deuteron energies above 9 MeV are due to the W^{183}(d, n) 34-day Re^{184} reaction.

The two uncertainties discussed above, namely, that due to variation of the ratio of 34-day Re^{184} to 165-day Re^{184} formed in the bombardment as a function of deuteron energy (~ 10%), and the Re^{184} (both isomers) formed by (d, n) reactions on W^{183} (~ 5%) were small by comparison with the 15% uncertainty in the half-life (34 ± 5 days) of Re^{184}. The total estimated uncertainty in the experimentally determined cross sections (Table 2. 4) for the W^{184}(d, 2n) 34-day Re^{184} reaction was about 25%.

The excitation function[36] for the reaction, Bi^{209}(d, 2n)Po^{209}, mentioned above, passes through a rather broad maximum of 540 mb between 14 and 16 MeV. Deuteron energies employed in the present work were not high enough to indicate the position of the maximum (Fig. 2. 5) for the W^{184}(d, 2n) 34-day Re^{184} excitation function. The experimentally determined cross sections ranged from about 3 to 380 mb for deuteron energies of 7 to 14 MeV, respectively.

2. 2. 2 Experimental Cross Sections for the Reactions W^{184}(d, p)W^{185} and W^{186}(d, p)W^{187}

The experimentally determined cross sections for W^{184}(d, p)W^{185} and W^{186}(d, p)W^{187} reactions were calculated on the basis of 30. 6% abundance of W^{184} and 28. 4% abundance of W^{186} in natural tungsten. The data are presented in Table 2. 5, and a plot of the data is shown in Fig. 2. 6. For comparison purposes, the W^{184}(d, 2n)Re^{184} excitation function is also shown in Fig. 2. 6.

From the data presented, it may be seen that the two excitation functions leading to the production of tungsten isotopes have the same general shape, but that the reaction cross sections of W^{186} are slightly higher. Both excitation functions increase from about 3 mb at 6 MeV to a fairly broad maximum at about 300 mb between 11 and 13 MeV. The excitation functions leading to the production of W^{185} and W^{187} are believed to be accurate to within about 10%

2. 2. 3 Selection of Deuteron Energy for Production of Radioactive Layer on Diffusion Samples

The original purpose in determining excitation functions for production of radioactive tungsten and rhenium isotopes by deuteron reactions with tungsten

TABLE 2.5

EXPERIMENTAL VALUES OF THE CROSS SECTIONS FOR THE REACTIONS W^{184} (d, p) W^{185} AND W^{186} (d, p) W^{187} AT VARIOUS DEUTERON ENERGIES

Foil No.	Deuteron Energy at Midpoint of Foil (MeV)	W^{184} (d, p) W^{185} Cross Section (mb)	W^{186} (d, p) W^{187} Cross Section (mb)
1	13.8	259	248
2	13.4	290	281
3	13.0	279	273
4	12.6	275	276
5	12.1	275	276
6	11.7	277	283
7	11.2	257	269
8	10.8	320	345
9	10.4	209	223
10	9.9	203	200
11	9.4	174	169
12	8.9	118	133
13	8.4	77.5	88.9
14	7.8	44.5	50.4
15	7.2	21.4	24.8
16	6.6	7.4	8.4
17	5.9	2.4	2.6

was to permit selection of an optimum deuteron energy for production of a thin radioactive "layer" of tungsten and rhenium tracers on the tungsten diffusion samples. With the curves (Figs. 2.5 and 2.6) now available, it was relatively simple to select this energy.

An optimum deuteron energy would correspond to cross sections high enough to produce sufficient tungsten and rhenium activity in a reasonable

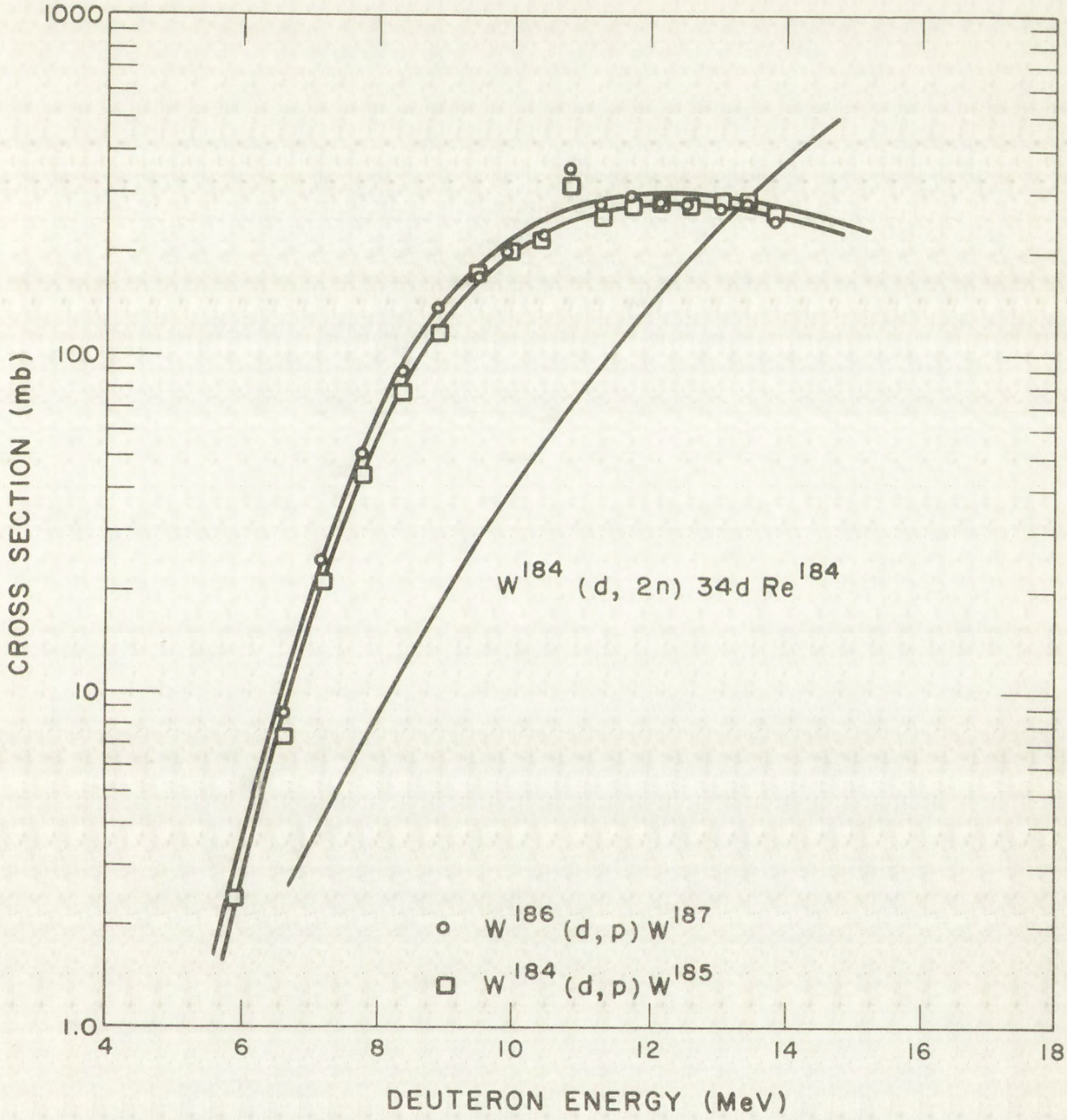

Fig. 2.6 Experimental Cross Sections for Deuteron Reactions on Tungsten as a Function of Deuteron Energy

bombardment time, yet low enough to hold the average deuteron penetration depth to a minimum. Furthermore, the decrease in cross section with decreasing deuteron energy (as the initial deuteron energy degraded through the tungsten) should be considerable so as to provide maximum activity on or slightly below the surface of the diffusion samples; in other words, an optimum deuteron energy would be on the steepest part of the curve (Fig. 2. 6).

With these criteria in mind, a deuteron energy of 9. 0 MeV was selected for bombardment of diffusion samples. The penetration depth of 9. 0-MeV deuterons in tungsten is 3. 6 mils, but 9. 0-MeV deuterons degrade to about 6. 0 MeV in only 1. 7 mils of tungsten. The corresponding cross sections for 75-day W^{185} production are 150 mb and 3 mb, respectively. The cross sections for 34-day Re^{184} production range from 20 mb at 9. 0 MeV to less than 1 mb at 6 MeV. The latter cross sections are for one rhenium isotope only, and other useful ones which would increase over-all rhenium activity would also be produced.

2. 2. 4 Half-Lives of Tungsten Isotopes

One of the best tungsten samples (Foil No. 6) from the excitation function study was counted routinely every two weeks over a period of 670 days (almost 9 half-lives) to determine an accurate value for the half-life of W^{185}. The data were programmed for an IBM-704 using the "Skitzo" code discussed in Section 2. 1. 4. In the first run, four parameters, the half-lives and zero-time activities of W^{185} and W^{187}, none of which were held constant, were determined. From the systematic trends which appeared in the deviations to the least-squares fit, the presence of trace amounts of another activity was suspected. Since the trace activity was probably W^{181}, another "Skitzo" run was made with six parameters, four of which were held constant, in an attempt to determine the zero-time activity and half-life of the impurity. The results of this run did indeed identify the impurity as having a half-life of 129. 5 days, thus confirming the presence of W^{181}. The W^{181} originated, of course, from (d, p) reactions on W^{180}, which has an abundance of only 0. 14% in natural tungsten. The zero-time activity of W^{181} was only 56 counts per minute compared to 6, 189 counts per minute of W^{185} and 676, 000 counts per minute of W^{187}.

A final run with six parameters, one of which (the W^{181} half-life) was held constant, gave the values 75.14 ± 0.63 days and 23.72 ± 0.06 hours for the half-lives of W^{185} and W^{187}, respectively. The uncertainties listed are 3 σ, which represent 99.73% confidence limits. The weighted variance, which is a measure of how closely statistical the data were, should be 1.00 for completely statistical data, as set up in the "Skitzo" code. For this last run, from which the half-life values were taken, the weighted variance was 1.106.

The 75-day half-life value of W^{185} did not agree with the half-life value (73 days) obtained from a "Skitzo" run of the data after only 44 days counting time (Section 2.1.4). However, this small difference (2.7%) was less than the experimental error in determining the cross sections leading to production of W^{185}. Therefore, the zero-time disintegration rates of W^{185} (Table 2.2) were not corrected. The value (23.72 hr) obtained for the W^{187} half-life after 44 days counting time did not change in the subsequent "Skitzo" run, which contained data over the longer counting period.

The half-life value (75.14 ± 0.63 days) obtained for W^{185} agrees with the 75.8 day half-life reported by Prestwood[37] and the half-life value (23.72 ± 0.06 hr) obtained for W^{187} agrees fairly well with the 23.85 ± 0.08 hr half-life reported by Eichholz.[38]

2.3 Summary

Excitation functions for the reactions, $W^{184}(d,p)W^{185}$, $W^{186}(d,p)W^{187}$, and $W^{184}(d,2n)$ 34-day Re^{184}, were measured for deuterons with energies ranging from 6 to 14 MeV by the stacked-foil technique. The excitation functions leading to the production of W^{185} and W^{187} have the same general shape and magnitude, but the reaction cross sections of W^{186} are slightly higher. Both excitation functions increase from about 3 mb at 6 MeV to a fairly broad maximum of 300 mb between 11 and 13 MeV. Cross sections leading to the production of 34-day Re^{184} ranged from about 3 to 380 mb for deuteron energies of 7 to 14 MeV. Deuteron energies employed were not high enough to indicate

the position of the maximum for the W^{184}(d, 2n) 34-day Re^{184} excitation function. From the above excitation functions, an energy of 9.0 MeV was selected for deuteron bombardment of tungsten diffusion samples to produce a thin layer of radioactive tungsten and rhenium tracers.

The decay of W^{185} was observed over a period of about nine half-lives, and a new half-life value of 75.14 ± 0.63 days, with the uncertainty expressed to 3 σ, was obtained. The half-life value obtained for W^{187}, also expressed to 3 σ, was 23.72 ± 0.06 hours.

Chapter 3

DIFFUSION EQUATION AND BOUNDARY CONDITIONS

3.1 Development of Fundamental Diffusion Equation

Diffusion in metals occurs by random motions of the atoms within the crystal lattice. Transfer of heat by conduction also occurs by random motions of atoms or molecules. Fick[39] recognized the analogy between the two processes and was the first to put diffusion on a quantitative basis by adopting the mathematical equation of heat conduction. The theory of diffusion, then, is based upon the assumption that the rate of transfer of a diffusing substance through unit area of a reference plane within the material is proportional to the concentration gradient measured normal to this plane. Thus,

$$F = -D\frac{\partial C}{\partial x}, \qquad (3.1.1)$$

where F, the diffusion current, is the rate of transfer per unit area of reference plane, C is the concentration of diffusing substance, and x is the coordinate normal to the plane along which diffusion occurs. Equation 3.1.1 is known as Fick's first law of diffusion. If the units of F are g/cm^2 sec and C is expressed in g/cm^3, it is readily seen that D is independent of grams of diffusing substance and has the units cm^2/sec. In vector notation and with diffusion occurring in three directions, Fick's first law becomes

$$\vec{F} = -D\nabla C = -D\left(\vec{i}\frac{\partial C}{\partial x} + \vec{j}\frac{\partial C}{\partial y} + \vec{k}\frac{\partial C}{\partial z}\right) , \qquad (3.1.2)$$

where $\vec{F}$ represents the current density at each point in the diffusion system.

Fick's second law may be derived as follows. Consider a small element of volume, dx dy dz = dV, within a diffusion system such as the one shown in Fig. 3.1. The coordinate axes x, y and z are along three mutually perpendicular unit vectors $\vec{i}$, $\vec{j}$ and $\vec{k}$, respectively. The total net loss of material diffusing out of this volume element per unit time should be equal to

$$-\frac{\partial C}{\partial t}\, dV.$$

The rate at which material diffuses into the element through face OABC is

$$\vec{i} \cdot \left[\vec{F}(x, y, z)\right] dy\, dz.$$

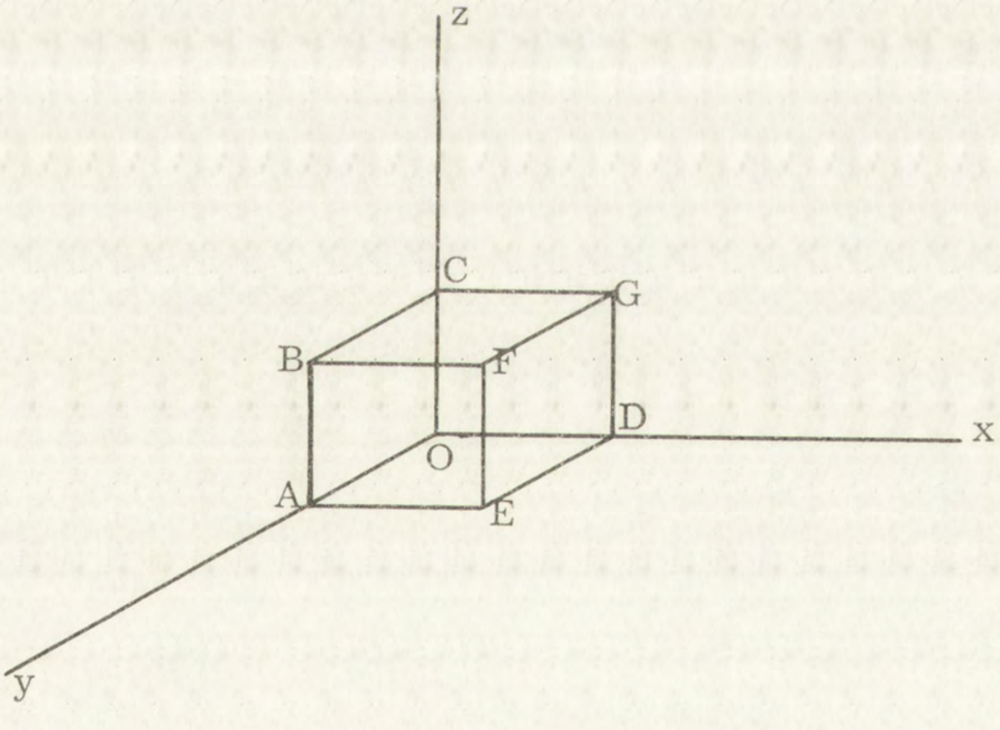

Fig. 3.1 Element of Volume

The rate at which material diffuses out of the element through face DEFG is

$$\vec{i} \cdot \left[\vec{F}(x, y, z) + \frac{\partial \vec{F}}{\partial x} dx\right] dy\ dz.$$

Therefore, the net loss between these two faces is

$$\vec{i} \cdot \frac{\partial \vec{F}}{\partial x} dx\ dy\ dz.$$

Similarly, the net losses between the other two pairs of faces are

$$\vec{j} \cdot \frac{\partial \vec{F}}{\partial y} dx\ dy\ dz \text{ and } \vec{k} \cdot \frac{\partial \vec{F}}{\partial z} dx\ dy\ dz.$$

Thus, the total net rate at which material diffuses out of the volume element, dV, is

$$-\frac{\partial C}{\partial t} dV = \left[\vec{i} \cdot \frac{\partial \vec{F}}{\partial x} + \vec{j} \cdot \frac{\partial \vec{F}}{\partial y} + \vec{k} \cdot \frac{\partial \vec{F}}{\partial z}\right] dx\ dy\ dz = \nabla \cdot \vec{F} dV. \qquad (3.1.3)$$

Then, from Eq. 3.1.2,

$$-\frac{\partial C}{\partial t} = \nabla \cdot \vec{F} = -\nabla \cdot (D\nabla C). \qquad (3.1.4)$$

In general, D is a function of concentration; but for self-diffusion where the chemical concentration is the same throughout the system and the difference in diffusion rates of isotopes can be neglected, D is independent of concentration. The isotope effect is nearly always less than experimental error and may be neglected.[40] Furthermore, D may be considered to be constant for any system in which the diffusing substance does not cause a macroscopic concentration gradient. For constant D, Eq. 3.1.4 becomes

$$\frac{\partial C}{\partial t} = D\nabla^2 C = D\left(\frac{\partial^2 C}{\partial x^2} + \frac{\partial^2 C}{\partial y^2} + \frac{\partial^2 C}{\partial z^2}\right), \qquad (3.1.5)$$

and for diffusion in one direction only, Eq 3.1.5 reduces to

$$\frac{\partial C}{\partial t} = D \frac{\partial^2 C}{\partial x^2} . \qquad (3.1.6)$$

Equation 3.1.6 is known as Fick's second law of diffusion. Similar derivations of Fick's second law may be found in almost any reference book or text on diffusion. See, for example, Crank's[41] treatment.

3.2 Solution of the Diffusion Equation

Of the various integrated forms of Fick's second law of diffusion, one of the most useful for diffusion studies and the one used in this work satisfies the boundary conditions of an infintely thin layer of tracer atoms diffusing into a semi-infinite diffusion medium. The boundary conditions are readily approximated experimentally, and obtaining D, the diffusion coefficient, from the experimental data is a relatively simple matter. Instead of a simple presentation of the solution and a statement that it may be verified by direct substitution, as is often done,[42,43] a solution based on the method of Laplace transforms is presented.

The partial differential equation to be solved, as stated above in Eq. 3.1.6, is

$$\frac{\partial C}{\partial t} = D \frac{\partial^2 C}{\partial x^2} ,$$

where $C(x,t)$ is the concentration, say in g/cm^3, t is the diffusion time, D is the diffusion coefficient and x is the coordinate along which diffusion occurs. An infinitely thin layer of material of surface density C_0 g/cm^2 diffuses into the semi-infinite medium. The initial condition is

$$C(x,0) = 0, \text{ for } x \neq 0 \qquad (3.2.1)$$

and the boundary condition is

$$\frac{\partial C(0,t)}{\partial x} = \left.\frac{\partial C}{\partial x}\right|_{x=0} = 0 \quad \text{for } t > 0. \qquad (3.2.2)$$

The total amount of diffusing material remains constant. Thus,

$$\int_0^\infty C(x,t)\, dx = C_0 \,. \qquad (3.2.3)$$

To facilitate the calculation for a semi-infinite medium, the system is reflected about the axis $x = 0$ so that

$$C(-x,t) = C(x,t) \qquad (3.2.4)$$

and

$$\int_{-\infty}^\infty C(x,t)\, dx = 2\, C_0 \,. \qquad (3.2.5)$$

Equations 3.1.6, 3.2.1 and 3.2.2 still apply. The natural boundary condition,

$$\lim_{x \to \pm\infty} C(x,t) = 0 \qquad (3.2.6)$$

also applies.

The Laplace transform $\overline{C}$ of $C(x,t)$ with respect to t is now defined,

$$\overline{C}(x,p) = \int_0^\infty C(x,t)\, e^{-pt}\, dt. \qquad (3.2.7)$$

Assuming differentiation under the integral sign to be valid,

$$\frac{\partial \overline{C}}{\partial x} = \int_0^\infty \frac{\partial C}{\partial x}\, e^{-pt}\, dt, \qquad (3.2.8)$$

and

$$\frac{\partial^2\overline{C}}{\partial x^2} = \int_0^\infty \frac{\partial^2 C}{\partial x^2}\, e^{-pt}\, dt. \tag{3.2.9}$$

Furthermore, by integration by parts,

$$\int_0^\infty \frac{\partial C}{\partial t}\, e^{-pt}\, dt = p\overline{C} - C(x,0). \tag{3.2.10}$$

Now taking the Laplace transform of Eq. 3.1.6, Eqs. 3.2.1, 3.2.9 and 3.2.10 yield

$$p\overline{C} = D\,\frac{\partial^2\overline{C}}{\partial x^2} \quad \text{for } x \neq 0. \tag{3.2.11}$$

Thus, Laplace transforms reduce Eq. 3.1.6 to an ordinary, linear differential equation which is readily solved. However, since there is a singularity at $x = 0$, different solutions for the regions $x > 0$ and $x < 0$ must be considered. Solving Eq. 3.2.11,

$$\overline{C} = A\, e^{qx} + B\, e^{-qx} \quad \text{for } x > 0 \tag{3.2.12a}$$

and

$$\overline{C} = E\, e^{qx} + F\, e^{-qx} \quad \text{for } x < 0, \tag{3.2.12b}$$

where

$$q = \sqrt{\frac{p}{D}}\ . \tag{3.2.13}$$

The condition of reflection for C, Eq. 3.2.4, applies also to the transform $\overline{C}$,

$$\overline{C}(-x,p) = \overline{C}(x,p) \tag{3.2.14}$$

as does the natural boundary condition, Eq. 3. 2. 6,

$$\lim_{x \to \pm\infty} \overline{C}(x,p) = 0. \qquad (3.2.15)$$

(Equation 3. 2. 2 does not yield a well-defined relation for $\overline{C}$ because the integration range in Eq. 3. 2. 8 includes the point t = 0, for which $\left.\frac{\partial C}{\partial x}\right|_{x=0}$ is not defined.)

Equation 3. 2. 15 applied to Eq. 3. 2. 12 requires that A = F = 0, and Eq. 3. 2. 14 requires that B = E. Thus, the solution to Eq. 3. 2. 11 for all x is

$$\overline{C} = B\, e^{-q|x|} . \qquad (3.2.16)$$

To evaluate B in the above equation, Eq. 3. 2. 7 must first be integrated over all x. Assuming that the x and t integrations can be interchanged,

$$\begin{aligned}\int_{-\infty}^{\infty} \overline{C}(x,p)\, dx &= \int_{-\infty}^{\infty} dx \int_{0}^{\infty} C(x,t)\, e^{-pt}\, dt \\ &= \int_{0}^{\infty} e^{-pt}\, dt \int_{-\infty}^{\infty} C(x,t)\, dx \\ &= 2\, C_0 \int_{0}^{\infty} e^{-pt}\, dt\end{aligned}$$

by Eq. 3. 2. 5. Performing the integration, the final result is

$$\int_{-\infty}^{\infty} \overline{C}(x,p)\, dx = \frac{2\, C_0}{p} . \qquad (3.2.17)$$

Substituting Eq. 3. 2. 16 into Eq. 3. 2. 17 and solving,

$$\frac{2\, C_0}{p} = \int_{-\infty}^{\infty} B\, e^{-q|x|}\, dx$$

$$= 2B\int_0^{\infty} e^{-qx}dx$$

$$= \frac{2B}{q}\,.$$

Thus,

$$B = \frac{q\,C_0}{p}$$

$$= \frac{C_0}{\sqrt{Dp}}$$

by Eq. 3.2.13. Substituting this value for B into Eq. 3.2.16,

$$\overline{C} = \frac{C_0}{\sqrt{Dp}}\,e^{-\sqrt{\frac{p}{D}}|x|}\,. \qquad (3.2.18)$$

The inverse Laplace transform of this expression yields the final solution,

$$C = \frac{C_0}{\sqrt{\pi Dt}}\,e^{-\frac{x^2}{4Dt}}\,. \qquad (3.2.19)$$

This exponential is the Gauss error curve. In logarithmic form, Eq. 3.2.19 becomes

$$\log_e C = \log_e\left(\frac{C_0}{\sqrt{\pi Dt}}\right) - \frac{x^2}{4Dt}\,. \qquad (3.2.20)$$

Equation 3.2.20 is a linear equation in $\log_e$ C and x^2, and thus D may be obtained from the slope of the graph of $\log_e$ C vs x^2 for constant diffusion time. In actual practice any quantity proportional to C such as specific activity may be used.

3.3 Boundary Conditions Satisfied by Deuteron Bombardment

As discussed in Chapter 2, the radioactive layer was to be produced on the diffusion samples by bombardment with 9-MeV deuterons. This should result in a layer of approximately exponentially decreasing rhenium and tungsten activity. Deuterons of 9-MeV energy degrade to approximately 6 MeV in about 1.7 mils of tungsten. The corresponding cross sections for the $W^{184}(d,p)W^{185}$ reactions at these energies are about 150 mb and 3 mb, respectively. The cross sections for 34-day Re^{184} production range from 20 mb at 9.0 MeV to less than 1 mb at 6 MeV. The latter cross sections are for one rhenium isotope only, and other useful ones which would increase over-all rhenium activity would also be produced. Thus, most of the activity would indeed be on the surface and just slightly below it. The expected concentration profile of the radioactive layer was verified by measurements on an unheated sample (Chapter 6). There it was shown that 90% of both the tungsten and rhenium activity was contained in the first mil of thickness of the diffusion samples.

One mil is a finite thickness, however, and the question arose as to whether the boundary condition of an infinitely thin layer would be satisfactorily fulfilled if the layer was one mil thick. Furthermore, defocusing a cyclotron beam to provide a completely uniform deuteron flux over an entire surface, say 5/8 in. in diameter, and maintaining this flux throughout the irradiation would be extremely difficult to accomplish. The average deuteron energy should remain fairly constant, but the beam pattern over the surface of the sample would vary. Thus, the further question arose as to whether a non-uniform layer would satisfactorily meet the boundary condition requirements.

To answer these questions, Dr. B. Kent Harrison of the Los Alamos Scientific Laboratory staff prepared a mathematical treatment starting with the fundamental diffusion equation. The essential conclusions of his treatment, which is given in detail in Appendix A, will be summarized briefly here.

It was shown that uniformity of the surface distribution of the radioactive layer is not an essential boundary condition requirement. Thus, for example,

the radioactive tracer could be concentrated in a single spot on the end of a diffusion sample, and need not be spread uniformly over the entire end surface. The thickness h of the radioactive layer is critical, however. For h less than $\sqrt{Dt}$, the observed diffusion coefficient will be too large by the approximate fractional error,

$$E = \frac{h^2}{6Dt} . \tag{3.3.1}$$

Thus, if $h = 0.245 \sqrt{Dt}$ the error in the diffusion coefficient will be about 1%.

Although it was not a problem in the present work, the effect on D of having a radioactive layer of variable thickness was also calculated.

Chapter 4

PREPARATION OF DIFFUSION SAMPLES

4.1 Tungsten Crystals

Single-crystal tungsten was obtained from the Linde Co., Division of Union Carbide Corp., East Chicago, Indiana. Their crystals are grown by an arc fusion process operating in an argon atmosphere. The starting material is high purity tungsten powder, and since no container is required in the fusion process, contamination is minimized. Linde Company's technical literature (Bulletins No. F-1397-A and F-1398-A) describe the tungsten crystals as being of high purity, having no porosity, and having crystallographic orientations controlled to within ± 5°. Density measurements by Linde on a tungsten single crystal could not distinguish between the real and theoretical value of 19.259 g/cm^3. The accuracy of their measurements was ± 0.02 g/cm^3. Lineage structure is to be expected in the crystals, but mismatch is specified as being less than 5°. (Lineage is defined here as areas which are misoriented with respect to each other by not more than 5°.) A final report[44] describing the properties of tungsten single crystals has been issued by Linde Company.

The first tungsten crystal (3/4 in. in diameter by 12 in. long) ordered from Linde Company had areas of mismatch greater than 9°, and was therefore returned. The replacement crystal was closer to specifications. Lineage mismatch appeared to be less than 5° over most of the crystal as determined by x-ray analysis of three samples cut from the center and each end of the 12 in.

length. Crystallographic direction of the crystal as ordered (<110> direction parallel to the cylinder axis within ± 5°) was also verified. A spectrochemical analysis on a piece of the crystal was performed in this Laboratory with results presented in Table 4.1. The results of carbon, hydrogen, nitrogen and oxygen analysis are also presented.

Table 4.1

ANALYSIS OF TUNGSTEN SINGLE CRYSTAL

Element	Concentration (ppm)	Element	Concentration (ppm)
Ag	< 3	Nb	<300
Al	< 30	Ni	< 30
B	< 10	Si	< 50
Ba	< 10	Sn	< 10
Be	< 3	Sr	< 30
Ca	< 30	Ta	< 0.1%
Co	< 30	Ti	< 30
Cr	< 30	V	<100
Cu	< 3	Zn	<100
Fe	< 30	Zr	< 30
K	< 30		
Li	< 10		
Mg	< 3	C	130 ± 10
Mn	< 10	H	< 10
Mo	<100	N	70 ± 5
Na	< 30	O	10 ± 1

The surface of the crystal as received was very rough. It was therefore centerless ground to remove all surface irregularities (final diameter 0.63150 in.), and then cut with a cutoff wheel into approximate 1/4-in. lengths. These pieces were mounted in a special jig for grinding the ends parallel to each other with a surface grinder. Because of the sectioning technique used, which will be described in Chapter 6, the diffusion samples had to be precision right-angle cylinders.

It was interesting to note that the tungsten crystals, although more ductile than powder-metallurgy tungsten, were quite notch sensitive, especially if the surface had any cold work. Electropolishing (tungsten as anode) in 10% sodium hydroxide solution at about 0.5 A/sq. in. will remove the cold-worked layers and reduce brittleness. Extended electropolishing brings out the lineage structure. Cleavage on the <100> plane at room temperature can occur. For example, cleavage occurred in one sample while an attempt was being made to inscribe an identification number on it with a Burgess Vibro-graver.

4.2 Surface Preparation

One end of each diffusion sample was highly polished to provide a flat surface for deuteron bombardment. A combination electro-mechanical polishing technique, which will be outlined briefly, was used. The procedure was developed by Group CMF-13, a physical metallurgy group of this Laboratory.

The samples were wet-polished with silicon carbide soft-back paper having successive grit numbers 320, 400 and 600. A final treatment with 4/0 paper using kerosene lubricant prepared the surface for electro-mechanical micropolishing. A polishing wheel covered with No. 1585 Buehler hard silk was charged with Linde A powder which was then saturated with a 10% solution of potassium ferricyanide ($K_3Fe(CN)_6$). Polishing was done with the sample as anode at 0.1 to 0.2 A and 10 V ($\sim$ 0.03 - 0.06 A/sq. in.). Reversing polarity momentarily during polishing was sometimes beneficial. Final polishing was done with Linde B powder on Buehler No. 1590 silk velvet. Average total polishing time per sample was 15 to 20 minutes.

4.3 Preannealing of Diffusion Samples

Prior to the deuteron bombardment, the samples were preannealed in vacuum (~ 10^{-6} mm Hg) for one hour at 2700 ± 25 °C to determine whether or not dimensional changes would occur, and to observe possible subgrainboundary movement. A resistance-heated tungsten tube furnace 2-1/2 in. diameter by 12 in. long was available for the anneal. The samples were suspended in the center of the tube in a previously outgassed basket assembly consisting simply of disks supported by wires which were hung from a rod extending across the top of the tube. The first layer of samples was covered with another disk which in turn held a layer of samples. The top layer was covered with a disk which served as a radiation shield. With this arrangement it was possible to anneal all the samples simultaneously, thus eliminating the variable of experimentally different annealing conditions.

About every 15 minutes the temperature was measured with a Leeds and Northrup optical pyrometer. The pyrometer was calibrated against a standard lamp up to 2000 °C and against a carbon arc with rotating disks up to the upper limit of the pyrometer. These corrections and the correction for the optical-quartz sight glass were applied to the observed temperature obtained by sighting into the side of the furnace through a small sight hole.

There were no measurable dimensional changes in any of the samples. In addition, metallographic examination of three samples before and after the anneal indicated essentially no subgrainboundary movement. Thermal etching did occur, however, revealing the lineage structure in each sample. Fig 4.1 is a metallograph of a thermally etched tungsten single crystal that had been prepared for the crystallographic lineage measurements. This crystal was not given the full polishing treatment described above.

The spectrochemical analysis and analysis for carbon, hydrogen, oxygen and nitrogen (small atoms which may be present in the crystal structure as interstitials) was repeated on a sample after annealing. The results of spectrochemical analysis after annealing were the same as those reported in Table 4.1. If changes occurred in the noninterstitial-atom content, the limits of

Fig. 4.1 Lineage Structure in Single-Crystal Tungsten. Thermal etching occurred after a one-hour vacuum anneal at 2700°C. Magnification ~ 6 X.

measurement were not low enough to detect them. Changes were reported for interstitial atom analysis, although their significance is questionable. Carbon content decreased from 130 ± 10 ppm to 120 ± 10 ppm while hydrogen increased from less than 10 ppm to 20 ± 5 ppm. Oxygen increased from 10 ± 1 ppm to 15 ± 1 ppm and nitrogen decreased from 70 ± 5 ppm to 55 ± 5 ppm. All these analyses were performed by Group CMB-1, the analytical group of this Laboratory.

4.4 Bombardment of Diffusion Samples with Deuterons

The polished ends of 14 diffusion samples were bombarded with 9.00 ± 0.05 MeV deuterons at the Los Alamos variable-energy cyclotron to provide a thin layer of tungsten and rhenium activity. The beam current was maintained between 2 and 3 μA for a total exposure of approximately 1500 μC for each sample. This exposure provided sufficient activity for diffusion experiments but was low enough (after 24-hour W^{187} and several short-lived rhenium isotopes died out) so that radiation was not a particular hazard during sectioning of the diffusion samples.

The target arrangement, diagrammed in Fig. 4.2, was similar to the one described in Chapter 2 for the excitation function study. Samples were held in a copper ring which provided thermal contact with the water-cooled metal holder. Target heating was not a problem, as evidenced by the fact that the target assembly was not warm to the touch immediately after irradiation. With 27 W input energy and 20 °C cooling water, the temperature drop through each sample, assuming no lateral heat loss, was estimated to be less than 1 °C.

Before irradiating the tungsten samples, the deuteron beam pattern had been measured by allowing it to impinge on a target of scotch tape backed up with titanium. A discernable pattern could be produced only with a very low beam current and low total flux. An elliptical pattern with major and minor axes of 1/2 in. and 1/4 in., respectively, precisely centered on the diffusion samples, was finally achieved.

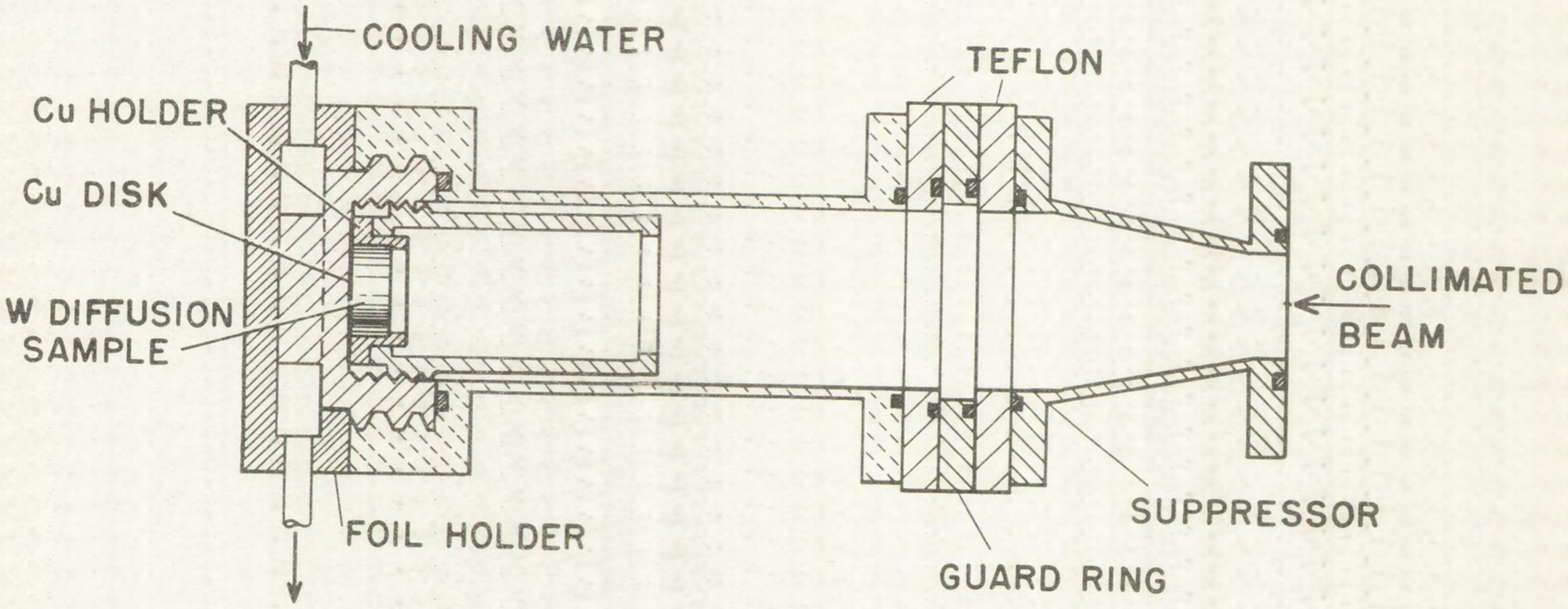

Fig. 4.2 Target Arrangement for Deuteron Bombardment of Diffusion Samples

Chapter 5

DIFFUSION HEATING OF SAMPLES

5.1 Induction Heating Furnace and Vacuum Equipment

An induction heating furnace used in conjunction with an eddy-current concentrator was available for diffusion heating of the samples. Power was supplied by a 25 kW Ther-Monic high frequency generator manufactured by the Induction Heating Corporation. Control was maintained with an Electr-O-Volt controller manufactured by the Minneapolis-Honeywell Regulator Company, Inc.

An eddy-current concentrator is a device used to greatly increase the efficiency of coupling of a crucible to the coils of an induction heater. The concentrators were designed by Mr. Donald E. Hull of this Laboratory who based his design on principles described by Northrop[45] in 1919 and by Babat and Losinsky[46] in 1940. Figure 5.1 is a sketch of a concentrator with crucible as it is used in a vacuum system. Note the shutter arrangement at the top which was necessary to prevent tungsten vapor from depositing on the optical-quartz window.

Among the advantages of a concentrator are (1) prevention of excess heating of the glass portion of the system, since much of the reflected radiation is absorbed by the water-cooled concentrator, (2) the attainment of very high temperatures with fairly large masses of material (for example, a tungsten crucible with samples weighed 189 grams) and (3) the very rapid heating of samples to equilibrium temperature and subsequent rapid cooling when the power is turned off. The latter advantage is particularly important for diffusion

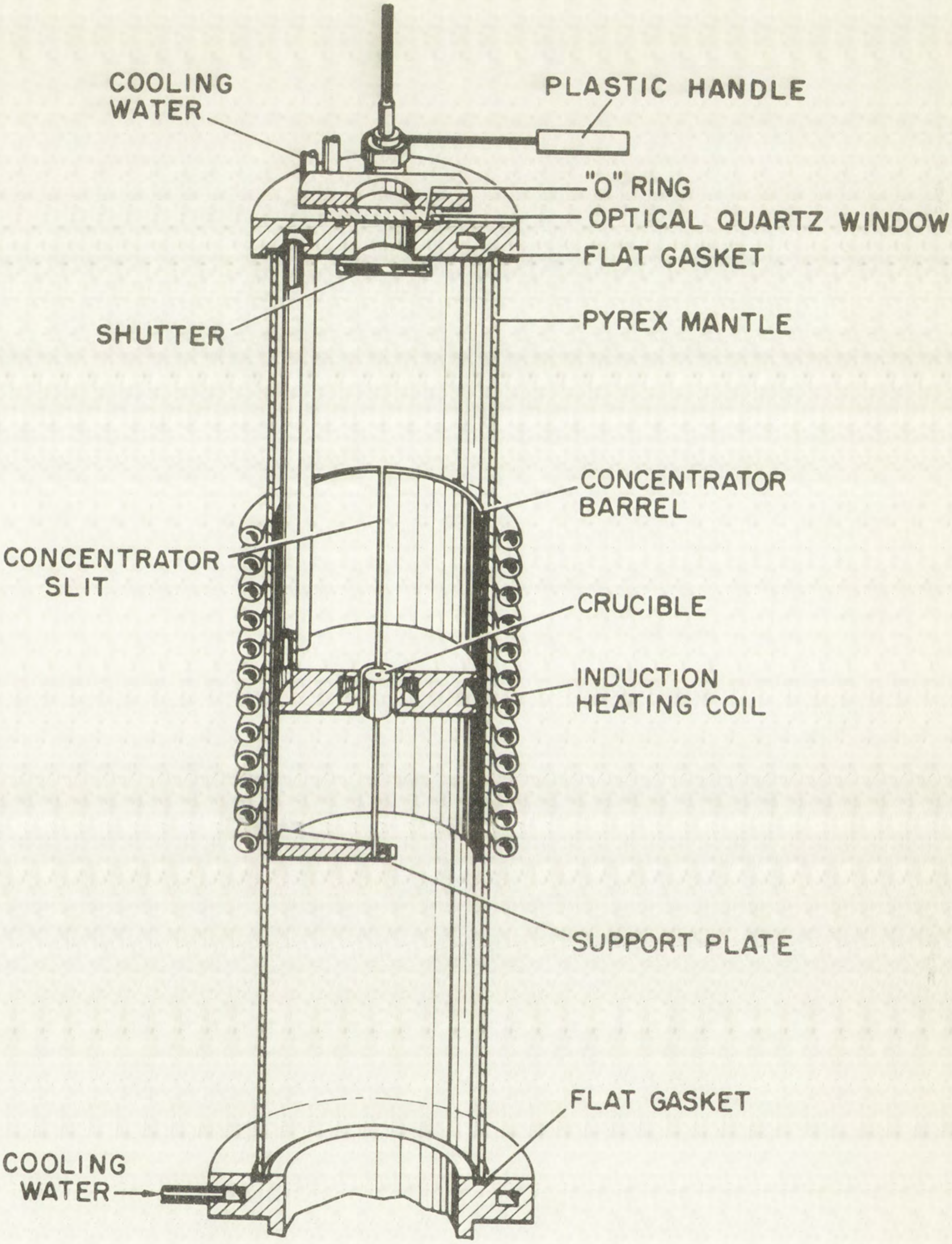

Fig. 5.1 Eddy-Current Concentrator in Vacuum System

work, since it essentially eliminates any correction for diffusion taking place during heating or cooling of the samples. For example, in one diffusion run a loaded crucible was heated from room temperature to 2890 °C in a little less than 2 minutes. When the power was turned off, it cooled from 2890 °C to 1900 °C in 30 seconds and to about 1300 °C in 1-1/2 minutes.

High vacuum in the system was maintained by an MCF-300 oil-diffusion pump manufactured by Consolidated Electrodynamics Corporation. The diffusion pump was backed up by a KC-5 fore pump manufactured by the Kinney Mfg. Division of the New York Air Brake Company. The roughing pump was also a Kinney mechanical pump, Model No. KC-15. Pressure in the system was measured with an NRC ionization gauge. Pressure for all runs was maintained between 5×10^{-5} and 5×10^{-6} mm of Hg. An over-all view of the equipment is presented in Fig. 5. 2

5. 2 Sample Arrangement

For three of the four diffusion runs samples were heated in a tungsten crucible as shown in Fig. 5. 3. The entire assembly, with the exception of the copper support plate, which was outside the heat zone, was made of tungsten. Three rods were used to support the crucible assembly rather than one as shown in Fig. 5. 1. The samples were positioned in the center of the crucible, which had a fairly thick top and bottom, to minimize heat losses through the ends. To minimize loss of radioactive material by evaporation, the samples were placed with their radioactive faces in apposition and were separated by a 1/2-in. diameter ring made from 30-mil tungsten wire. Since the samples were identical, only one from each pair was sectioned and analyzed. Note that in the above arrangement, samples were heated by radiation and conduction from the tungsten crucible, which in turn was heated by induction in the concentrator. The crucible and parts were outgassed prior to heating the diffusion samples.

For the fourth diffusion run it was necessary to heat the samples directly by induction heating in order to achieve a temperature higher than 3000 °C. A concentrator with a 3/4-in. diameter hole was used with the samples

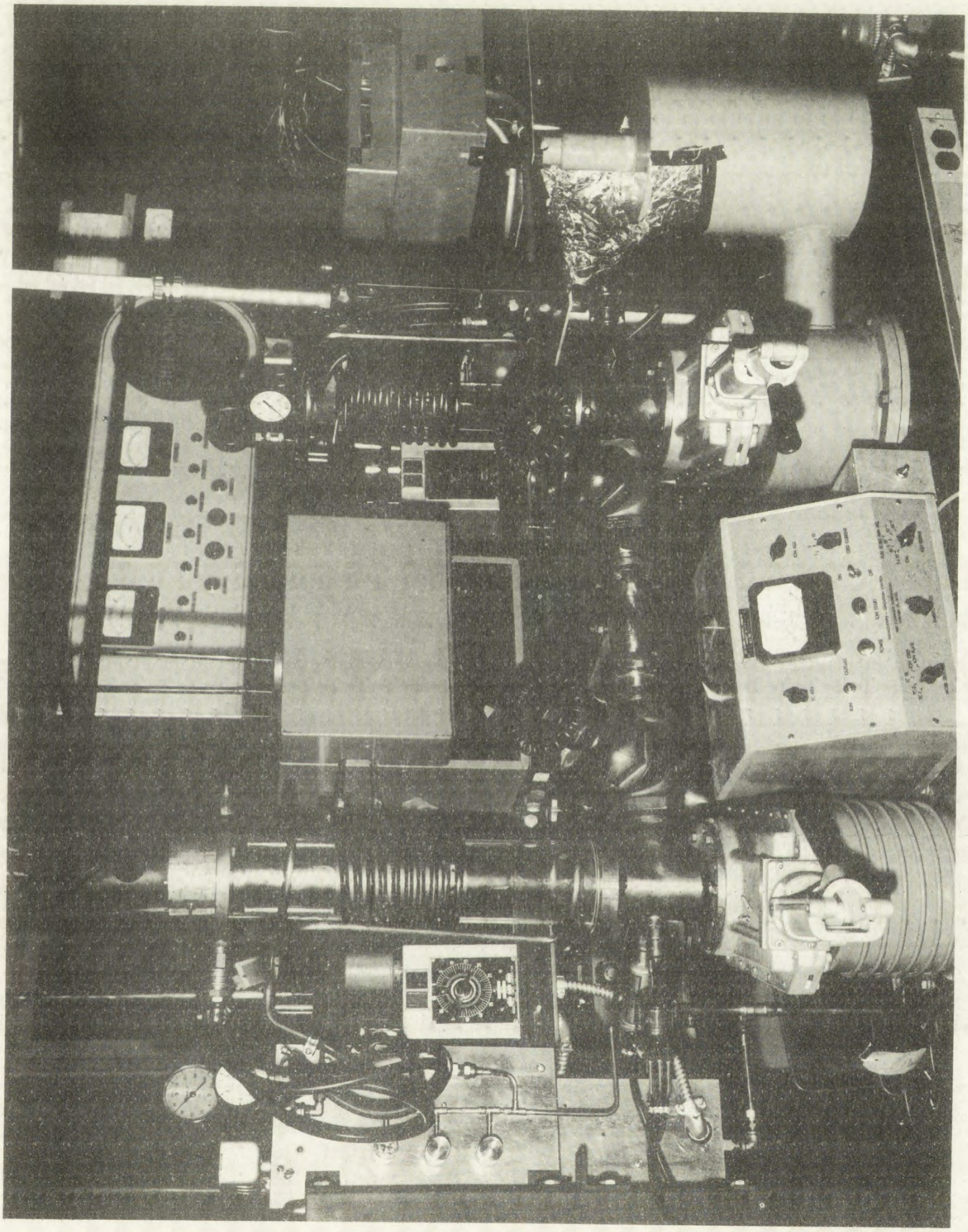

Fig. 5.2 View of Induction-Heating Apparatus

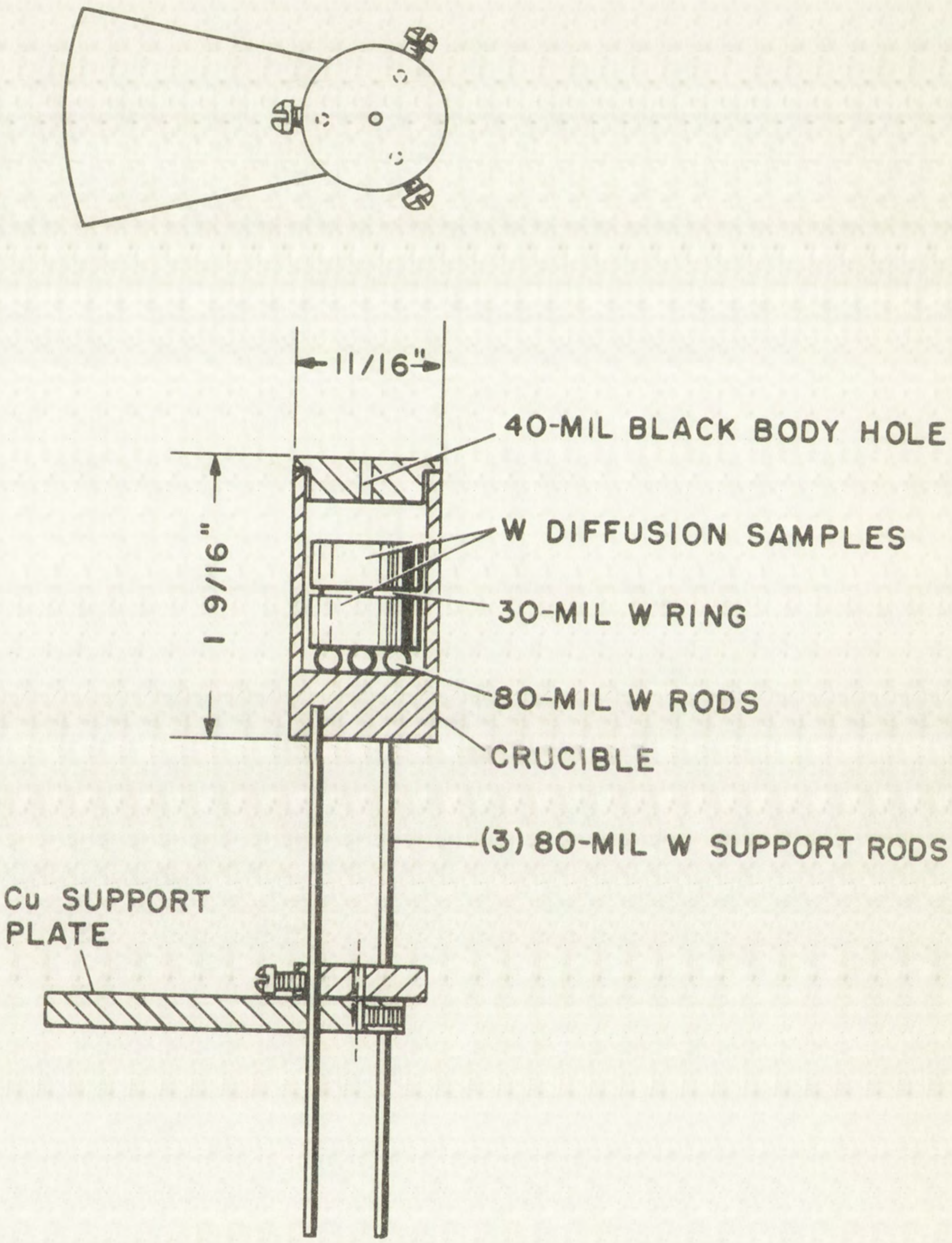

Fig. 5.3 Tungsten Crucible Assembly

mounted as shown in Fig. 5.4. (A concentrator with 1-in. diameter hole was used with the crucible.) Here again the entire assembly was made of tungsten with the exception of the copper support plate. Several radiation shields on each end minimized heat losses. The shields were slightly larger in diameter (0.6750 in. as compared to sample diameter of 0.6315 in.) than the samples. This arrangement was necessary to prevent electrical shorting which occurred if either sample made contact with the concentrator. For reasons not too well understood, shorting did not occur if only the radiation disks were in occasional contact with the concentrator. Sample weight held the assembly together inside the concentrator. As will be shown in Section 5.4, thermal gradients were not significantly different for samples in this assembly than they were for samples inside the crucible.

5.3 Temperature Measurement

Temperatures were measured with a calibrated Pyro disappearing-filament-type optical pyrometer. The temperature readings were corrected for transmissivity of the interposed optical-quartz window-reflecting mirror combination according to the equation

$$a\frac{1}{T_0} - \frac{1}{T_t} = \frac{1}{C} , \tag{5.3.1}$$

where T_0 is the observed temperature of the blackbody in degrees Kelvin, T_t is the "true" temperature in degrees Kelvin and a and C are constants. A derivation of this equation, which is based on Wien's law, is given by Dike.[47] The line of sight from the pyrometer led through a small hole into the chamber containing the samples, and since the chamber was for all practical purposes in radiation equilibrium, a "hohlraum", the light leaving the hole represented blackbody conditions. A calibration curve was prepared by observing the melting points of high purity metals (better than 99% pure). In this technique a small hole is drilled into the specimen, and the melting point is taken as the temperature at which the hole fills with liquid. The actual melting point

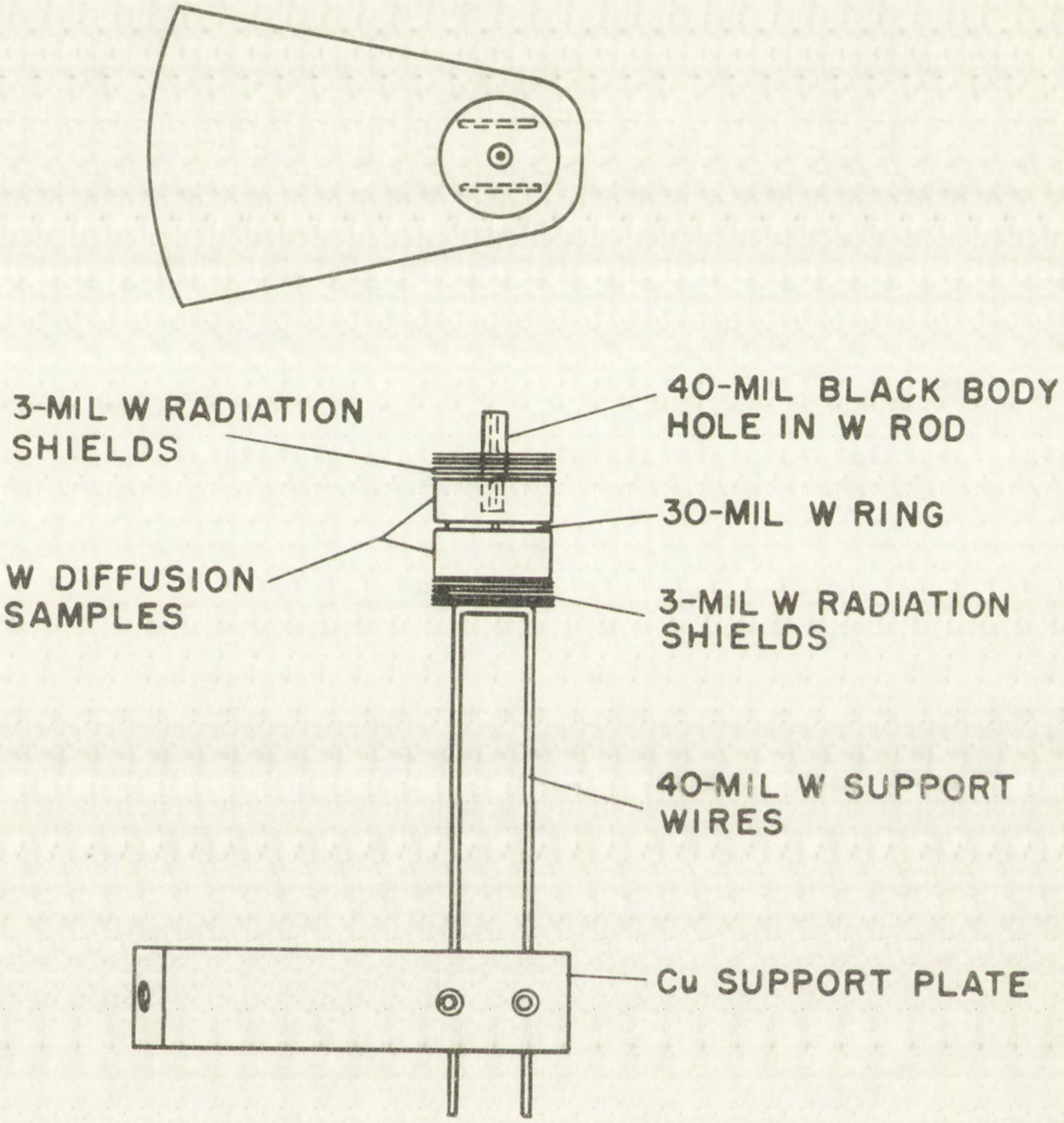

Fig. 5.4 Bare Sample Assembly

measurements were done by T. C. Wallace, Group CMB-3, who made three or four determinations which differed by not more than ± 15° for each high-melting metal. His data and the data for true melting points, which are given in Table 5.1, were programmed on an IBM-7090 for the best least-squares fit to Eq. 5.3.1. This equation, with the values for $a \pm \sigma_1$ and $1/C \pm \sigma_2$ where the σ's are the standard deviations, was used to convert the average of measured temperatures to true temperatures with their standard deviations.

Table 5.1

MELTING POINTS OF METALS USED FOR TEMPERATURE CALIBRATION GRAPH

Metal	Melting Point (°C)	Reference
Ta	2996 ± 25	Malter and Langmuir[48] (1939)
		Klopp, et al.[49] (1959)
		Pemsler[50] (1961)
Mo	2620 ± 20	Worthing[51] (1925)
		Taylor, et al.[52] (1961)
Nb	2468 ± 10	Schofield[53] (1957)
		Pemsler[50] (1961)
Rh	1966 ± 3	Metals Handbook[54]
Pt	1773 ± 1	Metals Handbook[54]
Co	1495 ± 1	Metals Handbook[54]

In the observation of temperatures during diffusion runs, the optical system and equipment was the same as was used by Wallace for the melting point observations, and correspondence between his and the author's reading of the pyrometer was verified. Precision of measurements was within ± 15°, which is better than the accuracy of the known melting points for high-melting metals as indicated in Table 5.1. Temperature measurements were made every 5 to 10 minutes on short runs, increasing to every 30 minutes for the longer runs. Any temperature change noted was corrected by changing the power level.

5.4 Temperature Gradients

Temperature gradients along the diameter and through the lengths of diffusion samples within the crucible (Fig. 5.3) were estimated by measuring temperatures in nonradioactive samples as follows. A lid to the crucible had five sight holes drilled through it instead of one. The four additional holes (0.050-in. diameter were 90° apart on a 7/16-in. diameter circle. Thus, it was possible to read surface temperatures at the center and near the edges of a blank sample. To read temperatures through the length of a top sample, three holes having depths of 1/16 in., 1/8 in. and 3/16 in., respectively, were drilled on a 7/16-in. diameter circle to line up with the holes through the crucible lid. A center hole was drilled completely through the sample. Thus, temperatures at the surface and at various depths through the top sample could be measured. To measure gradients through the bottom sample, another nonradioactive sample (which became the top sample in Fig. 5.3) had five holes drilled completely through it to line up with holes in the crucible lid above and the sample with graded hole depths which now became the bottom sample below. Thus it was possible to measure temperatures at the surface and at various depths within both samples. Temperature differences throughout did not exceed ± 15°.

Temperatures for the sample assembly shown in Fig. 5.4 were measured through three small sight holes which were drilled through the side of the concentrator. By carefully positioning the sample assembly inside the concentrator, it was possible to determine temperatures near the top, center and bottom along the length of the assembly on its outer surface. Here again the differences did not exceed ± 15°. Although the equilibrium internal temperature may have been slightly higher than the surface temperature, it is believed that these limits were still valid throughout the samples.

Chapter 6

SECTIONING OF DIFFUSION-HEATED SAMPLES

6.1 Introduction

A critical step in the measurement of the concentration profiles of the tungsten and rhenium tracers in the diffusion samples was the sectioning of layers for analysis. With the diffusion heating times employed, the useful portions of the concentration profiles were contained in the first 10 to 15 mils depth from the activated face. The experimental problem, then, was one of removing and collecting layers of the order of 0.5 to 1.0 mil thick with an uncertainty no greater than 0.05 mil, and with each new surface as nearly parallel as possible to its predecessor. In addition, it was desirable that the surfaces produced be physically specified so that their reproducibility could be checked.

In diffusion work, layer removal is most frequently accomplished with a lathe or a microtome, neither of which is suitable for sectioning tungsten. Tungsten is too hard for slicing with a microtome, and chipping occurs when lathe sectioning is attempted. Even though single-crystal tungsten has much better machining characteristics than powder-metallurgy tungsten, peripheral chipping occurred when sectioning with a lathe was attempted on a single-crystal cylinder. Removal of material from the lateral rather than end surface of the cylinder did appear to be possible with a sharp cutting tool, although there was still some danger of chipping at the ends.

Other possible methods of layer removal are chemical or electrolytic dissolution, and precision grinding. Electrolytic dissolution was tried with tungsten as anode in 10% sodium hydroxide solution. This method was abandoned, largely because of the problems associated with maintaining a uniform current density over the entire end surface of the cylinder. Chemical dissolution was not attempted because here again it was felt that preferential dissolution would occur. Precision grinding with an available surface grinder was investigated and found to be suitable for sectioning tungsten samples. The following parts of this chapter describe the surface grinder and the technique developed for mounting and sectioning the diffusion-heated samples. Since lateral grinding of the samples was done first, the mounting of samples, necessary for this operation and for layer removal, will be described first.

6. 2 Mounting of Samples

Since the diffusion samples were only 1/4 in. in length, some type of mounting device or technique to hold them securely for lateral grinding and for sectioning was necessary. Although several techniques were tried, including bakelite mountings and special jigs, the simplest and most effective technique was to increase the length of the sample by cementing another piece of metal to it. For this purpose precision right-angle cylinders, 3/4 in. in length and the same diameter as the diffusion samples, were machined out of nickel. Nickel was selected because in solution it is readily separated from tungsten by precipitation with dimethylgloxime. The underlying notion was that if cross contamination of activity from one layer to the next during sectioning was a problem, the nickel piece would be cemented to the radioactive end of the diffusion-heated sample and sectioning would be done in the direction of increasing radioactivity. The final layer would undoubtedly be contaminated with nickel, which would then have to be removed in order to obtain pure tungsten for counting. Cross contamination, however, was not a problem (see Section 6. 10), and therefore the nickel pieces were cemented to the cold end of the diffusion samples.

Two types of adhesive material were tested for cementing the pieces together--phenylsalicylate (Salol) and Eastman 910 Adhesive. Salol, which melts at about 40 °C, is water soluble and therefore quite convenient to use. However, it has insufficient strength for bonding nickel to tungsten in this application. Eastman 910 Adhesive (Eastman Chemical Products, Inc., subsidiary of Eastman Kodak Co., Kingsport, Tennessee) forms an extremely strong bond which is adequate for holding the two pieces together during both lateral and surface grinding. For high-strength bonding, the two surfaces must be very smooth and in intimate contact. Once these conditions are met, only a thin film of the adhesive is required.

The following procedure was used in cementing the pieces together. The two surfaces were prepared by polishing with 600-grit silicon-carbide paper. The samples were then cleaned by ultrasonic vibration in ethanol, and finally dried under a heat lamp. A thin film of Eastman 910 Adhesive was brushed on one of the surfaces. The other piece was pressed in position and held there with about a kilogram of weight. A snug-fitting Teflon ring 3/4 in. long and 1/8 in. thick was used for precisely centering the two pieces. Any excess adhesive was then forced out from between the two surfaces, but since the adhesive does not bond well with Teflon, the Teflon ring was readily removed after about twelve hours drying time.

6.3 Lateral Grinding

To avoid the effects of surface diffusion it is customary[55] in diffusion work to remove from the lateral surface of the diffusion sample a thickness equal to six to eight times the estimated value of $\sqrt{Dt}$. In the present work, this criterion ($8\sqrt{Dt}$) necessitated reducing the diameter of the samples from an original 0.63150 in. to a minimum of 0.5900 in. The diameter was reduced by grinding with a Dumore tool-post grinder mounted on a lathe. The grinding wheel used was a medium-soft, aluminum-oxide wheel with abrasive grain size of 60 (Catalog No. 3860K513E, Norton Company, Worcester, Mass.). There was no problem in holding the sample firmly in the lathe now that it was

1 in. long. The entire length of the specimen was reduced to the final diameter by reversing its position in the lathe and grinding both halves.

Since the original radioactivity on the end of the diffusion samples was essentially inside a circle 1/2 in. in diameter, there was little activity on the lateral surface even after diffusion heating. However, to reduce heating and to control this small amount of radioactivity, a wet brush was held against the sample during grinding. By occasionally dipping the brush in a pan of water, the ground particles were readily collected and the sample was never more than slightly warm to the touch.

6.4 Surface Grinding Machine and Choice of Grinding Wheel

A new Brown and Sharpe No. 618 Micromaster surface grinding machine (Brown and Sharpe Mfg. Co., Providence, R. I.) equipped with a magnetic chuck was used for sectioning the diffusion-heated samples. This machine (2900 rpm spindle speed) has a superior hydraulic longitudinal feed and hydraulic cross feed which results in very smooth table travel. The vertical-feed handwheel has wide-spaced graduations reading to 0.2 mil. For extreme accuracy of vertical adjustment, an auxiliary knob, adjacent to the handwheel, gives a fine vertical feed and is graduated to read to 0.1 mil. Thus, the depth of cut may be accurately advanced in increments of 0.1 mil or less.

The diffusion sample was held securely in a V-block which was placed on the magnetic chuck. Once sectioning had commenced, the sample was not removed from its original position until after the entire sectioning operation was complete, thus insuring that each new surface produced was precisely parallel to the previous one.

The simplest and most effective method for containment of radioactivity during sectioning turned out to be a loose-fitting plastic bag covering the grinding wheel, but exposing the magnetic chuck. The edges of the plastic bag around the magnetic chuck were firmly held in a metal frame which in turn was held by magnetism to the chuck. The bag, which was made of transparent polyethylene so that the grinding could be observed, was sufficiently loose

fitting so as not to interfere with table movement. Figure 6.1 gives an overall view of the surface grinder with plastic bag in place.

The mechanism of material removal with a properly cutting grinding wheel consists of a rupture of particles from the surface by the cutting action of the abrasive. A wheel that smears material or burnishes the surface is not cutting properly. The type of grinding wheel to use depends mainly upon the material being ground and the finish desired. Since there are numerous variants to consider in selecting a grinding wheel,[56] the Norton Co. was asked for their recommendations. Out of three types of grinding wheels recommended by the Norton Co. for grinding tungsten, one was selected (experimentally) as being best for this application. The wheel selected (Norton No. 39C 100J 5VK, 7 in. in diameter by 1/2 in. wide) is medium soft, and has a silicon-carbide abrasive (100 grain size) held together with a glass-type bond. This is a very free-cutting wheel which produces a smooth surface on single-crystal tungsten. With this free-cutting wheel, abrasive particles are removed from the wheel as they cut the tungsten surface, and little, if any, tungsten adheres to the wheel surface. The latter is an important consideration in minimizing cross contamination (see Section 6.10) from one layer to the next.

6.5 Specification of Ground Surface

The ground surfaces were physically specified so that their reproducibility could be measured occasionally. Since surface reproducibility was largely a function of the number and depth of grinding-wheel cuts, physical measurements of the surface indicated how many layers could be removed from a diffusion sample before "truing" the grinding wheel (the grinding wheel was trued dry with a single-point diamond). Two different types of measurement were made with instruments available at Los Alamos. These instruments, which permitted measurements of surface finish and flatness, will be described briefly, together with typical results obtained from measurements on the ground surface of single-crystal tungsten. It should be mentioned that single-crystal tungsten has better grinding characteristics than commercial powder-metallurgy

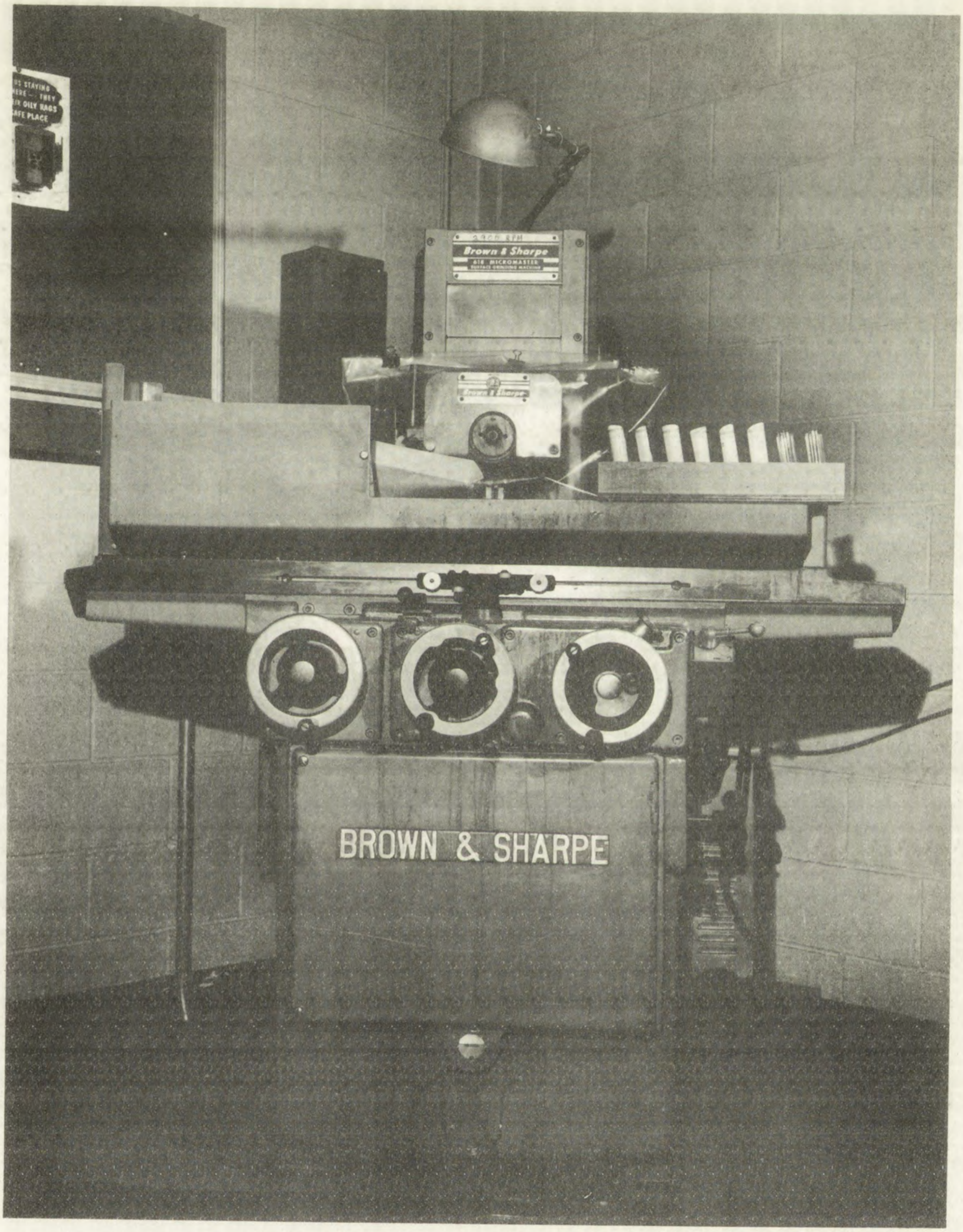

Fig. 6.1 Surface Grinding Machine with Plastic Bag for Containment of Radioactive Particles

tungsten, and only the results of measurements on single-crystal tungsten will be reported.

Surface roughness was measured with a Profilometer, which is a device used for converting the movements of a stylus or tracer tip, mounted on the end of an armature, into an electrical potential or current for operating a recorder or integrating instrument. With the Los Alamos instrument, the stylus is electrically driven back and forth across the surface to be measured, and the surface finish in μin. is read directly on a dial. To understand the meaning of the measurement, consider an imaginary line drawn through a cross-sectional view of the surface profile such that all areas above the line just fill the areas below the line. The number indicated on the Profilometer dial is the arithmetical average which would be obtained if an infinite number of measurements were made from surface peaks to the imaginary line and from surface valleys to this line. The reading obtained is obviously a function of the size of the tracer tip and the horizontal distance over which the measurements are averaged. The Los Alamos instrument has a 60°-cone diamond tracer with a 0.50-mil radius tip. The cutoff value used was 0.030 in. The maximum surface roughness obtained from measurements on several ground surfaces of tungsten single crystal was from 2 to 6 μin. Surface roughness did not exceed these values during sectioning.

As indicated above, the Profilometer cannot measure waviness if the distance between wave crests is greater than 30 mils. One of the best methods to measure waviness or flatness is the interference method which requires the use of an optical flat and a monochromatic light source. An optical flat is placed over the surface to be tested, so that a beam of light falling on the two is reflected partly by the optical flat and partly by the surface under test, which must itself be reasonably reflective. The beam returning from the surface under test lags behind the beam from the topical flat because it has had further to go. If the reflected beams combine in phase, there will be constructive interference and the eye will see a bright area; if the reflected beams combine out of phase, there will be destructive interference and the eye will see a dark area. Thus, the bands produced trace out contour lines, similar to the contour

lines on an ordinary map, the successive steps being half a wave length of the light used.

To make the measurement, the ground tungsten surface was hand rubbed once or twice on a flat top to remove grinding fuzz and enhance light reflection. A fringe pattern was then produced with an optical flat and a monochromatic helium light source. The helium wave length used was 5875.618 Å, and thus, one half wave length corresponds to a depth of about 11.6 μin. From the parallel bands produced, it was determined that the tungsten surface was flat within one band separation or within 11.6 μin.

The above described measurements of surface roughness and flatness indicate a surface reproducibility well within limits required for accurate sectioning of layers as thin as 100 μin. or 0.1 mil.

6.6 Micrometer Measurements and Sample Temperature

Thickness of the removed sections was determined by measurement of the length of the diffusion sample before and after layer removal. A Starrett precision micrometer caliper with scale graduations reading to 0.0001 in. was used for the measurements. All samples were measured without moving them from their original position in the V-block which was held by the magnetic chuck. With the top and bottom of the diffusion sample precisely parallel to each other, and with the measurements being made at the same location on the sample each time, precision of measurement was excellent. For example, ten measurements were made on one sample with the micrometer being removed each time. Ratchet pressure was used and the scale was not observed until the reading was made. All ten readings were the same to the fifth place.

In an actual sectioning procedure, the sample was measured twice, with micrometer ratchet pressure and with removal of the micrometer from the sample prior to the second measurement. The electromagnet was turned off during measurements to permit easy placement of the micrometer, but residual magnetism in the V-block held it firmly in its original position. The bottom of the diffusion sample was a reference plane for all measurements. Accuracy of measurement was estimated to be within ± 0.05 mil.

An experiment was done to correlate the micrometer readings with the actual mass of material removed as determined by mass measurements before and after sectioning. With 19.259 g/cm^3 as the density of single-crystal tungsten, the calculated mass removed checked to within 0.6% of actual mass removed for a penetration distance of 15 mils.

It was determined after a few experiments that heat from the electromagnet gradually raised the temperature of the V-block, and hence the sample, from room temperature to about 35 °C. The linear coefficient of thermal expansion of nickel is large enough (13×10^{-6} in./in. °C) to cause an error in measurement of layer thickness if the original length of the sample was measured prior to the attainment of thermal equilibrium. Therefore, a warm-up period (usually about an hour) prior to sectioning was required for the magnetic chuck and sample to reach thermal equilibrium.

Since dry grinding was employed, it was of interest to measure the sample temperature rise caused by the grinding process. A chromel-alumel thermocouple was placed very near the top surface of the sample through a small hole in the bottom of the sample. An ice bath was used for a reference junction, and millivolts were read with a potentiometer before and immediately after each cut. The temperature variation did not exceed 2 or 3 °C throughout the sectioning of several layers. Linear thermal expansion of the sample during grinding was, therefore, negligible.

6.7 The First Cut and General Procedure for Succeeding Cuts

In sectioning the diffusion samples, it was essential that the removed layers be parallel to each other and to the top radioactive surface. For example, an angle of 1° off parallel in positioning the sample can cause an error of 10% in the diffusion coefficient.[57] In this work, precise parallelism of successive layers was maintained by keeping the sample fixed throughout the entire sectioning process. However, the sample had to be carefully positioned prior to sectioning to insure that the first cut was parallel to the top radioactive surface. Since the samples were precision right-angle cylinders,

not much adjustment was necessary. Usually a small piece of thin shim stock placed under a corner of the V-block was all that was required to level the sample. Measurements of how parallel the top surface was to the magnetic chuck, and hence to the first layer, since the magnetic chuck was first ground with the grinding wheel, were made with a Starrett dial indicator mounted on a Brown and Sharpe permanent magnet base (Fig. 6.2). Scale graduations on the dial indicator were 0.0001 in., and the sample was leveled to within ± 0.0001 in. The maximum amount any sample was out of parallel, therefore, was of the order of 0.017°.

Before sectioning a sample, the grinding wheel was trued with a single-point diamond tip. Thereafter, the wheel was trued after removal of about 5 mils of tungsten. It was determined that the wheel needed truing less often, and surface reproducibility on the sample was better, if several light cuts were made rather than one deep cut. In general 0.3-mil cuts were made with up to three to four passes for each layer.

After a layer had been removed, the grinding wheel and the magnetic chuck were turned off to permit micrometer measurement and decontamination; the latter was done to prevent cross contamination of activity from one layer to the next. When the surface grinder was turned on to remove the next layer, the grinding wheel did not always come back to its original vertical position. Therefore, a preliminary pass was always made before advancing the wheel for the next cut. Because of this variability in the position of the grinding wheel, and also because part of the depth of cut represents a slight reduction in the diameter of the wheel, sectioning layers of exactly equal thickness was difficult. In the present work, with the exception of the concentration profile run, the first few layers were of the order of 1-mil thick, but the later ones were cut thicker, since specific activity decreased as the layers were cut deeper into the sample. Variations in thickness were of no consequence, however, since each layer thickness was carefully measured as described above.

An electrical safety device was installed on the surface grinder to prevent the grinder from operating unless the magnetic chuck was in the "hold" position.

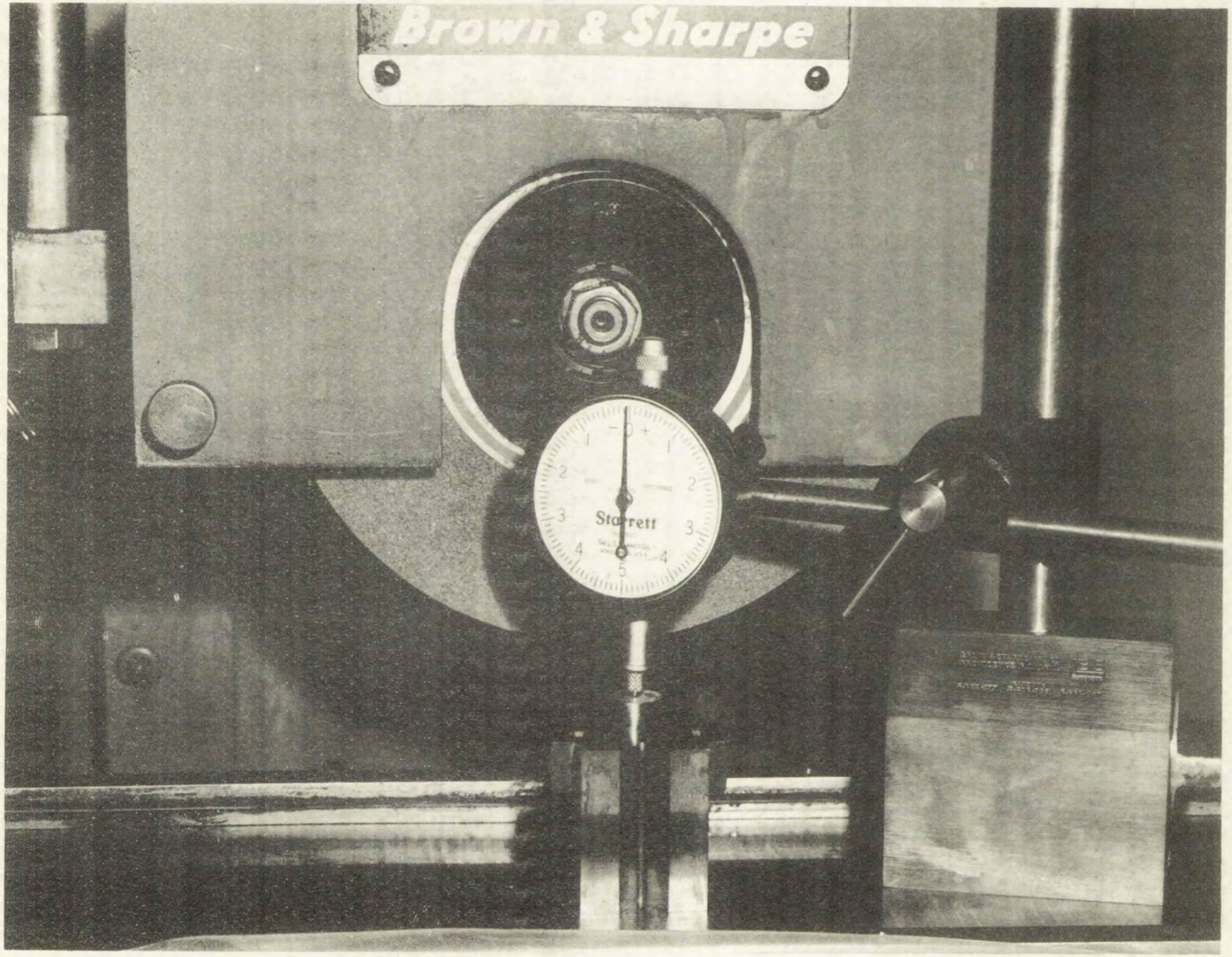

Fig. 6.2 View of Equipment for Positioning a Diffusion Sample Prior to the First Cut

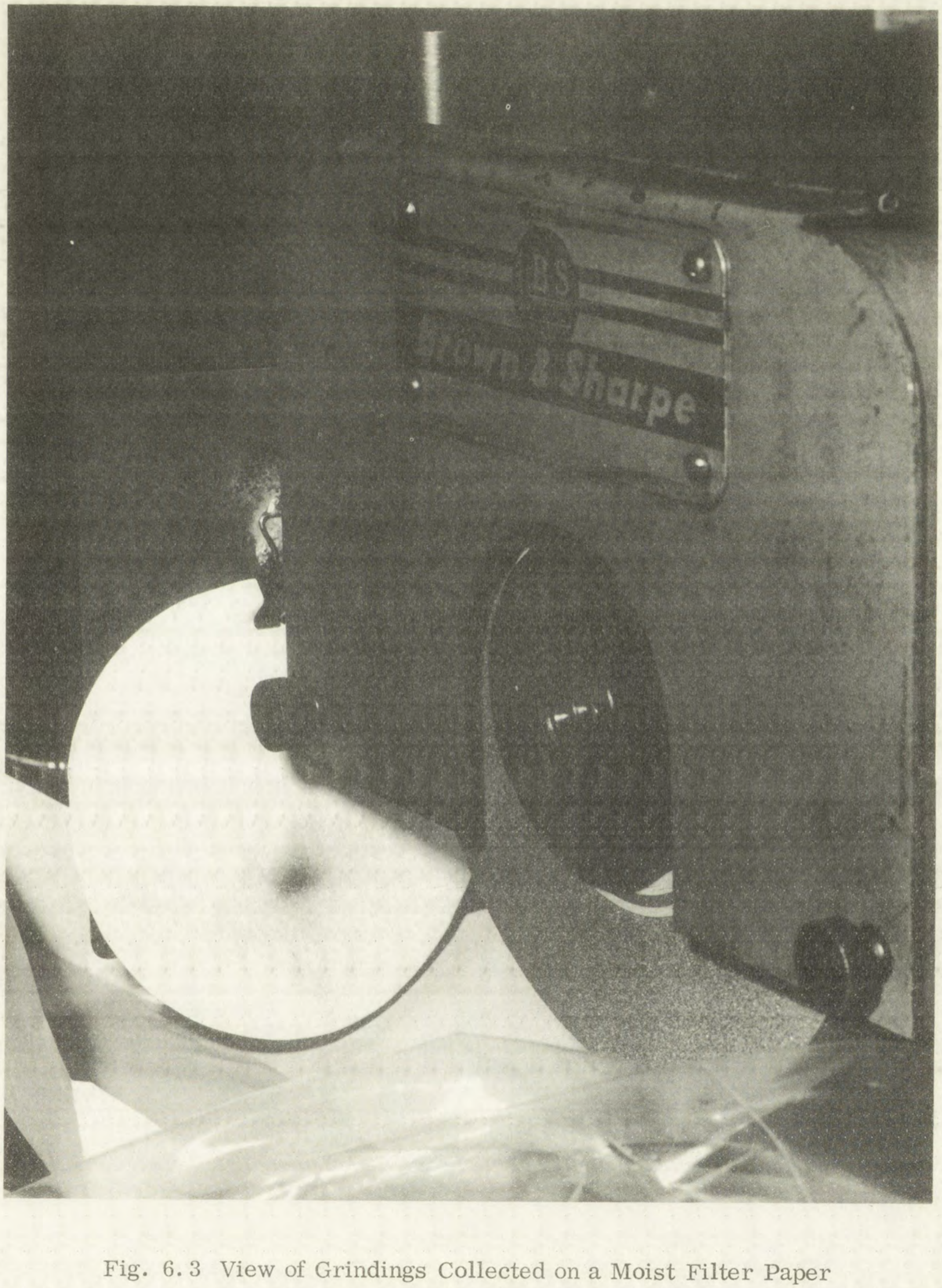

Fig. 6.3 View of Grindings Collected on a Moist Filter Paper

Another interesting point is that with practice one could judge fairly well the amount of tungsten on the collection filter paper simply by visual inspection. This practice was helpful in insuring that there was sufficient tungsten present for analysis. Since as little as 5 mg of tungsten could be analyzed, thin layers of the order 0.1 to 0.2 mil were practical.

Recovery of tungsten from each layer could be improved by about 20% by placing a rectangular tray made of white glazed paper on the magnetic chuck between the wheel and the collecting filter paper (Fig. 6.3). The paper tray was held in place by magnetism through metal paper clips glued to the bottom of it. The particles which collected in the tray were readily removed with a soft camel-hair brush. A separate brush and paper tray were used for collecting each layer.

6.9 Summary of Sectioning Procedure

Each diffusion-heated sample was first mounted, with Eastman 910 Adhesive, on a 3/4-in. nickel cylinder of the same diameter as the sample. Lateral grinding of the nickel-tungsten specimen was next accomplished, as described above, with a tool-post grinder mounted on an ordinary lathe. Layers of tungsten were then removed from the final specimen, which was now a precision right-angle cylinder about 9/16 in. in diameter by 1 in. long. The procedure was as follows.

The grinding wheel was trued, a plastic bag was fitted around it, and double-coated Scotch tape was used to line the inside of the grinding wheel housing. The diffusion sample was placed in the V-block, and was positioned on the magnetic chuck with the aid of a dial indicator to insure that the first layer removed would be parallel to the top radioactive surface. The top of the plastic bag was closed, the magnetic chuck was turned on, and the sample was allowed warmup time (about an hour) to reach thermal equilibrium (~ 35 °C). The plastic bag was then opened, the electromagnet was turned off, and duplicate measurements were made with a precision micrometer using ratchet pressure to establish the reference length of the sample. With the magnet turned on

again, a paper tray was placed in position, and two filter circles were moistened in a beaker of water and clipped to the metal mounting plate. With the plastic bag closed at the top, the grinding wheel was then turned on. The hydraulic-powered reciprocating table, which had been adjusted previously for total length of motion (6 to 8 in.), was also turned on. Vertical feed was then very slowly advanced until the wheel just touched the specimen. The hydraulic cross feed which had also been adjusted previously for slow, smooth motion was turned on. Three passes were then made advancing the fine, vertical-feed knob for a 0.3-mil cut on each pass. The grinding machine was then turned off, the bag opened, and the paper tray removed. Its contents were carefully brushed into a 50-mil lusteroid test tube. The filter paper was then removed, rolled into a roll, and placed in the same test tube. With the magnetic chuck turned off, duplicate length measurements were made with the micrometer to establish the layer thickness.

The steps employed to prevent cross contamination of activity from the first layer to succeeding layers were: 1) the removal of the light burr formed on the edge of the diffusion sample during grinding, by rubbing it with a fine emery stone, and 2) the thorough wiping of the inside of the plastic bag and all exposed parts with moist Kimwipes. After this procedure, steps for removal of the next layer were begun. A new paper tray and filter papers were positioned, the plastic bag was closed, and the grinding wheel and reciprocating table were turned on simultaneously. A preliminary pass was made without advancing the vertical feed, since the grinding wheel did not always return to its original position, after which the rest of the layer removal was the same as described above. A new brush was used for brushing out particles collected in each paper tray. After removal of about 5 mils of tungsten, the grinding wheel was trued with a single-point diamond tip placed next to the sample.

For the sectioning of each new sample, the plastic bag was replaced and the inside of the grinding-wheel housing was relined with double-coated Scotch tape.

The total time required for sectioning a sample, including time for preliminary preparations, was about 6 to 8 hours.

6.11 Concentration Profiles of Tungsten and Rhenium Tracers in the Initial Radioactive Layer

An unheated radioactive diffusion sample was sectioned, and each section was radiochemically analyzed for tungsten and rhenium to determine the distribution of these tracers as a function of depth in the initial radioactive layer. Concentration profile data for both tungsten and rhenium are presented in Table 6.2 and are plotted in Fig. 6.4. The tungsten concentration profile determination was essentially a verification of a portion of the $W^{184}(d,p)W^{185}$ excitation function measurement discussed in Chapter 2. The tungsten activity which should be in each section, as calculated from this excitation function, is also presented in Table 6.2 and is plotted as dotted lines in Fig. 6.4. As may be seen from the data, there is excellent agreement in the two sets of independently determined numbers. Since the rhenium activity in the sample did not result from the decay of a single radioactive isotope, a comparison of the rhenium concentration profile with the excitation function for the $W^{184}(d,2n)Re^{184}$ reaction is meaningless.

TABLE 6.2

EXPERIMENTAL DATA INDICATING CONCENTRATION PROFILES OF TUNGSTEN AND RHENIUM TRACERS IN AN UNHEATED SAMPLE

Thickness of Section (mils)	Cumulative Thickness (mils)	W Activity (c/min/mg)	Re Activity (c/min/mg)	Calculated* W Activity (c/min/mg)
0.50	0.50	89.20	94.22	84.00
0.50	1.00	41.87	29.84	43.60
0.58	1.58	12.47	6.64	14.27
0.77	2.35	2.89	1.17	2.95
0.75	3.10	0.14_3	0.02_2	--

*Calculated from the $W^{184}(d,p)W^{185}$ excitation function

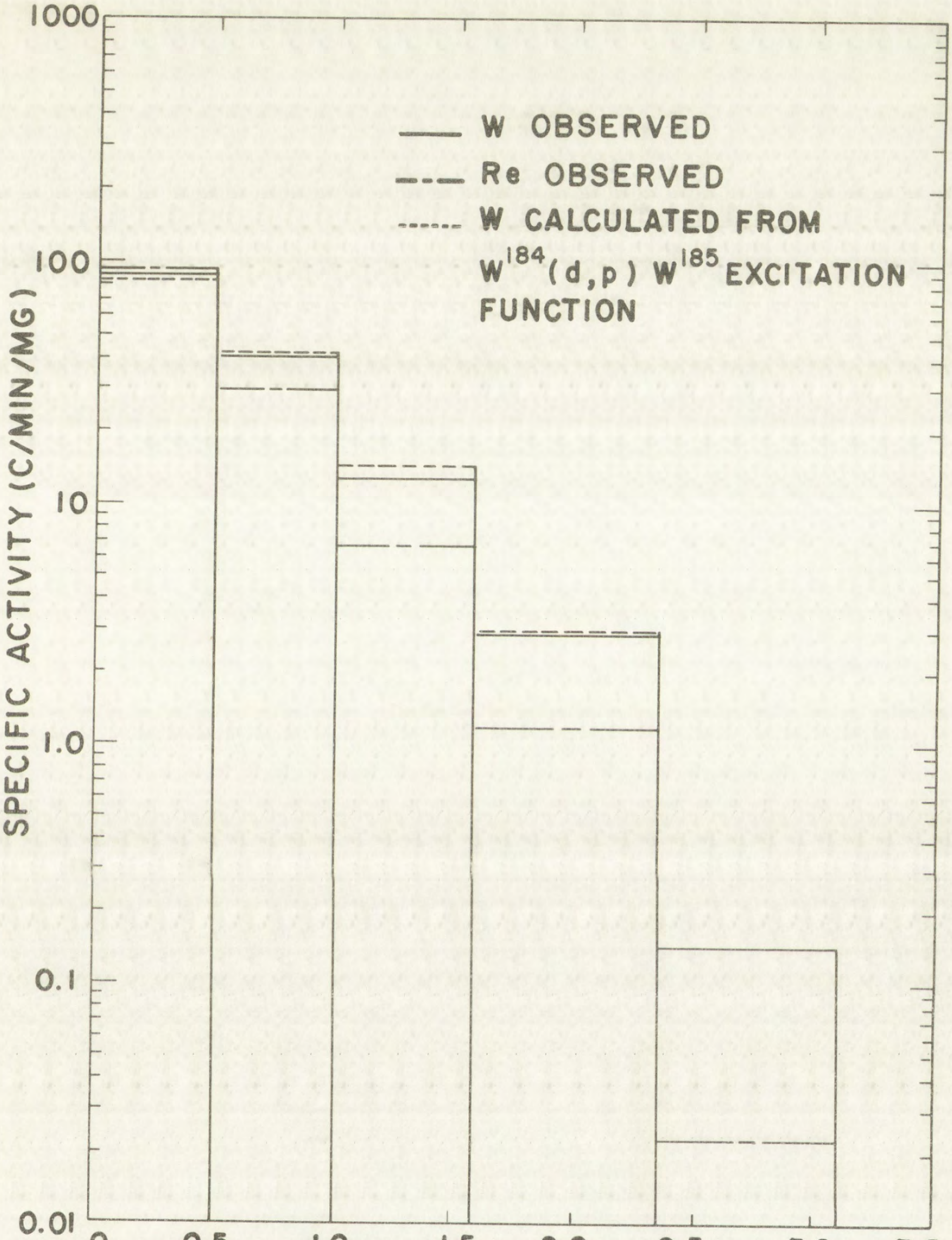

Fig. 6.4 Concentration Profiles of Tungsten and Rhenium Tracers in an Unheated Tungsten Diffusion Sample

From the analysis of the specific activity measurements of each section (Table 6. 2), it may be seen that approximately 87% of the tungsten activity and 93% of the rhenium activity is within the first mil thickness of the sample. This distribution of activity with depth thus closely approximates the boundary condition requirement discussed in Chapter 3.

Chapter 7

RADIOCHEMISTRY

7.1 Quantitative Analysis of Grindings

The sectioning of the diffusion-heated tungsten samples by grinding, as described in Chapter 6, provided a collection of particles composed of radioactive tungsten and rhenium, natural tungsten, silicon carbide, and a silicate material, probably $K_2Si_3O_7 \cdot Al_2Si_3O_6$. The latter two substances are the abrasive and the binding material used to hold the abrasive in the grinding wheel. The objective was to separate from this mixture pure fractions of tungsten and rhenium for counting.

Before development of the radiochemical procedures to be used, it was desirable to know the average weight per cent of each of the components in a collected layer of grindings. A gravimetric procedure, which is detailed in Appendix B, was developed for analysis of tungsten, silicon carbide and silica. The average results of analysis of ten layers are as follows. In a given weight of grindings, which constitute a layer, about 60% by weight is tungsten. The remaining 40% is made up of grinding wheel particles, 34% being silicon carbide abrasive and 6% being the soluble silicate binder. The average silicon content of a layer from the soluble silicate binder is only about 2%.

Of the total tungsten removed from the sample in the grinding off of one layer, 40 to 60% was actually collected for chemical processing. The remainder was in the form of fine dust that came to rest on all surfaces inside the plastic bag that enclosed the grinding operation. This dust was thoroughly

wiped off before the grinding of the next layer was undertaken. In general, the tungsten recovery was better for deeper grinding cuts than for shallower cuts. The theoretical weight of tungsten in a removed layer 0.1-mil thick was of the order of 10 mg.

7.2 Procedures for Radiochemical Analysis

The radiochemical procedures used for tungsten and rhenium were essentially modifications of existing procedures reported in the Nuclear Science Series.[58, 59] Certain modifications were introduced, however, because of the presence of silicon carbide and silicate particles from the grinding wheel.

In general, the method consisted of 1) dissolution of the grindings in a mixture of hydrofluoric and nitric acids followed by filtration to remove undissolved silicon carbide, 2) addition of rhenium carrier which was subsequently separated by precipitation as rhenium sulfide (Re_2S_7), 3) purification and conversion of rhenium to the final weighing form of tetraphenylarsonium perrhenate ($(C_6H_5)_4AsReO_4$), and 4) purification and conversion of tungsten to its final weighing form, the tungsten derivative of 8-hydroxyquinoline ($WO_2(C_9H_6ON)_2$). The yields for tungsten and rhenium were approximately 50% and 88%, respectively.

For diffusion work, the specific activity of each layer, or any quantity proportional to the specific activity, may be used in determining the penetration depth of the diffusing substance and hence its diffusion coefficient. The number of counts per minute per milligram of the tungsten derivative of 8-hydroxyquinoline was used as a measure of tungsten diffusion in the diffusion sample. A number proportional to the specific activity of rhenium in each layer was less obvious to determine, since, of course, there was no rhenium carrier present in the diffusion samples.

For the first diffusion run (2666 °C), the counts per minute per milligram of tetraphenylarsonium perrhenate were divided by the thickness of the removed layer. This technique was not satisfactory, however, because of the variation in the percentage of tungsten collected in each layer. Moreover, the radiochemical yield of tungsten was not sufficiently constant to provide a reliable number. Accordingly, for all the remaining runs, a tungsten analysis was

performed on each sample of dissolved grindings, and the rhenium data were corrected for tungsten recovery. Group CMB-1 performed the tungsten analyses by a spectrophotometric method.[60]

7.2.1 Dissolution of Grindings and Separation of Tungsten and Rhenium Fractions

The collected grindings from each layer were treated as follows. Grindings brushed from the paper tray (Chapter 6) were already in the bottom of a 50-ml lusteroid test tube. The moist filter paper roll with collected radioactive particles, also in the test tube, was allowed to dry. The particles were then brushed from the dry paper into the lusteroid tube with a stiff brush. Acid brushes worked very well, and a new one was used for each sample. Brushing the tungsten off the filter paper eliminated the need for dissolving the paper. The detailed chemical procedure established, applicable for as little as 5 mg of tungsten, is as follows. In this and subsequent procedures analytical, reagent-grade chemicals and distilled water were used throughout.

The grindings in a lusteroid centrifuge tube were dissolved in 0.5 ml of 48% hydrofluoric acid and one drop of 1:1 nitric acid. The finely divided tungsten dissolved vigorously as did the soluble silicate binder from the grinding wheel; silicon carbide abrasive from the grinding wheel did not dissolve. Silicon from the soluble silicate was strongly complexed as fluosilicic acid (H_2SiF_6), and did not interfere in subsequent chemistry. This was verified by negative spot tests (ammonium molybdate and benzidine) for silicic acid,[61] sensitive to 0.1 μ-gram, on samples of rhenium sulfide and tungsten sulfide. The dissolution reaction was tested for completeness by the addition of one drop of 1:2 nitric acid. It was necessary to keep the nitric acid content to a minimum to prevent oxidation of hydrogen sulfide gas which was later added. After dissolution, 10 to 15 ml of 1:1 hydrochloric acid was added, and the solution was filtered through a 5.5 cm Whatman No. 41h filter circle into a 25-ml volumetric flask. Filtration was superior to centrifugation because of the presence of "floaters". The flask was filled up to the mark with 1:1 hydrochloric acid, and, after equilibrium was established, 5 ml of the solution was pipetted out for spectrophotometric tungsten analysis. The remaining 20 ml was transferred to a 50-ml lusteroid

centrifuge tube. The amount of time the cold solution was in contact with the glass volumetric flask was held to a minimum, not more than 10 or 15 minutes, to minimize reaction of the glass with hydrofluoric acid. Two ml of rhenium carrier (the description of the rhenium carrier preparation is given in Section 7.2.3) was added, and the solution was warmed for 10-15 minutes to promote exchange. Care was taken to avoid excessive heating of the lusteroid tubes, which are rather heat sensitive. The solution was then cooled, and hydrogen sulfide gas was bubbled in to precipitate rhenium sulfide (Re_2S_7). The tungsten remained in solution as a fluoride complex (WF_6). Two or three drops of 1% aqueous Aerosol solution was added after which the mixture was centrifuged. The supernatant liquid containing the tungsten fraction was transferred to a 50-ml lusteroid centrifuge tube, and the rhenium fraction was set aside for further analysis as described in Section 7.2.3.

7.2.2 Tungsten Chemistry

Before continuing the procedure for analysis of the tungsten supernatant obtained above, a description of the preparation and standardization of the tungsten carrier solution will be given. The carrier solution was necessary, since one comparator sample (20 mg of inactive tungsten and 10 mg of inactive rhenium) was carried long with each set of four radioactive samples. In addition, it was of interest to determine a conversion factor (mg of tungsten derivative of 8-hydroxyquinoline ($WO_2(C_9H_6ON)_2$ per mg of tungsten in the standardized carrier solution) to compare with the theoretical value of 0.3646.

The carrier solution of tungsten (VI), 10 mg W/ml, was prepared from reagent-grade sodium tungstate ($Na_2WO_4 \cdot 2H_2O$) and distilled water. This solution was standardized using the procedure given in Appendix B. Since the Appendix B procedure requires the presence of salts, 50 ml of a 20% ammonium chloride solution was added for analysis of about 100 mg of tungsten.

In determining the mg of tungsten derivative of 8-hydroxyquinoline (oxine) obtained per mg of tungsten in the carrier solution, the procedure to be described below was used (commencing with the addition of the buffer solution) with the exception that beakers rather than centrifuge tubes were used and the

precipitate was filtered into a tared 60-ml sintered glass crucible of medium porosity for weighing. In a series of six determinations which varied by less than 1%, 100 mg of tungsten gave 273.7 mg of oxine precipitate for a conversion factor of 0.3654 mg of W/mg of oxine precipitate. This value is within 0.2% of the theoretical conversion factor.

Now, continuing with the analysis of the tungsten fraction obtained as described above, the detailed procedure established is as follows. Approximately 0.4 g of solid boric acid was added to the tungsten solution to complex hydrofluoric acid, after which tungsten sulfide (WS_3) precipitated. Any silicon present remained in solution as fluosilicic acid. The solution was heated at 60 to 70 °C for 10 to 15 minutes to aid in the dissolution of the boric acid and in the coagulation of the tungsten sulfide precipitate. Two or three drops of 1% Aerosol solution was added, after which the mixture was centrifuged, and the supernatant was discarded. (If the amount of tungsten present was marginal for analysis, cooling of the mixture in an ice bath prior to centrifugation helped increase the yield of tungsten sulfide, due to its decreased solubility at low temperatures.) The tungsten sulfide was washed once or twice with ~ 5 ml of 1:1 hydrochloric acid and was then dissolved in a minimum amount of conc. ammonium hydroxide and 1 drop of 30% hydrogen peroxide. Ten ml of water was added, and the mixture was centrifuged to remove undissolved boric acid. An aliquot of the supernatant corresponding to a maximum of 20 mg of tungsten was transferred to a 40-ml conical-tip glass centrifuge tube, after which the solution was scavenged once or twice with ~ 1 mg of ferric ion. (The aqueous ferric ion solution, 10 mg Fe/ml, was prepared from ferric chloride crystals ($FeCl_3 \cdot 6H_2O$) and distilled water. Five to 10 ml of conc. nitric acid was added, after which the solution was digested on a steam bath for 10 to 15 minutes to precipitate yellow tungstic oxide ($WO_3 \cdot xH_2O$). The mixture was centrifuged and the supernatant was discarded. The tungstic oxide was dissolved in 6 drops of conc. ammonium hydroxide, 10 ml of water was added, and 6 drops of glacial acetic acid was added. Next, 10 ml of a sodium acetate-acetic acid buffer solution (3.6 M $NaC_2H_3O_2$ and 1.0 M $HC_2H_3O_2$) was added, and the solution was heated to ~ 90 °C in a steam bath. (The tungsten derivative of oxine is best precipitated in the pH

range of 5.0 to 5.7. The pH of the above solution was ~ 5.4.) One ml of 5% oxine reagent (prepared by dissolving finely divided crystals of oxine in 2.0 M acetic acid) was added slowly and with vigorous stirring to the hot solution, which was then digested for 10 to 15 minutes to aid in the coagulation of the precipitate. The mixture was allowed to stand for 10 to 15 minutes after which it was filtered through a tared, 1-in. diameter Whatman No. 42 filter paper using a ground-off Hirsh funnel and a filter chimney. The precipitate was washed three times with 10-ml portions of ice water, and once with a 5-ml portion of ethanol. The sample was dried in a drying oven at 115 °C for 15 minutes, and then was allowed to cool for 20 minutes in the balance room, after which it was weighed. Finally, the sample was mounted with double-sided Scotch tape on a dural plate (2-1/2 in. x 3-1/2 in. x 1/16 in. thick), and was covered with a 0.5 mil thick Mylar film.

7.2.3 Rhenium Chemistry

The rhenium (VII) carrier solution used in this procedure and in the procedure given in Section 7.2.1 was prepared from reagent-grade potassium perrhenate ($KReO_4$) crystals obtained from A. D. Mackay, Inc., New York. Because of the low solubility of the salt, the carrier concentration was made up to 5 mg Re/ml instead of the usual 10 mg/ml.

The carrier solution was standardized according to the procedure to be given below (commencing with the addition of the solid sodium chloride), with the exception that beakers were used instead of centrifuge tubes, and the final precipitate was collected in tared sintered glass crucibles of medium porosity. Three analyses of approximately 100 mg of Re (20 ml of carrier solution) differed by only 0.3% and were within 0.2% of the stoichiometric amount of $KReO_4$ weighed out.

The detailed procedure established for the rhenium fraction obtained as described in Section 7.2.1 is as follows. The rhenium sulfide precipitate was washed once or twice with ~ 5 ml of 1:1 hydrochloric acid, after which it was dissolved in 8 to 10 ml of 1.0 M sodium hydroxide and 2 to 3 drops of 30% hydrogen peroxide. The solution was transferred to a 40-ml conical-tip glass centrifuge tube and heated at ~ 90 °C until it became clear. Fifteen to 20 ml of water

was added, after which the solution was scavenged once or twice with ~ 1 mg ferric ion. From 0.4 to 0.5 g of solid sodium chloride was added, after which the solution was reheated to 90 °C on the steam bath. Ten ml of an aqueous 1% solution of tetraphenylarsonium chloride, $(C_6H_5)_4AsCl$, was added slowly and with stirring to the hot solution to precipitate tetraphenylarsonium perrhenate, $(C_6H_5)_4AsReO_4$. The mixture was digested for 30 minutes at 90 °C on the steam bath to aid in the coagulation of the precipitate. After cooling, the mixture was filtered through a tared 1-in. diameter Whatman No. 42 filter circle using a ground-off Hirsh funnel and a filter chimney. The precipitate was washed three times with 10-ml portions of ice water and once with a 5-ml portion of ethanol. The sample was dried for 15 to 20 minutes at 115 °C, and then was allowed to cool for 20 minutes in the balance room, after which it was weighed. Finally, the sample was mounted with double-sided Scotch tape on a dural plate, and was covered with Mylar film.

7.3 Beta Counting Equipment and Procedure

The activity counted in the mounted samples of the tungsten derivative of 8-hydroxyquinoline was 75-day W^{185}, which decays by emission of 0.43-MeV beta particles. The 24-hr W^{187} had essentially died out by the time the samples were counted.

The samples were counted on the first shelf of a low background, propane-flow, proportional counter operating at atmospheric pressure at about 4200 volts. Electronic components were a Los Alamos Model PA-6 pulse amplifier and a Los Alamos Model SC-3C binary scaler. The low background (~ 1.6 c/m) was achieved by heavy shielding and by a Los Alamos Model SAC-1 anticoincidence counter actuated by a large scintillator located inside the shielding, above the proportional counter.

Each of the samples was counted twice for 60 or 120 minutes, depending upon its strength. Sample count rates were corrected for self-absorption, scattering, etc., with the counting efficiency curve previously mentioned (Fig. 2.2), and for decay time when necessary. The count rates for each sample were recorded in counts per minute per milligram.

7.4 Gamma Counting Equipment and Procedure

The activities counted in the mounted samples of tetraphenylarsonium perrhenate were principally the 34-day isomer of Re^{184} and 68-day Re^{183}, each of which decays by electron capture followed by emission of γ-rays. Examination of the γ-ray spectra at the time the rhenium samples were to be counted indicated that better counting data could be obtained by measuring the photopeak of the characteristic tungsten K x-ray rather than any of the relatively less intense γ photopeaks at higher energies. Figure 7.1 is a plot of the x-ray portion of the Re^{183}-Re^{184} scintillation spectrum of a typical sample. The counts in channels 19 through 43, encompassing the K x-ray peak, were totaled to obtain the rhenium count. The first small peak on the left of the tungsten x-ray is an iodine escape peak which originated from the sodium iodide crystal used in counting the samples. The two peaks to the right of the x-ray represent other γ-rays from Re^{183}-Re^{184}.

Each of the samples was counted from three to five times, allowing a fifty minute counting period, on an automatic γ-scintillation spectrometer used in conjunction with a modified RIDL Model 34-20 amplifier and 200-channel analyzer. The system recorded the analyzer output on punched tape, which was subsequently decoded to provide the data in tabular form.

One of the most active rhenium samples was used as a comparator sample, and was counted with each series of samples counted on the automatic γ-counter. All the samples were then corrected for decay according to the decay rate observed on the comparator sample. Corrections were also made for chemical yields.

To obtain a number proportional to the specific activity of rhenium in each layer ground off, the counts per minute of rhenium obtained for each sample were divided by the milligrams of tungsten in the solution to which the rhenium carrier was added, prior to radiochemical separation.

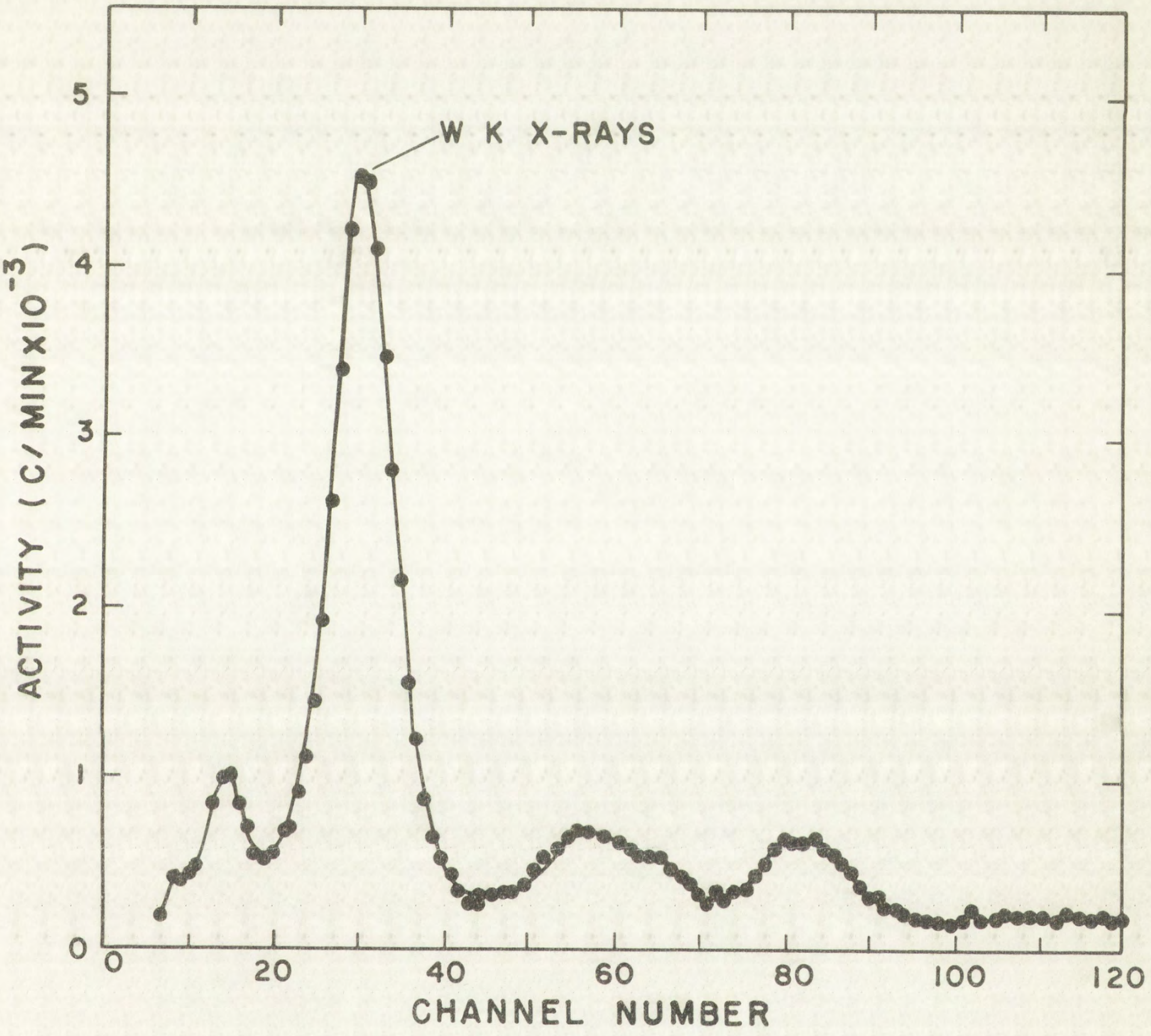

Fig. 7.1 X-Ray Portion of the Re^{183}-Re^{184} Scintillation Spectrum

Chapter 8

EXPERIMENTAL DATA

The subject matter of this chapter and the two which follow it represents the essential core of this research: the measurement of the tungsten and rhenium tracer distribution in the heated diffusion samples, the evaluation and organization of all sources of experimental error, and the analysis of the final results in terms of the frequency factor and enthalpy of activation for each of the two diffusion systems.

The tungsten and rhenium tracer concentrations were measured as a function of penetration depth for each of four samples. The samples had been heated at 2666, 2759, 2889, and 3228°C. The tracer distribution data for the four runs are presented in Tables 8. 1 through 8. 4.

In general, the errors listed in the tables are expressed as standard deviations. They include, in addition to counting errors, errors from cross contamination, from chemical processing, and from uncertainties in the β-counting-efficiency correction. The raw counting data have been corrected as described in Section 7. 3.

The penetration distances have been corrected for linear thermal expansion of the tungsten samples, i. e. , they represent the actual distances in the samples at high temperature, when the diffusion was taking place. Details of the corrections are given in Chapter 9.

For a given diffusion run with a heating time, t, it will be recalled that the concentration-penetration depth relation is represented by the expression

TABLE 8.1

EXPERIMENTAL DATA FOR DIFFUSION AT 2666 °C

Temperature - 2666 ± 46 °C
Average pressure - 7×10^{-6} mm Hg
Effective diffusion time - 2 hrs 59 min (1.074×10^4 sec)

Section No.	Thickness of Section (mils)	x^a (cm x 10^3)	x^2 (cm^2 x 10^6)	W Activity (c/min/mg)	Re Activity (c/min/mg W)
1	0.75	0.97_4	0.94_8	119.35 ± 2.82[b]	76.47 ± 0.78[c]
2	0.65	2.79	7.78	50.04 ± 1.52	28.59 ± 0.30
3	0.70	4.54	20.61	22.08 ± 0.67	15.21 ± 0.18
4	0.50	6.10	37.21	8.10 ± 0.25	4.59 ± 0.06
5	0.70	7.65	58.52	1.78 ± 0.07	1.39 ± 0.06

From least-squares analysis: $D(W) = (3.31 \pm 0.23) \times 10^{-10}$ cm^2/sec

$D(Re) = (3.35 \pm 0.45) \times 10^{-10}$ cm^2/sec

Corrected:[d] $D(W) = (2.00 \pm 0.13) \times 10^{-10}$ cm^2/sec

$D(Re) = (2.03 \pm 0.27) \times 10^{-10}$ cm^2/sec

[a] x, which is the distance from the original interface to the midpoint of the section, has been corrected for linear thermal expansion.

[b] Total σ includes, in addition to counting statistics: σ (cross contamination) = 0.6%, σ (chemical processing) = 1.2%, σ (β-counting-efficiency correction) = 2.0%.

[c] Total σ includes, in addition to counting statistics: σ (cross contamination) = 0.6%, σ (chemical processing) = 0.7%.

[d] Corrections were 1) 36% for initial thickness of radioactive layer (Eq. 3.3.1), and 2) 3.5% for sample misalignment and finite thickness of sections, for a total reduction of 39.5% in the observed D values.

TABLE 8.2

EXPERIMENTAL DATA FOR DIFFUSION AT 2759 °C

Temperature - 2759 ± 47 °C
Average pressure - 9×10^{-6} mm Hg
Effective diffusion time - 12 hrs 13 min (4.398×10^4 sec)

Section No.	Thickness of Section (mils)	x[a] (cm x 10^3)	x^2 (cm^2 x 10^4)	W Activity (c/min/mg)	Re Activity (c/min/mg W)
1	1.05	0.16_9	0.028	39.12 ± 0.92[b]	19.81 ± 0.38[c]
2	1.10	0.42	0.173	29.98 ± 0.73	16.99 ± 0.43
3	1.05	0.70	0.483	19.00 ± 0.50	12.48 ± 0.33
4	1.05	0.97	0.943	10.67 ± 0.31	7.40 ± 0.51
5	1.22	1.26	1.600	5.37 ± 0.17	4.44 ± 0.61
6	1.13	1.57	2.471	1.98 ± 0.07	1.70 ± 0.39
7	1.15	1.87	3.486	0.58_5 ± 0.03	0.71 ± 0.40

From least-squares analysis: $D(W) = (4.74 \pm 0.14) \times 10^{-10}$ cm^2/sec
$D(Re) = (5.60 \pm 0.12) \times 10^{-10}$ cm^2/sec

Corrected:[d] $D(W) = (4.41 \pm 0.13) \times 10^{-10}$ cm^2/sec
$D(Re) = (5.30 \pm 0.11) \times 10^{-10}$ cm^2/sec

a. x, which is the distance from the original interface to the midpoint of the section, has been corrected for linear thermal expansion.

b. Total σ includes, in addition to counting statistics: σ (cross contamination) = 0.6%, σ (chemical processing) = 0.7%, σ (β-counting-efficiency correction = 2.0%.

c. Total σ includes, in addition to counting statistics: σ (cross contamination) = 0.6%, σ (Re chemical processing) = 0.7%, σ (W chemical processing) = 1.5 - 2.5%.

d. Corrections were 1) 5.2% for initial thickness of radioactive layer (Eq. 3.3.1), and 2) 1.61% for sample misalignment and finite thickness of sections, for a total reduction of 6.8% in the observed D values.

TABLE 8.3

EXPERIMENTAL DATA FOR DIFFUSION AT 2889 °C

Temperature - 2889 ± 51 °C

Average pressure - 2×10^{-5} mm Hg

Effective diffusion time - 6 hrs (2.16×10^{4} sec)

Section No.	Thickness of Section (mils)	x[a] (cm x 10^3)	x^2 (cm^2 x 10^4)	W Activity (c/min/mg)	Re Activity (c/min/mg W)
1	0.85	1.12	0.013	41.95 ± 0.98[b]	21.52 0.46[c]
2	2.40	5.35	0.286	34.25 ± 0.84	17.80 ± 0.44
3	1.15	9.98	0.996	19.75 ± 0.52	12.39 ± 0.22
4	1.10	12.90	1.66	10.31 ± 0.28	6.99 ± 0.38
5	0.82	15.40	2.37	4.92 ± 0.17	4.30 ± 0.11
6	1.33	18.21	3.32	2.28 ± 0.12	2.22 ± 0.04
7	1.07	21.34	4.55	0.81 ± 0.04	0.76 ± 0.10

From least-squares analysis: $D(W) = (1.31 \pm 0.03) \times 10^{-9}$ cm^2/sec

$D(Re) = (1.66 \pm 0.04) \times 10^{-9}$ cm^2/sec

Corrected:[d] $D(W) = (1.24 \pm 0.03) \times 10^{-9}$ cm^2/sec

$D(Re) = (1.55 \pm 0.04) \times 10^{-9}$ cm^2/sec

a. x, which is the distance from the original interface to the midpoint of the section, has been corrected for linear thermal expansion.

b. Total σ includes, in addition to counting statistics: σ (cross contamination) = 0.6%, σ (chemical processing) = 0.8%, σ (β-counting-efficiency correction) = 2.0%.

c. Total σ includes, in addition to counting statistics: σ (cross contamination) = 0.6%, σ (Re chemical processing) = 0.67%, σ (W chemical processing) = 1.2 - 1.9%.

d. Corrections were 1) 3.8% for initial thickness of radioactive layer (Eq. 3.3.1) and 2) 1.5% for sample misalignment and finite thickness of sections, for a total reduction of 5.3% in the observed D values.

TABLE 8.4

EXPERIMENTAL DATA FOR DIFFUSION AT 3228°C

Temperature - 3228 ± 60°C

Average pressure - 2×10^{-5} mm Hg

Effective diffusion time - 88 ± 2 min (5.28×10^3 sec)

Section No.	Thickness of Section (mils)	x[a] (cm x 10^3)	x^2 (cm^2 x 10^4)	W Activity (c/min/mg)	Re Activity (c/min/mg W)
1	2.05	2.67	0.071	13.14 ± 0.35[b]	6.13 ± 0.11[c]
2	1.30	7.06	0.498	10.57 ± 0.32	5.84 ± 0.19
3	0.85	9.86	0.972	9.60 ± 0.28	5.41 ± 0.20
4	1.00	12.29	1.510	7.61 ± 0.24	4.61 ± 0.60
5	1.00	14.90	2.220	6.19 ± 0.20	4.25 ± 0.18
6	1.13	17.70	3.133	4.44 ± 0.13	3.34 ± 0.15
7	1.17	20.75	4.306	3.23 ± 0.12	2.17 ± 0.29
8	1.67	24.44	5.973	1.54 ± 0.06	1.60 ± 0.26
9	1.18	28.17	7.935	0.82 ± 0.04	0.75 ± 0.22
10	1.08	30.95	9.579	0.50 ± 0.03	0.51 ± 0.10

From least-squares analysis: $D(W) = (1.36 \pm 0.02) \times 10^{-8}$ cm^2/sec

$D(Re) = (1.90 \pm 0.10) \times 10^{-8}$ cm^2/sec

Corrected:[d] $D(W) = (1.34 \pm 0.04) \times 10^{-8}$ cm^2/sec

$D(Re) = (1.86 \pm 0.11) \times 10^{-8}$ cm^2/sec

a. x, which is the distance from the original interface to the midpoint of the section, has been corrected for linear thermal expansion.

b. Total σ includes, in addition to counting statistics: σ (cross contamination) = 0.6%, σ (chemical processing) = 0.8%, σ (β-counting-efficiency correction) = 2.0%.

c. Total σ includes, in addition to counting statistics: σ (cross contamination) = 0.6%, σ (Re chemical processing) = 0.7%, σ (W chemical processing) = 1.3 - 2.3%. The first Re point was omitted for least-squares analysis.

d. Corrections were 1) 1.5% for initial thickness of radioactive layer (Eq. 3.3.1) and 2) 0.6% for sample misalignment and finite thickness of sections, for a total reduction of 2.1% in the observed D values.

$$C = \frac{C_0}{\sqrt{\pi D t}} e^{-x^2/4Dt} , \qquad 3.2.19$$

where x is the penetration depth and C is the concentration of the diffusing tracer, expressed in the tables as counts/min/mg W. The diffusion constants D(W) and D(Re) were obtained for each run by least-squares fits of the above expression (left in its non-linear form) to the sets of C-vs-x data given in the tables. Variation in the C axis only was considered, and each C value was weighted by the square of the reciprocal of its standard deviation. The program for the least-squares analysis was prepared by Moore and Zeigler[62], and the problems were run on a Los Alamos IBM 7090.

The data presented in Tables 8.1 through 8.4 are plotted in Figs. 8.1 through 8.4 in terms of $\log_e C$ vs x^2 for visual comparison of tungsten and rhenium diffusion rates. The plots follow the linear relationship as expected for volume diffusion.

The D values obtained from least-squares analyses were corrected for 1) the initial thickness of the radioactive layer, 2) possible sample misalignment, and 3) finite thickness of the sections taken for analysis. These corrections and the experimental errors are treated in detail in the next chapter.

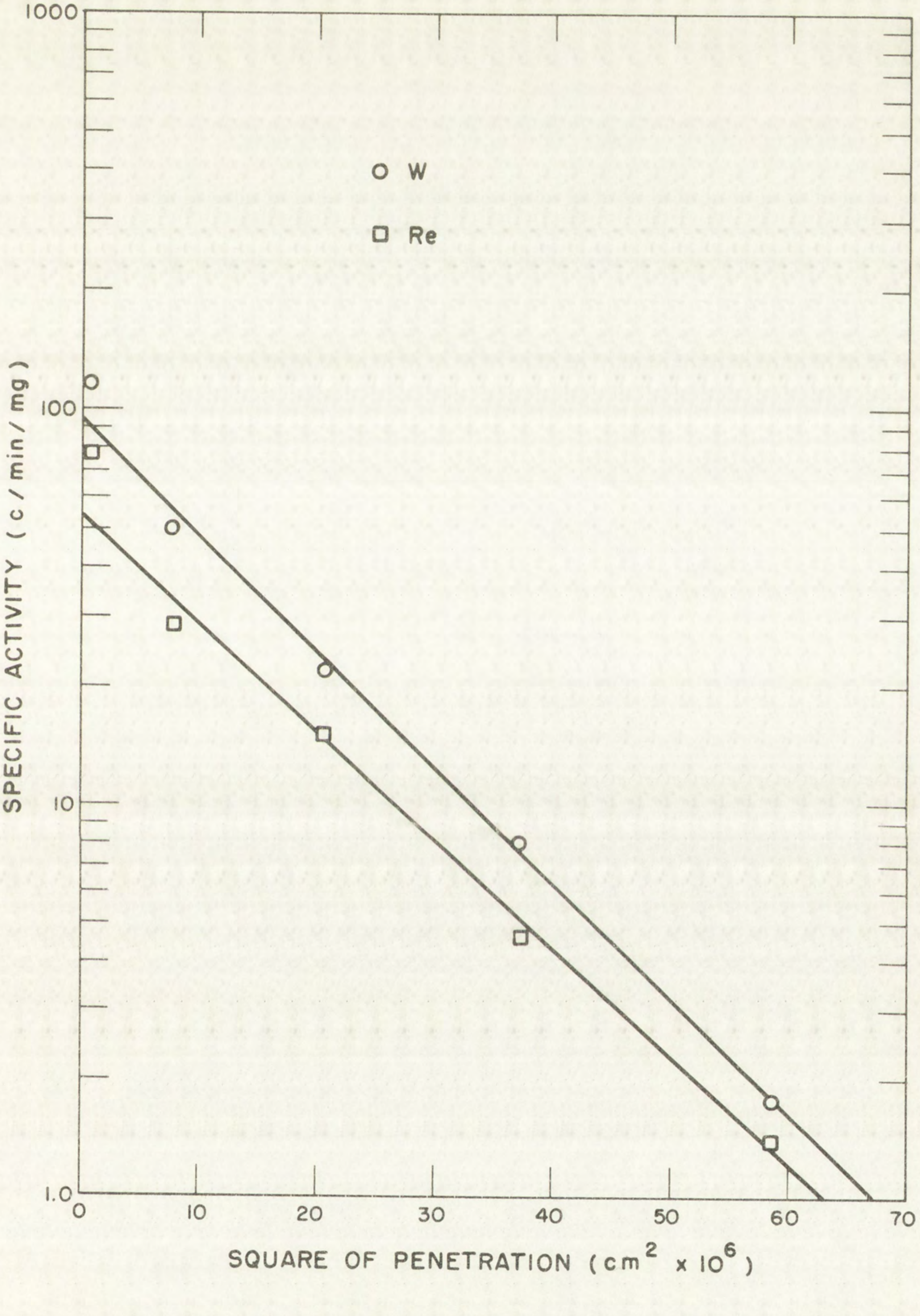

Fig. 8.1 Log Specific Activity vs Square of Penetration for Diffusion at 2666°C

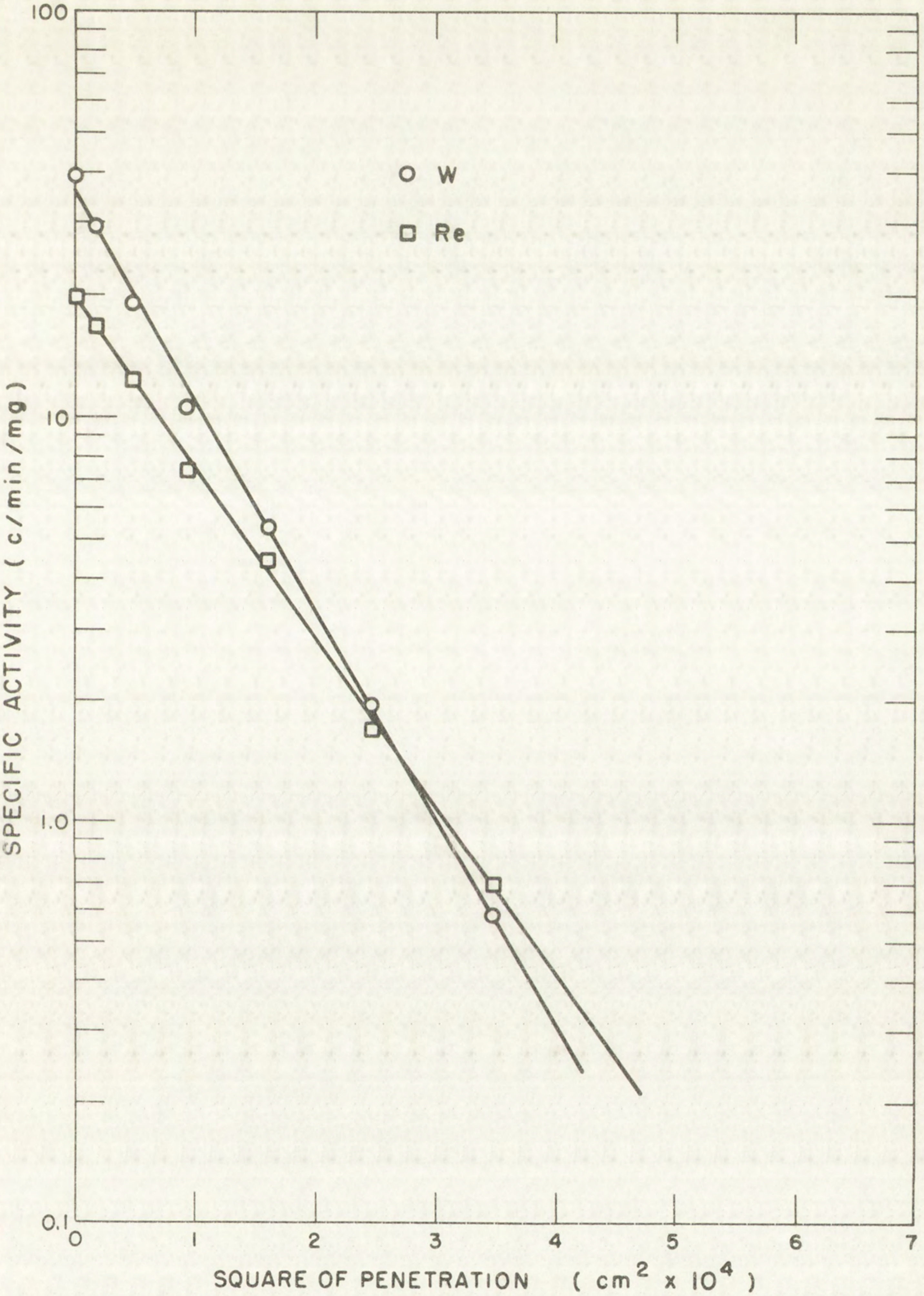

Fig. 8.2 Log Specific Activity vs Square of Penetration for Diffusion at 2759°C

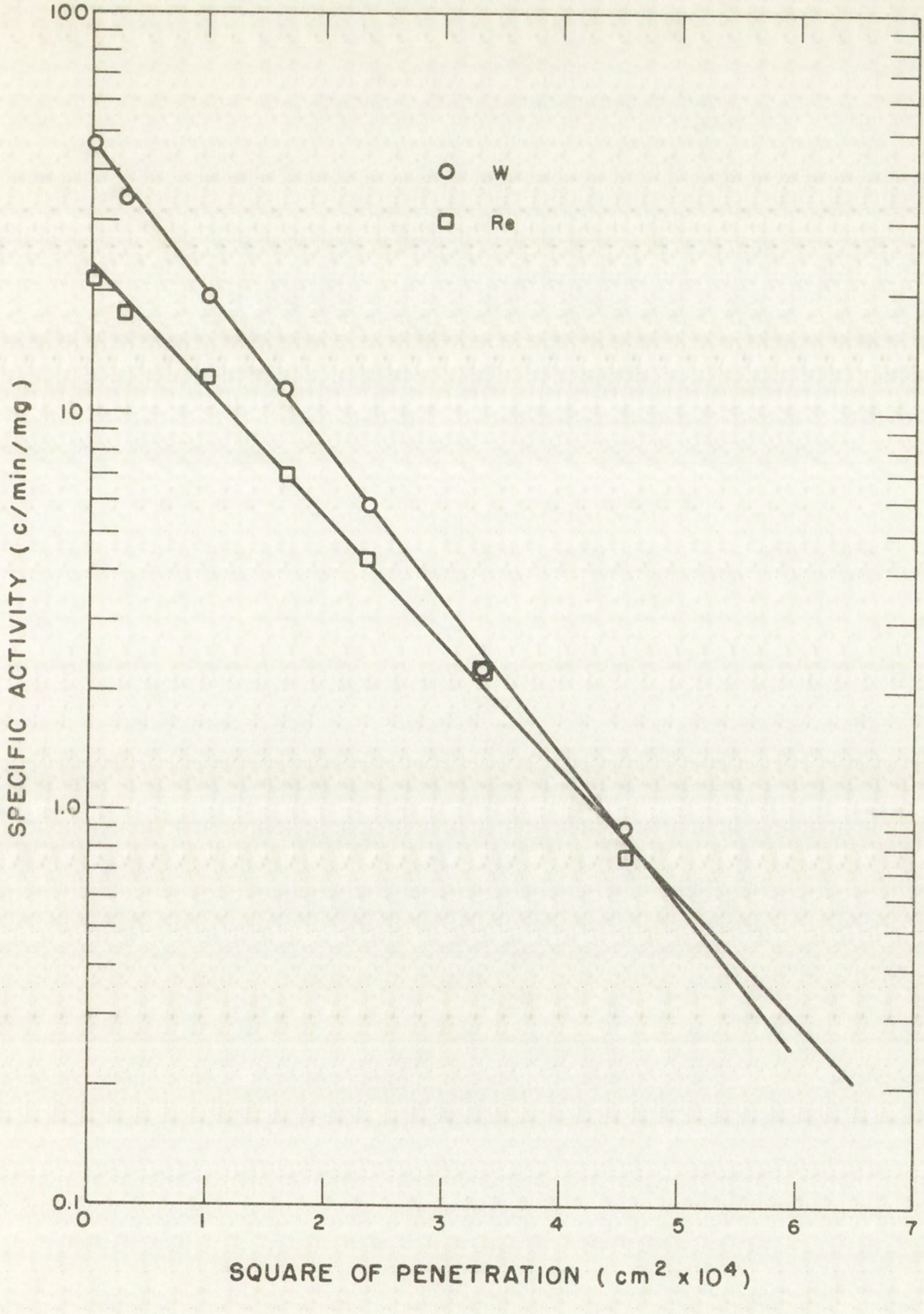

Fig. 8.3 Log Specific Activity vs Square of Penetration for Diffusion at 2889°C

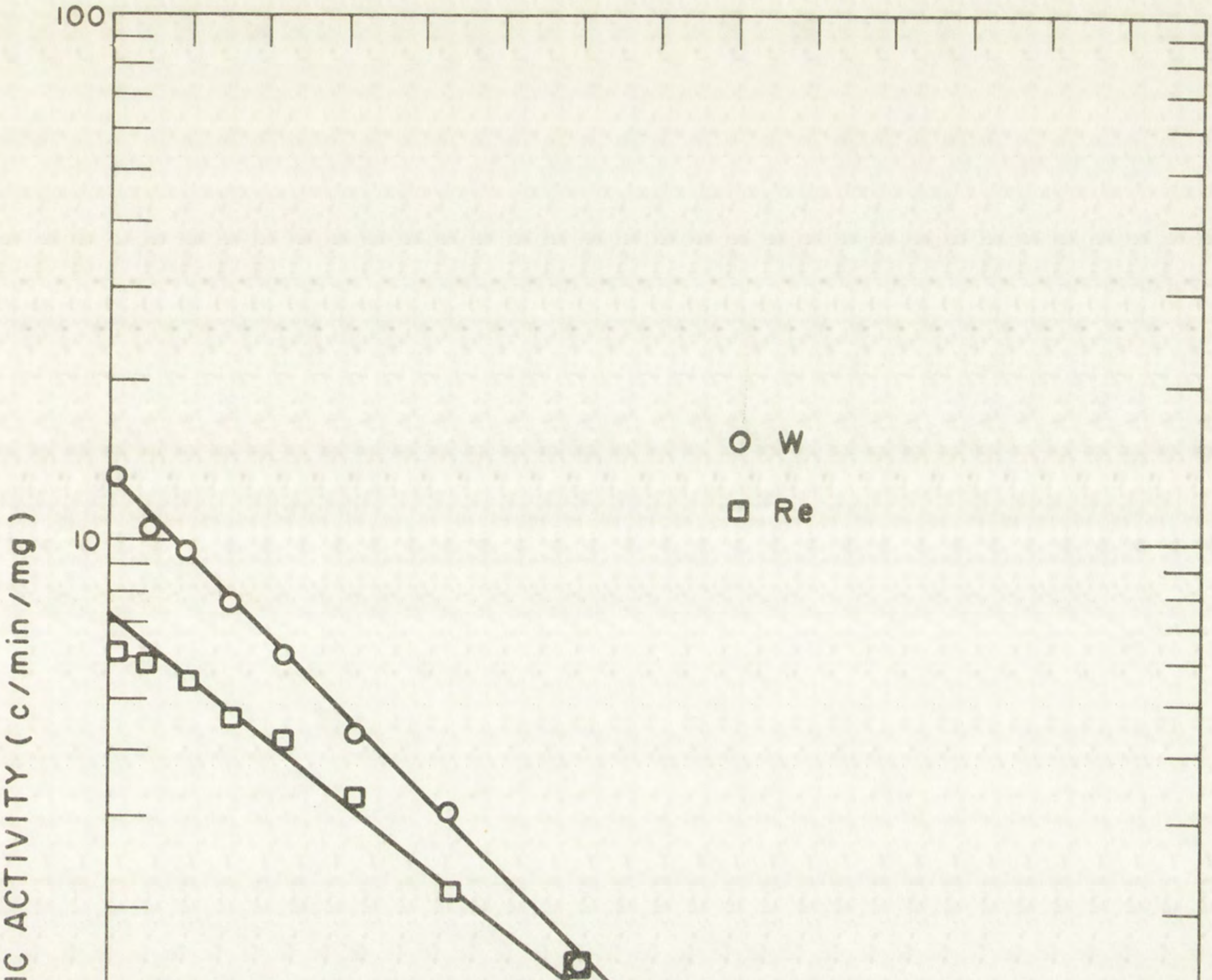

Fig. 8.4 Log Specific Activity vs Square of Penetration for Diffusion at 3228°C

Chapter 9

DISCUSSION OF ERRORS AND CORRECTIONS

A rather thorough error analysis was made on all experimental data and techniques. For conservatism, standard errors (σ) rather than probable errors ($0.67\ \sigma$) were used in counting statistics, and were estimated for all other known random errors. Applicable relative standard errors were combined (square root of the sum of the squares) for each point of the data in order that they would be reflected in the least-squares analyses. Corrections to the data were made for known systematic errors when justified. The combining of standard errors, and the corrections made to the diffusion coefficients were noted in the tables of Chapter 8.

Table 9.1 is an outline of all the errors considered. Many of these have been discussed or mentioned briefly in previous chapters, but are included here for completeness. The remainder of this chapter is devoted to a discussion of the errors listed in Table 9.1.

9.1 Errors Associated with Activation of the Diffusion Samples

Possible sources of error from items I-A, I-B and I-C (Table 9.1) are negligible for the following reasons. The variation of deuteron energy (± 0.05 MeV) would cause only slight variations in the initial distribution of the tracers as a function of depth. Moreover, the shape of this distribution was the same for all points on the bombarded face of the sample.

TABLE 9.1

OUTLINE OF POSSIBLE SOURCES OF ERROR

I. Errors associated with activation of the diffusion samples.
   - A. Variation in deuteron energy.
   - B. Nonperpendicular incidence of deuterons at the surface of the diffusion samples.
   - C. Non-uniform distribution of radioactivity on the surface of the diffusion samples.
   - D. Initial thickness of radioactive layer.
   - E. Deuteron damage to tungsten.

II. Errors associated with diffusion heating of the samples.
   - A. Temperature measurement and temperature gradients.
   - B. Effective diffusion time measurements.
   - C. Evaporative loss of radioactivity.
   - D. Linear thermal expansion of tungsten.

III. Errors associated with sectioning of diffusion-heated samples.
   - A. Linear expansion of tungsten and nickel during grinding.
   - B. Surface diffusion effects.
   - C. Cross contamination of activity from one layer to succeeding layers.
   - D. Micrometer measurements.
   - E. Sample misalignment.
   - F. Error in taking the penetration distance, x, at the midpoint of each section.
   - G. Thickness and number of sections.

IV. Errors associated with chemical processing and counting of samples.
   - A. Chemical processing.
   - B. Efficiency correction for β counting.
   - C. Radioactive decay.
   - D. Counting errors.

Since abnormal incidence of the deuteron beam on the samples would not affect the average range of 9.00-MeV deuterons in tungsten, the average penetration depth would be constant and layers of activity corresponding to constant deuteron energy would be parallel to the top surface. In fact, there would be some advantage in positioning the samples so that the beam would strike the surface at an oblique angle, and thus decrease the thickness of the radioactive layer parallel to the top interface.

There was no error due to non-uniform distribution of radioactivity on the surface of the samples. This point has been discussed in Section 3.3.

The error due to the initial thickness of the radioactive layer, which was also discussed in Section 3.3, is calculable (Eq. 3.3.1), and, therefore, corrections were made to the data as indicated in the tables of Chapter 8. For the first diffusion run (2666 °C), a low estimate of the required diffusion time resulted in a considerable error in D as calculated from Eq. 3.3.1. Since the correction is good only for small α (see Appendix A) a verification of the magnitude of the error was made as follows. Equation 46 (Appendix A) which gives the concentration of activity in a diffusion sample as a function of x (in Appendix A notation, $x = z$) and t for an initial distribution of activity P(u), was substituted into Eq. 51, which gives the fractional error in D. The result of this substitution is

$$C(x) = \frac{1}{x} \frac{\int_{-\infty}^{\infty} u \, e^{-(x-u)^2/4Dt} \, P(u)du}{\int_{-\infty}^{\infty} e^{-(x-u)^2/4Dt} \, P(u)du} . \qquad 9.1.1$$

Equation 9.1.1 was then integrated numerically at an x value (penetration depth) of 6×10^{-3} cm which was arbitrarily chosen from the concentration-penetration data for the 2666 °C run (Fig. 8.1). The values for P(u) were taken off the initial concentration profile curve (Fig. 6.4). The numerical integration indicated an error in D of 36%. For the remaining diffusion runs, the errors in D due to an initial thickness of radioactive layer, h, were 5.2%, 3.8% and 1.5% as calculated from Eq. 3.3.1 for the diffusion runs at 2759, 2889, and 3228 °C, respectively.

The problem of deuteron damage to the tungsten diffusion samples and its subsequent effect on diffusion is an interesting one. In a typical deuteron

irradiation of tungsten with a total beam current of 1500 μC, ~ 10^{16} 9.00-MeV deuterons strike the tungsten and, after traveling their total range, come to rest, forming a layer of deuterium, at a penetration depth of about 3.6 mils. Only very few deuterons (~ 0.01%) undergo nuclear reactions to form radioactive isotopes. The deuterium gas (~ 0.0004 cc at STP) diffuses out of the samples at temperatures above, say 400 to 500 °C.

Undoubtedly, radiation damage to tungsten includes formation of vacancies through which diffusion of tungsten or rhenium atoms could be enhanced. However, if the radiation-induced vacancies were annealed out prior to the occurrence of significant diffusion, this enhancement would be minimized or eliminated completely. Although deuterium ions, being heavier than neutrons, would perhaps produce more radiation damage than neutrons for a given integrated flux, the recovery of tungsten from radiation damage caused by neutrons is applicable. By residual electrical resistivity measurements, Thompson[63] studied the recovery of neutron-irradiated tungsten. He concluded that tungsten vacancies migrate at 400 °C with an activation energy for migration of only 1.7 eV. Recovery as indicated by Thompson's electrical resistivity measurements was essentially complete at temperatures slightly above 450 °C.

Since radiation-damage effects in metals are somewhat similar to cold-working effects, it is of interest to compare the above results by Thompson with recovery in cold-worked tungsten. Koo[64] showed by residual resistivity measurements that cold-work vacancies in tungsten anneal out at 350 °C with an activation energy of 1.7 eV. Pugh[65] reported that, for cold-deformed tungsten, vacancies and interstitials are eliminated just above 400 °C as indicated by electrical resistivity measurements, and that migration and annihilation of dislocations occur just above 500 °C as indicated by a recovery of mechanical properties.

Since the lowest temperature for any diffusion run was 2666 °C, it is reasonable to assume, on the basis of the recovery data given above, that radiation-damage effects on diffusion rates were negligible or nonexistent. Furthermore, the linearity of the plots of log C vs x^2, (Figs. 8.1 through 8.4) indicates the absence of significant radiation-damage effects. If, indeed, diffusion was enhanced through the first 3.6 mils (0.84×10^{-4} cm) of tungsten, a flattening of the curve over that distance would have occurred.

9.2 Errors Associated with Diffusion Heating of the Samples

The uncertainty in temperature measurement and the variation of temperature throughout the samples during diffusion heating have been discussed in Sections 5.3 and 5.4. The standard error for each temperature is listed in the tables of Chapter 8.

For the shortest diffusion run (88 min at 3228°C), the uncertainty in effective diffusion time was 2 min or 2.3%. This error was included in the standard deviation shown for the diffusion coefficient on this run. For all other diffusion runs, the uncertainty in effective diffusion time was less than 0.5%, and was therefore ignored. Because of very rapid heating and cooling of the samples made possible by induction heating (Chapter 5), uncertainy in diffusion-time measurements was very small.

The vapor pressure of tungsten (item II-C, Table 9.1), usually considered to be very low, is appreciable at temperatures above 75% of the melting point of tungsten. Loss of radioactivity by evaporation could have been a problem were it not for the special experimental arrangement (Figs. 5.3 and 5.4) during diffusion heating. The radioactive faces were in apposition and were separated by a 1/2-in.-diameter ring made from 30-mil tungsten wire. Essentially all the radioactivity was contained within a 1/2-in.-diameter circle on the diffusion samples. At the high temperatures of diffusion heating, the tungsten rings formed an effective seal for containment of tungsten gas between the two radioactive surfaces. The only gas escape route was through the small opening where the two ends of the tungsten ring came together. The problem, therefore, was reduced to one of molecular flow through an orifice or short tube. The following calculation estimates the amount of radioactive tungsten lost by evaporation during the highest temperature (3501°K) diffusion run. Loss of radioactive rhenium would be of the same order of magnitude.

The equation relating vapor pressure to loss of material through a small orifice is

$$G = \frac{P\,K\,A\,t}{17.14}\left(\frac{M}{T}\right)^{\frac{1}{2}} \qquad 9.2.1$$

where G is the grams of material lost, P is the vapor pressure in mm Hg, K is a correction factor (necessitated because the thickness (l) of the wall, in which the orifice of area πa^2 was located, was not vanishingly small compared to a), A is the area (cm^2) of the orifice (πa^2), t is the time (sec), M is the molecular weight of the effusing gas, and T is the temperature in degrees Kelvin. The derivation of Eq. 9.2.1, which is based on the kinetic theory of gases, is discussed in detail by Dushman.[66] At 3500 °K the vapor pressure of tungsten is 5.64×10^{-3} mm Hg,[67] the area of the orifice was estimated to be 2.0×10^{-3} cm^2, and an estimated[68] value for K is 0.42. The value obtained for G for the highest temperature diffusion run is 3.40×10^{-4} g. Since this value corresponds to a loss from both surfaces, only half that amount or 1.70×10^{-4} g was lost from each sample. The corresponding thickness loss over a 1/2-in.-diameter circle was only 0.0028 mils. In terms of atoms, 5.51×10^{17} atoms were lost from each sample, of which 3.8×10^{6} or $\sim 10^{-9}\%$ were radioactive as estimated from the specific activity of the first layer removed from an unheated diffusion sample (Table 8.2). Thus, loss of radioactivity by evaporation was not a problem. Further verification was the linearity of the log C vs x^2 plots (Figs. 8.1 through 8.4).

The author is not aware of any experimental determination of the linear coefficient of thermal expansion for tungsten (item II-D in Table 9.1) in the temperature range 2600 °C to 3200 °C. Therefore, an estimated value of 8.25×10^{-6} cm/cm-°C was used. This value was obtained by an extrapolation of the data first reported by Worthing[69] and later confirmed by other investigations.[70] Worthing's linear expansion coefficients for well-annealed tungsten wire at 1300 and 2300 °K are 5.19×10^{-6} cm/cm-°C and 7.26×10^{-6} cm/cm-°C, respectively.

Because thermal expansion characteristics of single-crystal tungsten cylinders may be different from those for polycrystalline tungsten wire, and also because of extrapolation uncertainties, an estimated error of 20% in the extrapolated coefficient is reasonable. On the basis of the coefficient $8.25 \pm 1.65 \times 10^{-6}$

cm/cm-°C, therefore, the errors in the corrections to penetration distances did not exceed 0.6%. As an example of the magnitude of the correction, a penetration distance of 10 mils measured at room temperature was corrected to 10.27 ± 0.05 mils for diffusion at 3228°C.

9.3 Errors Associated with Sectioning of Diffusion-Heated Samples

The linear thermal expansion of tungsten and nickel during sectioning (item III-A, Table 9.1) has been treated in Section 6.6, and was found to be negligible.

Surface diffusion effects were eliminated by lateral grinding prior to sectioning as discussed in Section 6.3.

Experimental measurements indicated cross contamination of activity from one layer to succeeding layers was about 0.6%.

The technique of micrometer measurements, along with estimates as to their precision and accuracy, has been discussed in Section 6.6. The accuracy of measurement was estimated to be ± 0.05 mil. Since the bottom of the diffusion sample was the reference plane for all measurements, the error in the position of the midpoint of each section was constant and was equal to ~ 0.035 mil.

The errors indicated by items III-E, III-F and III-G of Table 9.1 were estimated from a formula derived by Shirn, et al.[71] The necessary corrections were then applied to the diffusion coefficients as indicated in Tables 8.1 through 8.4. From Shirn's formula, an observed diffusion coefficient is too large because of misalignment and finite thickness of sections by the fractional error

$$E = \frac{d^2_{ave} + 3\,\frac{s^2}{4}}{24\,Dt}, \qquad 9.3.1$$

where d is the average thickness of sections (cm) and s is the misalignment distance (angle of misalignment in radians times the sample diameter). Since the maximum angle of misalignment for any sample was only 0.017° (Section 6.7) or 3×10^{-4} radians ($s = 4.5 \times 10^{-4}$), the misalignment contribution to the total error

was small. The experimentally observed diffusion coefficients for diffusion at 2666°C, 2759°C, 2889°C and 3228°C were reduced, on the basis of these corrections, by 3.5%, 1.6%, 1.5% and 0.6%, respectively. The corrections are noted in the tables of Chapter 8.

9.4 Errors Associated with Chemistry and Counting of Samples

Errors in chemical processing (item IV-A, Table 9.1), including weighing uncertainties, did not exceed 1.2% for the tungsten samples. For the rhenium samples, which included a tungsten analysis as explained in Section 7.2, the chemistry and weighing errors did not exceed 2.6%.

The efficiency correction for β counting has been described in Section 7.3. The estimated error for this correction was 2%.

Most of the samples obtained from a diffusion run were counted the same day so that radioactive decay corrections were not needed for the fairly long-lived isotopes being counted (75-day W^{185} and 34-day Re^{184}). However, corrections for radioactive decay were made when the corrections were significant.

Counting errors varied from 0.5% to 5% with an average error of 2.3% for tungsten samples and from 0.5% to 20% with an average error of 5.1% for rhenium samples.

9.5 Summary of Errors and Corrections

The significant, known, random errors which were combined for inclusion in the least-squares analyses of the diffusion data are as follows. The identification at the left refers to items listed in Table 9.1.

III-C	Cross contamination - 0.6%
IV-A	Chemical processing (W samples) - 0.6 to 1.2%
IV-A	Chemical processing (Re samples) - 1.4 to 2.6%
IV-D	Counting statistics (W samples) - 0.5 to 5% with an average of 2.3%
IV-D	Counting statistics (Re samples - 0.5 to 20% with an average of 5.1%

IV-B Error in β-counting-efficiency correction - 2.0%.

The significant, known, random errors not included in the least-squares analyses for determination of diffusion coefficients were 1) the error in the micrometer measurement of the penetration distance x (a constant error, item III-D, Table 9.1) and 2) the small error in the corrected value of x due to the linear thermal expansion of tungsten (item II-D, Table 9.1). These errors were not included because they represent deviations along the x axis, and only those along the specific-activity axis were essential for the analyses. (Usual procedure in least-square analysis is to consider only deviations along one axis, which, according to Parratt,[72] sacrifices little in accuracy. The axis along which the deviations are greater is chosen for the least-squares treatment.)

The known systematic errors, for which corrections were made to the experimentally measured diffusion coefficients, were 1) error due to initial thickness of radioactive layer (item I-D, Table 9.1), and 2) errors due to misalignment and finite thickness of sections (items III-E, III-F, and III-G, Table 9.1). For diffusion runs at temperatures 2666, 2759, 2889 and 3228°C, the errors caused by the initial thickness of the radioactive layers were 36%, 5.2%, 3.8% and 1.5%; the errors caused by misalignment and finite thickness of sections were 3.5%, 1.6%, 1.5% and 0.6%. The appropriate corrections were made as indicated in the tables of Chapter 8.

Since random errors were combined, as mentioned above, for least-squares analyses of the data, the total standard errors in the experimentally-observed diffusion coefficients were obtained from the results of the least-squares analyses. These were 6.6%, 2.9%, 2.1% and 2.9% for tungsten self-diffusion coefficients, and 13.4%, 2.1%, 2.4% and 5.7% for the coefficients obtained for rhenium diffusion in tungsten at diffusion temperatures of 2666, 2759, 2889, and 3228°C, respectively. Temperature uncertainty for each diffusion run is not included in the above percentages, but is included in the temperature-dependent rate laws to be discussed in the next chapter.

As a final comment at the conclusion of this chapter, the author would like to endorse the words of Parratt[73] concerning errors in science: "Elimination of errors often strains the ingenuity, judgment, and patience of the best of experimenters."

Chapter 10

RESULTS AND DISCUSSION

10.1 Temperature Dependence of Self-Diffusion in Tungsten and of Rhenium Tracer Diffusion in Tungsten

A summary of the diffusion coefficients obtained, along with standard errors for both the diffusion coefficients and the corresponding temperatures at which they were determined are presented in Table 10.1.

TABLE 10.1

SUMMARY OF DIFFUSION DATA

D for W Self-Diffusion (cm^2/sec)	D for Re Diffusion in W (cm^2/sec)	Temperature (°K)
$(2.00 \pm 0.13) \times 10^{-10}$	$(2.03 \pm 0.27) \times 10^{-10}$	2939 ± 46
$(4.41 \pm 0.13) \times 10^{-10}$	$(5.30 \pm 0.11) \times 10^{-10}$	3032 ± 47
$(1.24 \pm 0.03) \times 10^{-9}$	$(1.55 \pm 0.04) \times 10^{-9}$	3162 ± 51
$(1.34 \pm 0.04) \times 10^{-8}$	$(1.86 \pm 0.11) \times 10^{-8}$	3501 ± 60

The data of Table 10.1 fit the usual Arrhenius relationship, $D = D_0 e^{-Q/RT}$ where D is the diffusion coefficient, in cm^2/sec, D_0 is the frequency factor, in cm^2/sec, Q is the activation energy in calories/mole, R is the universal gas constant (1.987 cal/mole-deg), and T is the temperature in degrees Kelvin. Figure 10.1 is a plot of log D vs 1/T for both tungsten and rhenium

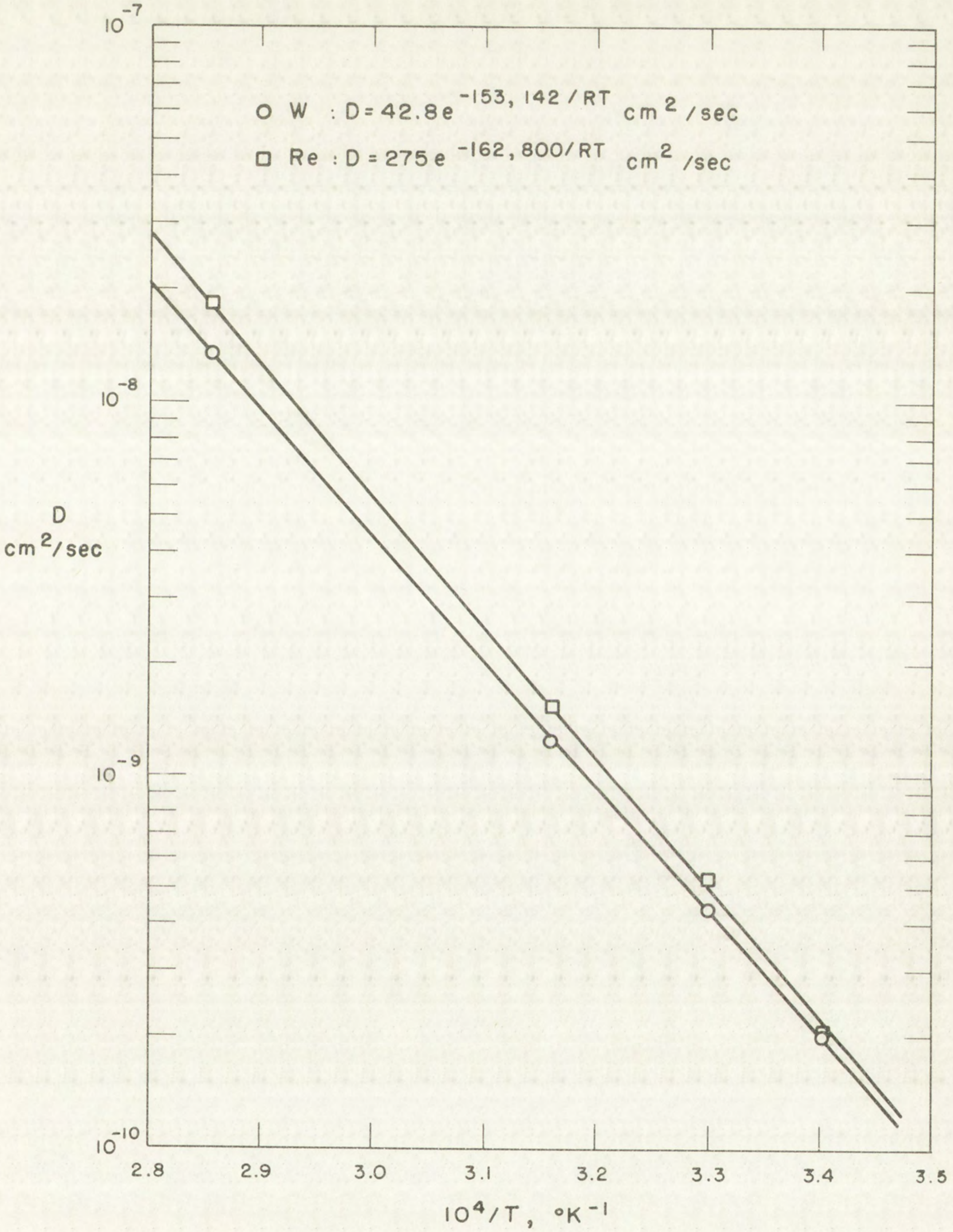

Fig. 10.1 Plot of Log D vs 1/T for Diffusion of Tungsten and Rhenium Tracers in Tungsten

diffusion. From the plot it is seen that rhenium diffusion was consistently more rapid than tungsten diffusion in each of the diffusion runs with the difference in rates increasing at higher temperatures.

To obtain the best values for activation energies and frequency factors, the data of Table 10.1 were programmed for least-squares fit to the function, $D = D_0 e^{-Q/RT}$. A FORTRAN code was written by Zeigler and Moore[27] based upon an approach suggested by Deming.[74] With this approach, deviations in both axes were included in the regression analysis, which was run on the Los Alamos IBM 7090. The final results were,

$$D(W) = (42.8 \pm 4.8)\, e^{-(153{,}142 \pm 633)/RT} \text{ cm}^2/\text{sec},$$

$$D(Re) = (275 \pm 110)\, e^{-(162{,}800 \pm 2498)/RT} \text{ cm}^2/\text{sec}.$$

The standard errors in activation energies indicated above are quite small considering the fairly large uncertainties in diffusion temperatures (Table 10.1). However, these small deviations for activation energies are indicative of the internal consistency of temperature measurement for each of the diffusion runs.

10.2 Consistency of Data with Empirical Rules of Diffusion

It is of interest to compare the above data for self-diffusion in tungsten with values predicted from empirical rules derived from observations on other self-diffusion systems. Since any mechanism for self-diffusion involves the straining of atomic bonds, it is reasonable to attempt correlations of the activation energy for self-diffusion with quantities which reflect the strength of atomic binding. Thus, LeClaire[75] has suggested the relationship

$$Q = 38\, T_m \text{ cal/mole} , \qquad 10.2.1$$

where Q is the activation energy, and T_m is the absolute melting temperature. With T_m equal to 3683°K for tungsten, the activation energy should be about 140 kcal/mole.

Nachtrieb and Handler[76] propose that the activation energy should be related to the latent heat of melting, ΔH_m, by the relationship

$$Q = 16.5\,\Delta H_m \text{ cal/mole.} \qquad 10.2.2$$

They consider that the self-diffusion process is analogous to a local melting of the lattice, and that the number of participating atoms is essentially constant for all metals. Equation 10.2.2 is equivalent to Eq. 10.2.1 for metals in which the entropy of melting is a constant equal to 2.3 cal/mole-°K. In such cases, $\Delta H_m = 2.3\ T_m$. For tungsten, $\Delta S_m = 2.29$ cal/mole-°K, which satisfies the condition for equivalence of Eqs. 10.2.1 and 10.2.2. With a value of 8420 cal/mole[77] for the latent heat of melting of tungsten, the activation energy should be 139 kcal/mole.

Sherby and Simnad[78] have attempted an empirical correlation of the activation energy for self-diffusion with the absolute melting temperature, crystal structure and "valence" of pure metals. Their relationship is

$$D = D_0\, e^{-(K_0 + V)\, T_m/T} \text{ cm}^2\text{/sec}, \qquad 10.2.3$$

where K_0 is a constant which depends only on the crystal structure of the metal, V is a constant determined in an uncertain way by the valence of the metal, and the other terms are as previously defined. Sherby and Simnad have suggested that D_0 should equal 1 cm^2/sec for many metal systems, although they point out that D_0 values may perhaps be higher for body-centered cubic metals than for face-centered cubic metals.[79] (Experimental values of D_0 reported in the literature[7] vary from 10^{-8} to 10^7, which is not of much help in judging the validity of this notion.) The value of K_0 for body-centered cubic lattices is 14. Assuming a valence of 6 for tungsten, Eq. 10.2.3 yields an activation energy of 146 kcal/mole. The activation energy for tungsten self-diffusion obtained in the present

work (153.1 ± 0.6 kcal/mole) agrees to within 5% of the value obtained from Eq. 10.2.3, and to within 10% of the values obtained from Eqs. 10.2.1 and 10.2.2.

A summary of experimental and predicted values of D_0 and Q for self-diffusion in tungsten is presented in Table 10.2. From the data presented, it would appear that an activation energy of the order of 120 kcal/mole is far too low for volume self-diffusion in tungsten.

TABLE 10.2

SUMMARY OF EXPERIMENTAL AND PREDICTED VALUES OF D_0 AND Q FOR SELF-DIFFUSION IN TUNGSTEN

Direct Measurements

Q (kcal/mole)	D_0 (cm^2/sec)	Temp. Range (°C)	Investigator
135.8	6.3×10^7	1287-1453	Vasil'ev and Chernomorchenko[14] (1956)
120.5	0.54	2000-2700	Danneberg[18] (1961)
153.1	42.8	2660-3230	Present Work (1962)

Indirect Measurements

Q (kcal/mole)	D_0 (cm^2/sec)	Investigator
142	11.5	van Liempt[15] (1945)
160		Green[16] (1959)
125		Schnitzel[17] (1959)

Predicted Values

Q (kcal/mole)	D_0 (cm^2/sec)	Reference
140		LeClaire[75] (1949)
139		Nachtrieb and Handler[76] (1954)
146	1.0	Sherby and Simnad[78] (1961)

A few comments on the values of D_0 and Q obtained by direct measurements (Table 10.2) are in order. Both Danneberg and the Russian investigators used polycrystalline tungsten in their work, rather than single-crystal tungsten. Volume self-diffusion coefficients can be measured in polycrystalline metals provided the diffusion temperatures are sufficiently high for volume diffusion to dominate grain-boundary diffusion. Grain-boundary diffusion has a lower activation energy, and thus tends to predominate at lower temperatures. Diffusion temperatures above 75% of the melting point of the metal should be sufficiently high to mask most of the effects of grain-boundary diffusion. For tungsten, 75% of the melting point is 2558 °C, whereas the temperature range of measurement in the Russian work was 1287-1453 °C. The unusually large D_0 value which they obtained is indicative of a large positive entropy of activation, which in turn suggests a "loosening" of the lattice or grain-boundary diffusion. The contribution of grain-boundary diffusion to the measured diffusion results in a lower activation energy than would be expected for volume diffusion alone, and for this reason their value of 135.8 kcal/mole is probably low. Although Danneberg's temperature range of measurement was higher (2000 to 2700 °C), his results may also have been affected by grain-boundary diffusion.

The technique described by Danneberg for his self-diffusion work was direct, but somewhat unusual. The tracer was applied to 0.2 mm polycrystalline tungsten wire by electrophoresis of tungsten trioxide suspended in alcohol with calcium chloride as conducting salt. The tungsten trioxide was then reduced to tungsten by some method unmentioned in his paper. After diffusion heating, lateral layers 1 to 5 microns thick were removed from the wires electrolytically and the activity of the resulting solution was measured with a scintillation counter. An experimental uncertainty in this technique is nonuniform removal of layers. The author's experience in attempting to remove layers electrolytically from the end surface of cylindrical tungsten diffusion samples has been mentioned in Section 6.1. It was difficult to maintain uniform current density over the entire surface to be dissolved. Although uniform current density could have perhaps been more easily achieved along the length of a wire than on the end surface of a cylinder, Danneberg still had the problem of preferential dissolution because of

varying surface energies over the polycrystalline tungsten wire. Moreover, Danneberg really had no way of knowing whether or not each layer he removed electrolytically was precisely concentric with the center of the wire. The uncertainty in diffusion coefficients due to nonuniform removal of layers can be appreciable.

In the present work, diffusion samples were single-crystal tungsten, and the temperature range of measurement (2660-3230 °C) was well above 75% of the melting point of tungsten. In addition, the direct sectioning technique, which is generally considered most accurate for diffusion work,[19,20] was employed. The technique of activating the diffusion samples directly by bombardment with deuterons may be criticized because of the resulting finite "layer" of activity and because of deuteron damage to the first 3.6 mils of the tungsten diffusion samples. However, it has been shown elsewhere in this report that valid corrections were made to the diffusion coefficients for finite thickness of the initial tracer activity, and that these corrections were small for long diffusion times. Evidence has also been presented indicating that radiation damage effects due to deuteron bombardment of the diffusion samples were rapidly annealed out at the high diffusion-heating temperatures employed in this work, and, therefore, that enhancement of diffusion through the initial portion of the diffusion samples was unlikely. Moreover, the linearity of the concentration-penetration curves ruled out diffusion enhancement through the first 3.6 mils of tungsten. Total penetration distance for all runs except the one at lowest temperature was from 8 to 10 mils.

The small standard errors of 11.2% in D_0 and of 0.4% in Q obtained by least-squares analysis of the tungsten self-diffusion coefficients at each diffusion temperature, with standard errors for both diffusion coefficients and temperatures included in the analysis, are indicative of the excellent fit of the data.

10.3 Mechanisms of Diffusion; Semiempirical Correlations

10.3.1 Mechanisms of Diffusion

A few of the suggested mehanisms for volume diffusion are illustrated in Fig. 10.2. Each model will be described briefly by considering the possible motion of a single diffusing atom through a nearly perfect lattice.

In the ring mechanism, the diffusing atom moves by interchanging its position with that of another lattice atom by a process involving the correlated rotation of two or more atoms about a common center. The rotation of a two-membered ring is often called an interchange or direct exchange mechanism. The more common case, for a cubic lattice, is a ring of four members.

In the interstitial mechanism illustrated in Fig. 10.2, the diffusing atom moves by jumping from an interstitial position to an adjacent interstitial position. This mechanism is believed to be responsible for diffusion of small solute atoms in a solvent lattice of large atoms.

In the vacancy model for diffusion, a diffusing atom moves by jumping into a neighboring vacant lattice site. This mechanism is dependent upon the existence or formation of point imperfections (vacant lattice sites) in the crystal lattice and upon their movement.

In the "relaxion" model, the diffusing atom moves more or less freely within a small region of disorder in the crystal. The disordered region (relaxion) consists of about 12 to 14 atoms which have relaxed inward around a lattice vacancy. The relaxion moves through the crystal, amoeba-like, by a process likened to a local melting and freezing of the relaxion at the edges.

10.3.2 Semiempirical Correlations

It is difficult to establish which of the above-mentioned mechanisms of diffusion is operative in a given diffusion system from the experimentally measured frequency factor, D_0, and the energy, or more precisely, enthalpy of activation, Q, which appear in the equation representing the temperature dependence of the

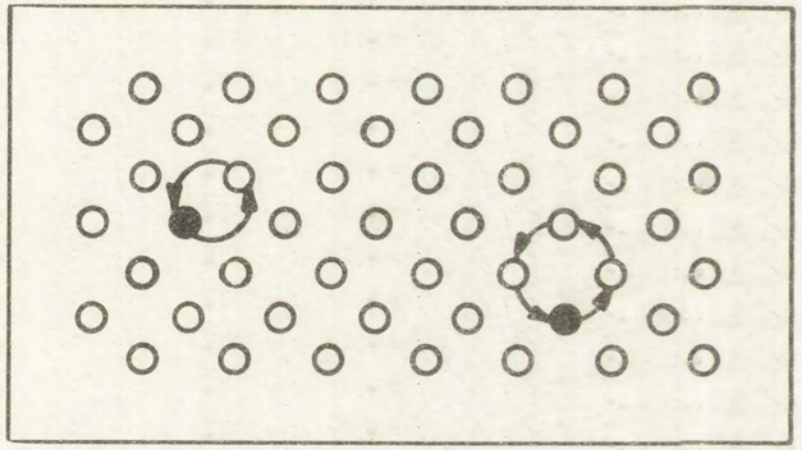

RING MECHANISM

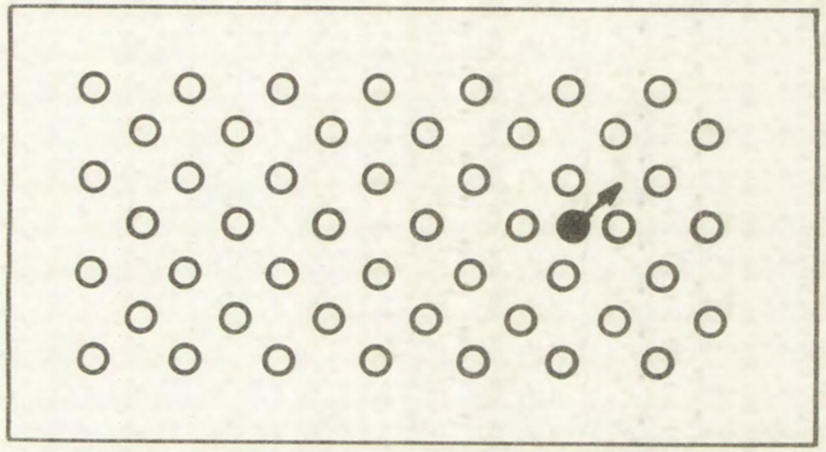

INTERSTITIAL MECHANISM

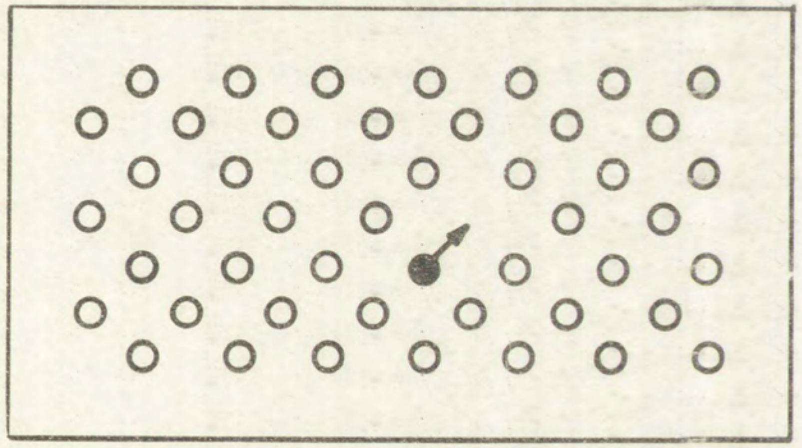

VACANCY MECHANISM

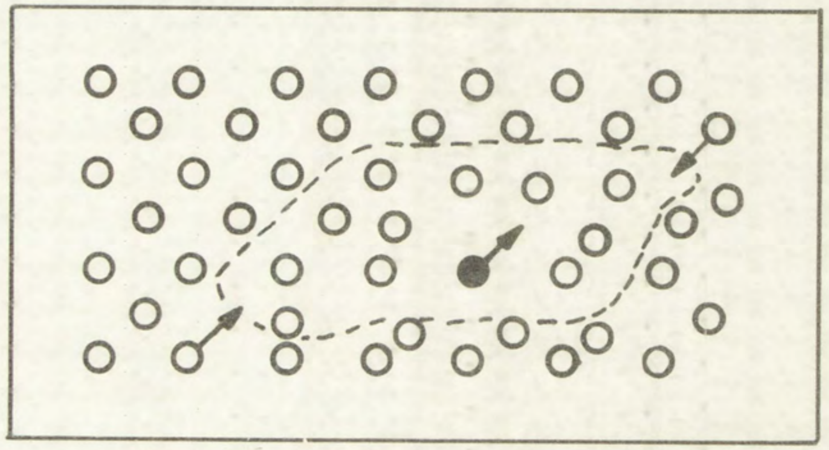

RELAXION MECHANISM

Fig. 10.2 Mechanisms for Volume Diffusion

diffusion coefficient. As Lazarus[80] points out, the theory of diffusion in metals is not completely understood, and much theoretical work remains to be done.

Calculations, from first principles, of entropies and energies of activation for a given self-diffusion system to prove or disprove a particular diffusion mechanism or model are laborious and sometimes inconclusive. For example, the classic work of Huntington and Seitz[81, 82] on the vacancy mechanism of self-diffusion in copper gives an activation energy which disagrees with experiment by about 35%. Calculations of this type will not be attempted here. However, proposed mechanisms have been considered on the basis of semiempirical correlations which relate observed frequency factors and activation energies with various macroscopic properties of the crystal such as melting temperature, latent heat of melting, and certain elastic constants.

Nachtrieb and Handler[76] have suggested that the relaxion mechanism is operative if the activation energy is related to the latent heat of melting by the previously-mentioned expression

$$Q = 16.5\, \Delta H_m \text{ cal/mole.} \qquad 10.2.2$$

Although Eq. 10.2.2 may be associated with the relaxion mechanism, for self-diffusion in tungsten it certainly is not conclusive, since Eq. 10.2.2 is essentially equivalent to the strictly empirical correlation of LeClaire.

Zener[7] has proposed a useful relationship for cubic metals to differentiate between a ring or vacancy mechanism. His relationship is

$$D = \gamma a^2 \nu\, e^{-\Delta F/RT} = \gamma a^2 \nu\, e^{\Delta S/R}\, e^{-\Delta H/RT} \text{ cm}^2\text{/sec}, \qquad 10.3.2.1$$

where γ is a numerical factor whose value depends upon the lattice geometry and the mechanism, a is the lattice parameter, and ν is the Debye frequency. The free energy in Eq. 10.3.2.1 is the isothermal work required to move the diffusing atom into its next position in the lattice, whether it be by a ring mechanism or by a vacancy mechanism. Zener's next relationship connects the entropy of activation, the observed temperature derivative of the shear modulus of the metal, the melting point, and the activation enthalpy by the expression

$$\Delta S = \frac{\lambda\beta\Delta H}{T_m} \text{ e.u.} \qquad 10.3.2.2$$

In Eq. 10.3.2.2, β is the dimensionless quantity, $-d(\mu/\mu_o)/d(T/T_m)$, where μ is the shear modulus at temperature T and μ_o is μ extrapolated to 0°K. The empirical constant λ, which represents the fraction of ΔH used in straining the lattice, has been found to be approximately + 0.55 for the vacancy mechanism and approximately unity for the ring mechanism.

The values of ΔS and ΔH derived from the present measurements, together with T_m and with a value of β used by Zener, may now be substituted into this expression to obtain a λ for self-diffusion in tungsten. First, an experimental ΔS is obtained from the expression

$$\Delta S = R\log_e \frac{D_0}{\gamma a^2 \nu} \text{ e.u.}, \qquad 10.3.2.3$$

where D_0 is the experimentally-determined frequency factor, 42.8 $cm^2\ sec^{-1}$, γ is a numerical factor assigned a value of 6 by Zener for a ring mechanism in body-centered cubic metals, $\nu = 6.4 \times 10^{12}\ sec^{-1}$ and $a = 3.16 \times 10^{-8}$ cm. With these data, $\Delta S = 14.0$ cal/mole °K. Next, from the present work, $\Delta H = 153.1$ kcal/mole. T_m has been given previously as 3683°K. Finally, Zener uses $\beta = 0.35$, based on Köster's[83] measurements of elastic constants for tungsten. With these values, λ turns out to be 0.96, approximately as expected for self-diffusion by the ring mechanism.

Also, by combining Eqs. 10.3.2.1 and 10.3.2.2, with the usual Arrhenius relationship, an expression for calculating D_0 is obtained,

$$D_0 = \gamma a^2 \nu\, e^{\lambda\beta Q/T_m R}\ cm^2/sec, \qquad 10.3.2.4$$

where $Q = \Delta H$, the experimentally measured activation energy. The calculated value of D_0 from Eq. 10.3.2.4 for self-diffusion in tungsten, which is 58 cm^2/sec, compares favorably with the upper limit of the observed D_0, 48 cm^2/sec. This evidence also favors a ring mechanism as based on Zener's theory.

LeClaire[9] has extended and refined Zener's theory to permit differentiation among interstitial, vacancy or ring mechanism for self-diffusion in cubic metals from the observed values of Q and D_0 and from the elastic constants of the metals. In addition, an expression is given for estimating the number of rings of atoms participating in the mechanism. Analysis of the present data in the light of LeClaire's refinements eliminates the interstitial and vacancy mechanisms for self-diffusion in tungsten, and strongly favors the ring mechanism. LeClaire's expression for calculating the number of rings participating in the mechanism is

$$\log_e N_r = \log_e \frac{D_0}{a^2\nu} + \frac{Q}{R}\left(\frac{\mu'}{\mu_0} - \frac{\rho'}{\rho_0}\right) , \qquad 10.3.2.5$$

where N_r is the number of distinct rings composed of r atoms, ρ' is the temperature derivative of the density of the metal and ρ_0 is the density at 0°K. The other terms are as previously defined. LeClaire lists a value of $- 0.84 \times 10^{-4}$ $°K^{-1}$ for the expression in parentheses for tungsten. Based on the present observed values of D_0 and Q, N_r for self-diffusion in tungsten is found to be 10.4. This value is not too far from the theoretical value of 6 rings, composed of four atoms each, for a body-centered cubic lattice. For rings of two atoms, N_r is theoretically unity. For an interstitial mechanism in body-centered cubic lattices, LeClaire has shown that N_r should equal 0.5

Buffington and Cohen[10] have also given an extended treatment of Zener's theory, but with consideration of the vacancy mechanism only. Danneberg[18] has attempted to show that self-diffusion in tungsten occurs by a vacancy mechanism based on the model of Buffington and Cohen. However, Danneberg's values of D_0 and Q are believed to be in error. The author's values of D_0 and Q do not fit Buffington and Cohen's vacancy model.

In summary, based on Zener and LeClaire's semiempirical correlations of these mechanisms, the vacancy and interstitial mechanisms are eliminated, and the ring mechanism is strongly favored for self-diffusion in tungsten. The relaxion model cannot really be tested from constant pressure measurements of D_0 and Q alone.

The above discussion has been limited to self-diffusion in tungsten, which, of course, is more amenable to theoretical interpretation than impurity diffusion in tungsten. However, the question of how rhenium tracer diffuses through a tungsten lattice is an interesting one. Observed impurity diffusion in metals proceeds at rates either faster, slower or the same as for self-diffusion, and the reasons for the differences in diffusion rates are only poorly understood. The theory of impurity diffusion in metals has not yet advanced as far as the theory for self-diffusion in metals. Lazarus[84] and LeClaire[85] have recently presented theoretical treatments on impurity diffusion in metals based on first principles, but no discussion of theory or correlation effects will be presented here.

The rates observed for rhenium tracer diffusion in single-crystal tungsten were greater than for self-diffusion in tungsten for each of the diffusion runs, and the activation energy for rhenium diffusion in tungsten is significantly higher. Because rhenium atoms have nearly the same charge and size as tungsten atoms, it is reasonable to conjecture that the mechanism operative in tungsten self-diffusion is also operative for diffusion of tracer rhenium atoms through a tungsten lattice.

Chapter 11

SUMMARY

The diffusion of radioactive tungsten and rhenium tracers in single-crystal tungsten has been measured by the direct sectioning technique. Cylindrical specimens prepared from the single-crystal material were activated on one end by deuteron bombardment at the Los Alamos cyclotron. They were then heated in an induction furnace for measured periods of time, and parallel sections were ground off and radiochemically analyzed to determine the distribution of the tracers as a function of depth. Four diffusion heatings were performed, at temperatures of 2666°, 2759°, 2889°, and 3228°C. The distributions of the tungsten and rhenium tracers resulting from the diffusion runs were used to calculate diffusion coefficients for tungsten and rhenium at each of these four temperatures, and the variation of the diffusion coefficients with temperature were used to obtain activation energies.

Prior to the experimental work, general diffusion calculations were performed to establish criteria for thinness and uniformity of the initial tracer layer. In order to determine an optimal deuteron energy for production of a tracer layer meeting these criteria, a stack of tungsten foils was bombarded with 14.0 MeV deuterons and radiochemically analyzed to establish the tracer-production cross sections as a function of deuteron energy (or, for the diffusion samples, as a function of deuteron penetration depth).

The reactions for which excitation functions were determined are $W^{184}(d,p)W^{185}$, $W^{186}(d,p)W^{187}$, and $W^{184}(d,2n)$ 34-day Re^{184}. The excitation

functions leading to the production of W^{185} and W^{187} were found to have the same general shape and very nearly the same magnitude. Both excitation functions increase from about 3 mb at 6 MeV to a fairly broad maximum of 300 mb between 11 and 13 MeV. Cross sections leading to the production of 34-day Re^{184} range from about 3 to 380 mb for deuterons with energies ranging from 7 to 14 MeV. Deuteron energies employed were not high enough to indicate the position of the maximum for the $W^{184}(d,2n)$ 34-day Re^{184} excitation function.

During the course of the experimental work, it was convenient to observe the decay of W^{185} and W^{187}, and new half-life values are reported for these two isotopes. The values determined, with uncertainties expressed to $3\ \sigma$, are 23.72 ± 0.06 hours for W^{187} and 75.14 ± 0.63 days for W^{185}. The decay of W^{185} was observed over a period of about nine half-lives.

In accordance with the above excitation function data, a deuteron beam energy of 9.0 MeV was adopted for activation of the diffusion samples. The thin, approximately exponentially-decreasing, radioactive layer produced by 9.0 MeV deuterons was shown to satisfactorily meet boundary-condition requirements of the one-dimensional diffusion equation. Activation of the diffusion samples by deuteron bombardment has the advantage that the tracer atoms are born in the crystal lattice, thus eliminating the possibility of diffusion blocking by oxide films or other impurities which may be present when radioactivity is deposited on the surface of diffusion samples by other methods.

Diffusion heating of the samples in high vacuum was accomplished by an induction-heating arrangement which included an eddy-current concentrator. Temperatures were measured by optical pyrometry and the system was calibrated by reference to the melting points of tantalum (2996 °C), molybdenum (2620 °C), niobium (2468 °C), and rhodium (1966 °C). In addition to the advantage of attainment of very high diffusion-heating temperatures, induction heating essentially eliminates uncertainties in effective diffusion-time measurements because of very rapid heating and cooling of the diffusion samples.

Sectioning of the diffusion-heated samples was accomplished by grinding with a precision, reciprocating-table surface grinding machine equipped with a magnetic chuck. About 50 ± 10% of the tungsten in each layer was

collected for analysis. Cross contamination of activity from one layer to succeeding layers was negligible when proper precautions were taken. This technique had the advantage of insuring parallelism of each removed layer, since the sample was not removed from its mounting during the entire sectioning process. Layers as thin as 0.2 mil were practical. It was found that in a given weight of grindings, which constitute a layer, about 60% by weight was tungsten; the remaining 40% was made up of grinding wheel particles.

Radiochemical procedures were developed for separating pure fractions of tungsten and rhenium from the ground particles collected in each layer. Briefly, the radiochemistry consisted of 1) dissolution of the grindings in a mixture of hydrofluoric and nitric acids followed by filtration to remove undissolved silicon carbide (silicon from soluble silicates was converted to the very stable fluosilicic acid which remained in solution and did not interefere in subsequent chemistry), 2) addition of rhenium carrier which was subsequently separated by precipitation as rhenium sulfide, 3) purification and conversion of rhenium to the final weighing form of tetraphenylarsonium perrhenate for mounting and gamma counting, and 4) purification and conversion of tungsten to its final weighing form, the tungsten derivative of 8-hydroxyquinoline, for mounting and beta counting.

The diffusion data obtained for self-diffusion in single-crystal tungsten and diffusion of rhenium tracer in single-crystal tungsten over the temperature range 2660 °C to 3230 °C have been presented in Table 10.1. These data fit the usual Arrhenius relationship; $D = D_0 \, e^{-Q/RT}$ where D is the diffusion coefficient in cm^2/sec, D_0 is the frequency factor in cm^2/sec, Q is the activation energy in calories/mole, R is the universal gas constant in calories/mole-°K, and T is the temperature in degrees Kelvin. The temperature-dependence of the diffusion coefficients in the two systems, obtained by least-squares analysis of the data, is well represented by the equations

$$D(W) = (42.8 \pm 4.8) \, e^{-(153,100 \pm 600)/RT} \ \mathrm{cm^2/sec},$$

and

$$D(\mathrm{Re}) = (275 \pm 110)\, e^{-(162,800 \pm 2,500)/RT}\ \mathrm{cm^2/sec.}$$

The D_0 and Q values obtained for tungsten self-diffusion were analyzed in the light of current theories reported in the literature, and it appears that tungsten self-diffusion occurs by a ring mechanism. The theory of impurity diffusion in metals has not advanced sufficiently to establish a mechanism for diffusion of rhenium tracer in tungsten. However, the high activation energy indicates that there are no easy diffusion paths for rhenium atoms; and since rhenium atoms have nearly the same charge and size as tungsten atoms, it is reasonable to conjecture that rhenium tracer may diffuse through a tungsten lattice by a similar mechanism.

Chapter 12

SUGGESTIONS FOR FUTURE RESEARCH

The technique, described in this research, of heating diffusion samples in an induction furnace has the advantage of attainment of very high temperatures, and, in addition, the advantage of very rapid heating and cooling of the diffusion samples, thus minimizing or eliminating the error in determining effective diffusion times. Induction heating would be particularly applicable to diffusion studies on the high-melting refractory metals. The sectioning of diffusion-heated samples with a precision surface-grinding machine is both rapid and accurate. The technique is applicable for the sectioning of many soft metals as well as hard, brittle metals which cannot be sectioned on a lathe.

Production of a radioactive layer of tracer atoms on diffusion samples by bombardment with deuterons can be applied to many metal systems. Impurity diffusion as well as self-diffusion can often be measured in the same diffusion sample because of the occurrence of competing reactions (i.e., (d,xn) reactions). Examples of metal systems in which both self-diffusion and impurity diffusion may be studied concurrently after deuteron activation are:

Hf^{180}(d,p) 42.5-day Hf^{181}, Hf^{179}(d,2n) 600-day Ta^{179}

Mo^{98}(d,p) 67-hr Mo^{99}, Mo^{95}(d,2n) 60-day Tc^{95}

Os^{190}(d,p) 14.6-day Os^{191}, Os^{192}(d,2n) 74-day Ir^{192}

Ta^{181}(d,p) 112-day Ta^{182}, Ta^{181}(d,2n) 68-day W^{181}.

Alpha particles have relatively short ranges in metals and may also be used for production of a radioactive layer of impurity atoms on diffusion samples.

For example, bombardment of yttrium with alpha particles produces 62-day Nb^{91} and 10.2-day Nb^{92} by (α, n) reactions. Due to the corrosive properties of yttrium, considerable care would be necessary; however, current interest in the metal makes the example worthwhile. Another example is bombardment of zirconium with alpha particles to produce mainly Mo^{93}.

The examples mentioned above produce impurity tracer atoms of approximately the same size as the solvent metal. Activation of diffusion samples with impurity tracer atoms of much smaller size than the solvent metal would be of interest, since diffusion of small solute atoms through a lattice of large solvent atoms is thought to occur by a different mechanism (interstitial) than diffusion of solute atoms through a lattice of solvent atoms of approximately the same size. A possible method of activating any metal diffusion sample with relatively small 53-day Be^7 atoms is to coat the sample with graphite and bombard it with He^3 particles. By recoil some of the 53-day Be^7 atoms from the reaction $C^{12}(He^3, 2\alpha)\ Be^7$ would become imbedded in the diffusion sample, and would remain there after removal of the graphite. The excitation function for this reaction has been measured,[26] and, although fairly long bombardment times would be necessary, the technique is practical.

In activating diffusion samples by bombardment with deuterons or alpha particles, care must be taken that the boundary conditions required by the solution to the diffusion equation are satisfactorily met. If excitation functions for the particular reactions of interest are not available, good estimates of optimum particle energies to use and their corresponding cross sections are sometimes possible from theoretical considerations and from comparison with available experimental data on comparable isotopes. The concentration profile of an initial radioactive layer after bombardment can always be obtained by sectioning a sample which has not been diffusion-heated.

When impurity tracer atoms are produced on the diffusion samples by nuclear reactions, chemical concentration gradients of the tracer are avoided and the requirement of constant D in Ficks' second law is readily met.

The ease of activation and the variety of impurity tracer atoms which can be produced by nuclear reactions on numerous metal systems provides for many interesting problems. As Lazarus[84] points out, impurity diffusion in pure metals is only poorly understood. The accumulation of reliable data would be of considerable aid to the theorists.

APPENDIX A*

EFFECT ON DIFFUSION MEASUREMENTS OF IRREGULARITIES IN THE INITIAL LAYER OF DIFFUSING MATERIAL

One of the most useful integrated forms of Fick's diffusion law is

$$C = \frac{C_0}{\sqrt{\pi\ Dt}}\ e^{-x^2/4Dt} ,$$

where C is the concentration of the tracer, D is the diffusion coefficient, x is the coordinate along which diffusion proceeds, and t is the diffusion time. The boundary conditions imposed to obtain this solution require a uniform, infinitely thin layer of tracer diffusing into an infinitely thick diffusion medium. These conditions must be closely approached experimentally in order for Fick's law to be fulfilled. The dual questions of how thick can the infinitely thin layer be and how non-uniform can the uniform layer be, under the boundary condition requirements, have never been adequately answered in the literature as far as one of the writers has been able to determine. (See, for example, LAMS-2562.[12] These two questions are particularly important if the diffusing radioactive layer is to be formed by a (d, p) reaction on the diffusion samples. In this case, the radioactive layer will have a finite thickness of approximately exponentially-decreasing concentration. In addition, irregularities in surface distribution of the radioactivity are likely. To answer these questions, therefore, a mathematical treatment starting with the fundamental diffusion equation is necessary.

---

*Appendix A, written by B. Kent Harrison and Robert L. Andelin, first appeared as an internal Los Alamos Scientific Laboratory Report in October, 1961. It is reproduced here in its entirety.

The fundamental diffusion equation is

$$D\nabla^2 C = \frac{\partial C}{\partial t} \,,$$

where C is the concentration of the tracer and t is the diffusion time. In cylindrical coordinates the equation becomes

$$\frac{1}{D}\,\frac{\partial C}{\partial t} = \frac{\partial^2 C}{\partial r^2} + \frac{1}{r}\,\frac{\partial C}{\partial r} + \frac{1}{r^2}\,\frac{\partial^2 C}{\partial \theta^2} + \frac{\partial^2 C}{\partial z^2} \,. \qquad (1)$$

The initial concentration is assumed to be given by a function, $B(r,\theta,z)$:

$$C(r,\theta,z,0) = B(r,\theta,z) \,. \qquad (2)$$

The coordinate system is oriented as shown below:

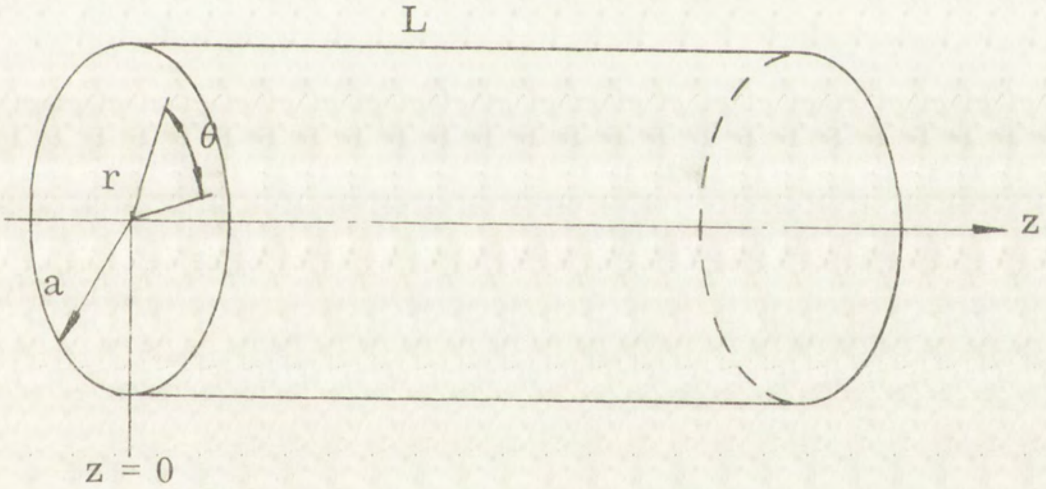

For convenience in calculations a mirror image of the rod in the region $z < 0$ is assumed. This provides symmetry under $z \rightarrow -z$ and does not affect the final result. The rod is also assumed to be of infinite length. The boundary conditions are now:

$$\left(\frac{\partial C}{\partial z}\right)_{z=0} = 0 \,, \qquad (3)$$

$$\left(\frac{\partial C}{\partial r}\right)_{r=a} = 0 \ , \tag{4}$$

$$\lim_{|z|\to\infty} C(r, \theta, z, t) = 0 \ , \tag{5}$$

$$\lim_{t\to\infty} C(r, \theta, z, t) = 0 \ . \tag{6}$$

Equations (3) and (4) may be obtained from "Mathematics of Diffusion", J. Crank, Oxford, Clarendon Press (1956). Equations (5) and (6) are obvious.

The differential equation is solved by separation of variables in steps. Writing

$$C(r,\theta, z, t) = E(r, z, t)F(\theta) \ , \tag{7}$$

one obtains from Eq. (1)

$$\frac{r^2}{E}\left(\frac{E_t}{D} - E_{rr} - \frac{E_r}{r} - E_{zz}\right) = \frac{F_{\theta\theta}}{F} \ . \tag{8}$$

Each side of Eq. (8) must be equal to a constant which is written as $-n^2$ to insure single-valuedness of F (n is an integer or 0). Solving for F gives

$$F(\theta) = \alpha \sin n\theta + \beta \cos n\theta \ . \tag{9}$$

The left-hand side of Eq. (8) becomes

$$\frac{E_t}{D} - E_{rr} - \frac{E_r}{r} - E_{zz} + \frac{n^2 E}{r^2} = 0 \ . \tag{10}$$

$$C(r,\theta,z,t) = \sum_{n=0}^{\infty} \sum_{k=1}^{\infty} \left[F_{nk}(z,t) \sin n\theta + G_{nk}(z,t) \cos n\theta \right] J_n(\lambda_{nk} r) , \qquad (17)$$

where

$$\lambda_{nk} J'_n(\lambda_{nk} a) = 0. \qquad (18)$$

In this expression F_{nk} and G_{nk} are solutions of Eq. (14) subject to Eqs. (3), (5), and (6).

To solve Eq. (14) $F_{nk}(z,0)$ and $G_{nk}(z,0)$ are needed. These are found by setting $t = 0$ in Eq. (17) and using Eq. (2):

$$B(r,\theta,z) = \sum_{n=0}^{\infty} \sum_{k=1}^{\infty} \left[F_{nk}(z,0) \sin n\theta + G_{nk}(z,0) \cos n\theta \right] J_n(\lambda_{nk} r). \qquad (19)$$

The coefficients of the double Fourier-Bessel series of Eq. (19) are now found in the usual manner:

$$G_{0k}(z,0) = \frac{1}{\pi a^2 [J_0(\lambda_{0k} a)]^2} \int_0^a dr\, r\, J_0(\lambda_{0k} r) \int_{-\pi}^{\pi} B(r,\theta,z) d\theta , \qquad (20)$$

$$G_{nk}(z,0) = \frac{2\lambda_{nk}^2}{\pi(\lambda_{nk}^2 a^2 - n^2)[J_n(\lambda_{nk} a)]^2} \int_0^a r J_n(\lambda_{nk} r) dr \int_{-\pi}^{\pi} B(r,\theta,z) \cos n\theta \, d\theta , \qquad (21)$$

$$F_{nk}(z,0) = \frac{2\lambda_{nk}^2}{\pi(\lambda_{nk}^2 a^2 - n^2)[J_n(\lambda_{nk} a)]^2} \int_0^a r J_n(\lambda_{nk} r) dr \int_{-\pi}^{\pi} B(r,\theta,z) \sin n\theta \, d\theta. \qquad (22)$$

Now the quantity measured in a typical diffusion experiment is proportional to the total amount of tracer in a disc or layer at position z and diffusion time t. This quantity is

$$\lim_{|z| \to \infty} M(z,t) = 0 \ , \tag{28}$$

$$\lim_{t \to \infty} M(z,t) = 0 \text{ and} \tag{29}$$

$$M(z,0) = \int_0^a r\,dr \int_{-\pi}^{\pi} B(r,\theta,z)d\theta. \tag{30}$$

Writing equation (14) as

$$\frac{1}{D} M_t + \lambda^2 M - M_{zz} = 0 \ , \tag{31}$$

it now becomes an easy matter to solve for M using the Laplace transform. Setting

$$m(z,s) = L_t[M(z,t)] = \int_0^{\infty} e^{-st} M(z,t)dt, \tag{32}$$

$$P(z) = M(z,0) = \int_0^a r\,dr \int_{-\pi}^{\pi} B(r,\theta,z)d\theta, \tag{33}$$

then

$$L_t\left[\frac{\partial M}{\partial t}\,(z,t)\right] = sm(z,s) - P(z) \ , \tag{34}$$

and

$$L_t\left[\frac{\partial^2 M}{\partial z^2}\,(z,t)\right] = \frac{\partial^2 m(z,s)}{\partial z^2}. \tag{35}$$

Equation (31) becomes

$$\frac{1}{D}(sm - P) + \lambda^2 m - \frac{\partial^2 m}{\partial z^2} = 0, \tag{36}$$

while Eq. (27) and Eq. (28) become

$$\left(\frac{\partial m}{\partial z}\right)_{z=0} = 0\ , \tag{37}$$

and

$$\lim_{z \to \infty} m(z,s) = 0. \tag{38}$$

If

$$\omega^2 = \lambda^2 + \frac{s}{D}, \tag{39}$$

Eq. (36) becomes essentially

$$\frac{d^2 m}{dz^2} - \omega^2 m = \frac{P(z)}{D}\ , \tag{40}$$

which has the general solution

$$m(z,s) = \frac{1}{D\omega}\int_0^z \sinh \omega(z-u)\ P(u)\ du + \beta \sinh \omega z + \alpha \cosh \omega z. \tag{41}$$

Equation (37) requires

$$\beta = 0 . \tag{42}$$

Equation (41) may now be written in the form

$$m(z,s) = e^{\omega z}\left[\frac{1}{2\omega D}\int_0^z e^{-\omega u}\, P(u)\, du + \frac{\alpha}{2}\right] + e^{-\omega z}\left[-\frac{1}{2\omega D}\int_0^z e^{\omega u}\, P(u)\, du + \frac{\alpha}{2}\right]. \tag{43}$$

Equation (38) now yields

$$\alpha = \frac{1}{D\omega}\int_0^{-\infty} e^{\omega u}\, P(u)\, du = -\frac{1}{D\omega}\int_0^{\infty} e^{-\omega u}\, P(u)\, du. \tag{44}$$

That the two integrals are equal may be seen by replacing u with -u in either of them, since $P(-u) = P(u)$ by Eq. (33) and the symmetry requirement stated at the beginning of the discussion. One obtains finally

$$m(z,s) = \frac{1}{D\omega}\int_0^z \sinh \omega(z-u)\, P(u)\, du - \frac{1}{D\omega}\cosh \omega z \int_0^{\infty} e^{-\omega u}\, P(u)\, du. \tag{45}$$

Performing the inverse Laplace transform under the integral sign in Eq. (45) the final result is

$$M(z,t) = \frac{1}{2\sqrt{\pi D t}}\int_{-\infty}^{\infty} e^{-(z-u)^2/4Dt}\, P(u)\, du. \tag{46}$$

From Eq. (33)

$$P(z) = \int_0^a r\, dr \int_{-\pi}^{\pi} B(r,\theta,z)\, d\theta. \tag{46a}$$

M(z, t) is thus the same as the concentration (as a function of z and t) in a semi-infinite slab due to an initial distribution P(z). If $B(r, \theta, z)$ has the form

$$B(r, \theta, z) = Q(r, \theta) R(z), \tag{47}$$

then P(z) is proportional to R(z) and the r, θ dependence may be essentially ignored. $B(r, \theta, z)$ will take the form of Eq. (47) for a given experimental arrangement if the thickness of the initial tracer layer is constant. In the case of the radioactive layer formed from deuterons, this condition (Eq. 47) is approximately met if the deuterons have the same average energy over the surface of the end of the rod. In this case $R(z) = e^{-\mu z}$ where μ is the linear absorption coefficient of the deuterons in the target material, and Q is proportional to the deuteron beam intensity which may vary with r and θ over the rod end surface.

Whatever the detailed behavior of P(z), if it can be approximated by the function

$$\begin{aligned} F(z) &= \frac{K}{h} \quad \text{for} \quad |z| < h \quad \text{and} \\ F(z) &= 0 \quad \text{for} \quad |z| > h \quad , \end{aligned} \tag{48}$$

for h small enough, the assumption

$$M = \frac{K}{\sqrt{\pi D t}} e^{-z^2/4Dt} \tag{49}$$

--which is implicitly made in the measurement and graphing process-- is justified. This may be proved by substituting F(z) for P(z) in Eq. (46):

$$M(z, t) = \frac{K}{2h\sqrt{\pi D t}} \int_{-h}^{h} e^{-(z-u)^2/4Dt} \, du = \frac{K}{2h} \left[\operatorname{erf}\left(\frac{h-z}{2\sqrt{Dt}}\right) + \operatorname{erf}\left(\frac{h+z}{2\sqrt{Dt}}\right) \right]. \tag{50}$$

Equation (50) is, of course, the solution of the diffusion equation for a semi-infinite slab with initial layer thickness h. Equation (50) is approximately Eq. (49) for small h.

The error made in D from using an initial layer of finite thickness h may be calculated in the following manner. The quantity, $\partial/\partial(z^2) \ln M$,

measures the slope of the curve ln M vs z^2. It equals $-1/4\,Dt$ for Eq. (49). Thus the quantity

$$C(z) = 1 + 4\,Dt \frac{\partial}{\partial(z^2)} \ln M, \tag{51}$$

which is zero for Eq. (49), measures the fractional error in the slope (slope = $-(1 - C)/4\,Dt$). From equation (50),

$$C(z) = 1 - \frac{4}{z}\sqrt{Dt/\pi}\; \frac{e^{-(h^2+z^2)/4\,Dt}\sinh(hz/2\,Dt)}{\operatorname{erf}\left(\frac{h-z}{2\sqrt{Dt}}\right) + \operatorname{erf}\left(\frac{h+z}{2\sqrt{Dt}}\right)}\;. \tag{52}$$

If $\alpha = h/\sqrt{Dt}$ is small, then $C(0) \cong C(h) \cong \alpha^2/6$. Thus, if $h < 0.24\sqrt{Dt}$, the percentage error in the slope (and hence in D) will be $\leq 1\%$.

For an initial layer described by

$B(r,\theta,z) = \frac{K}{h}$ for $|z| < h$, $0 \leq \theta \leq \gamma$; and $B = 0$ elsewhere, we have

$P(z) = K'$ for $|z| < h$ and

$P(z) = 0$ for $|z| > h$

and the previous comments apply.

If the initial tracer layer had a circular wedge form as illustrated,

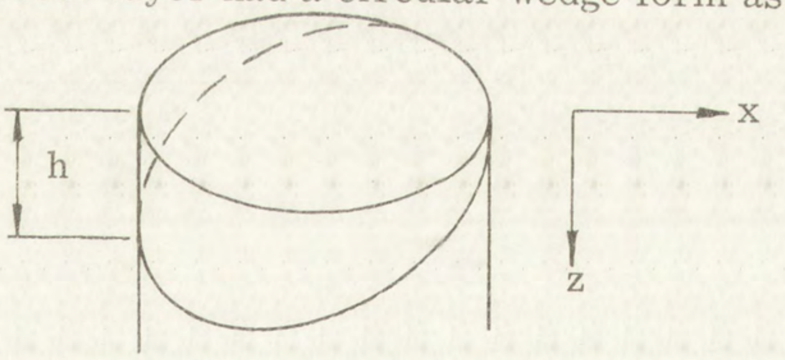

then B = K within the volume and B = 0 outside the volume.

The oblique plane has the equation

$$\frac{2z}{h} + \frac{x}{a} = 1.$$

Integration of Eq. (46a) yields

$$P(z) = Ka^2 \left[\cos^{-1}(2y - 1) - 2(2y - 1)\sqrt{y - y^2} \right] \text{for } y \leq 1 \;,$$

where $y = |z|/h$, and $P(z) = 0$, $y \geq 1$. Now if $\alpha = h/\sqrt{Dt}$, as before, and

$$H(x) = \cos^{-1}(2x - 1) - 2(2x - 1)\sqrt{x - x^2} \;, \tag{53}$$

then the calculated P(z), with Eq. (46) and Eq. (51) yields

$$C(z) = \frac{\displaystyle\int_0^1 dx \, \frac{hx}{z} \, H(x) \, e^{-\alpha^2 x^2} \sinh\left(2\alpha^2 \frac{xz}{h}\right)}{\displaystyle\int_0^1 dx \, H(x) \, e^{-\alpha^2 x^2} \cosh\left(2\alpha^2 \frac{xz}{h}\right)} \;. \tag{54}$$

Thus,

$$C(0) = \frac{\displaystyle\int_0^1 dx \, 2\alpha^2 x^2 \, H(x) \, e^{-\alpha^2 x^2}}{\displaystyle\int_0^1 dx \, H(x) \, e^{-\alpha^2 x^2}} \;.$$

For small α, to order α^2,

$$C(0) = 2\alpha^2 \frac{\displaystyle\int_0^1 dx \, x^2 \, H(x)}{\displaystyle\int_0^1 dx \, H(x)} \;. \tag{55}$$

Integrating Eq. (55) by parts, one has

$$C(0) = \frac{2\alpha^2}{3} \frac{\int_0^1 x^3 \sqrt{x - x^2}\, dx}{\int_0^1 x \sqrt{x - x^2}\, dx} = \frac{7\alpha^2}{24} .$$

Thus, for $h < 0.6$ Dt, the slope is obtained to within about 1%.

APPENDIX B

GRAVIMETRIC PROCEDURE FOR ANALYSIS OF TUNGSTEN, SILICON CARBIDE, AND SILICA

The procedure herein described was used for analysis of the particles collected in sectioning a tungsten diffusion sample with a surface grinding machine. The grinding wheel was the source of silicon carbide abrasive and soluble silicate binder in the collected particles. Since silica was included in the analysis, a fusion dissolution was required rather than a hydrofluoric acid-nitric acid dissolution. (Silicon tetrafluoride, which forms on dissolution of soluble silicates, is somewhat volatile when heated.) The presence of alkali salts from fusion dissolution of the particles interfered with the usual[86] tungsten analysis which involves precipitation of tungstic acid in the presence of the alkaloid cinchonine. Therefore, another procedure using tannin and involving a tannin-cinchonine-tungstic acid complex was used. In this method, originally due to Schoeller and Jahn[87] and later studied by Lambie,[88] alkali salts are actually necessary for satisfactory flocculation of the precipitate. The method is especially useful for analysis of small amounts of tungsten (as little as 5 mg may be analyzed), and is quantitative to within 0.5%. The procedure given below is for analysis of less than 200 mg of tungsten.

The entire analysis involves 1) dissolution of the particles in a sodium hydroxide-potassium nitrate flux under controlled conditions so that tungsten and silicates dissolve, but not silicon carbide, 2) taking up the cooled melt in water and filtering off the silicon carbide which is then dried and weighed, 3) precipitating a tannin-cinchonine-tungstic acid complex which is finally ignited

to tungstic oxide containing some silica, 4) determining the amount of silica in the tungstic oxide precipitate by treating it with hydrofluoric acid to volatilize silicon tetrafluoride, and 5) combining this weight of silica with that found in the filtrate (from tungstic acid complex precipitate) by evaporation and dehydration analysis. In the present work, comparator samples were analyzed along with the actual samples. A weighed piece of tungsten single crystal and a weighed chip from a spare grinding wheel constituted a comparator sample. The detailed procedure established is as follows.

A 20-ml nickel crucible (high form, highly polished) was filled slightly less than 1/3 full with sodium hydroxide pellets and potassium nitrate crystals in the ratio of about 4:1. The mixture was fused slowly at low heat (less than 350 °C) until the melt was quiescent, after which it was allowed to cool. Collected grindings from a layer were weighed and distributed on top of the cool melt. The crucible was heated very slowly to about 310 °C, and held there until the reaction with tungsten was complete and the melt was quiescent (Note 1). The melt was allowed to cool with a hooked platinum stirring rod in it. After cooling, the solidified melt was removed from the crucible with the platinum stirring rod (some heat was often necessary), and was dissolved in 50 ml of water in a 100-ml platinum dish. The crucible was carefully washed with water, and the washings were added to the solution. To remove any dissolved nickel from the solution, a small amount (~ 0.02 g) of solid sodium peroxide was added, after which the solution was heated at ~ 80 °C for about five minutes (Note 2). Any nickel present was immediately oxidized to nickel (III) oxide hydrate which came out of solution as a black, easily-filterable precipitate. After cooling, the solution was filtered with gentle suction through a 9-cm Whatman No. 50 filter paper mounted on a No. 00 porcelain Hirsh funnel with perforated plate. The filter paper was thoroughly washed with 1.0 M ammonium hydroxide solution, and the filtrate and washings were transferred to a 400 or 600-ml beaker, and were set aside. The filter paper containing silicon carbide was thoroughly washed with 1:1 hydrochloric acid, and finally with water (Note 3), after which it was folded around the silicon carbide and placed in a platinum crucible. The paper was then dried,

charred, and ignited for 10 minutes at about 800 °C in a muffle furnace. The sample was cooled for 30 minutes, in a dessicator, to balance room temperature, and was weighed. The ignition was repeated until a constant weight of silicon carbide was obtained. Several drops of phenolpthalein solution were added to the tungsten-containing filtrate obtained above, which had a volume of 200 to 300 ml, after which 1:1 hydrochloric acid was carefully added until the solution became colorless. The solution was heated to ~ 50 °C, and 0.5 g of ashless tannin from a freshly prepared aqueous solution was added (10 ml of a solution containing 2.5 g of tannin per 50 ml of water). Next, 10 ml of 1:1 hydrochloric acid was added to precipitate the brown tungstic oxide-tannin complex (Note 4). The creamed pulp of about one half of a 9-cm Whatman No. 41 filter circle was added to the mixture. With vigorous stirring, 5 ml of a solution containing 5% cinchonine alkaloid in 1:3 hydrochloric acid was added to the warm solution (Note 5), and the mixture was allowed to stand over night. Next, the mixture was filtered through a 9-cm Whatman No. 41h filter circle mounted in a No. 00 Hirsh funnel (Note 6). The precipitate and filter paper were thoroughly washed with cold ammonium chloride-cinchonine wash solution (Notes 7 and 8), and the filtrate, including washings, were set aside. After folding the filter paper around the precipitate, it was placed in a large (50 cc), uncovered platinum crucible for ignition. The paper was dried, charred, and the carbon was volatilized at a very low red heat, after which the precipitate (still uncovered) was ignited for 10 minutes in a muffle furnace at 800 °C (Note 9). After ignition, the crucible was cooled for 30 minutes, in a dessicator, to balance room temperature, and was weighed. The precipitate was then moistened with hydrofluoric acid, and after evaporation to dryness, was reignited at 800 °C to constant weight of tungstic oxide (WO_3); pure, dry tungstic oxide is not hygroscopic. The loss in weight represented the silica (SiO_2) originally present in the sample (Note 10). Next, the filtrate and washings obtained above were transferred to a platinum dish, and were evaporated to dryness. The residue was heated for an hour at 110 °C, and, after cooling, 10 ml of conc. hydrochloric acid was added. After standing for 2 minutes, the mixture was warmed for 5 to 10 minutes, and was finally diluted to 100 ml with hot water. The mixture was

filtered while still hot through Whatman No. 42 filter paper, and the dehydrated silica was washed thoroughly with hot 1:20 hydrochloric acid, and finally with hot 1:50 sulfuric acid. The filter paper was folded around the silica and was placed in a deep platinum crucible. After carefully drying, charring and volatilizing the paper, the crucible was covered with a tightly fitting cover, and ignited at 1200 °C for 15 minutes. The sample was cooled in a dessicator and weighed, and then reignited to constant weight; pure, dry silica is not hygroscopic. Total silica was obtained by adding this weight of silica to that obtained by loss of weight of the tungstic oxide after treatment with hydrofluoric acid.

NOTES

1. Temperature control was important for several reasons. At temperatures much higher than 350 °C, the nickel crucible and silicon carbide abrasive started to dissolve. In addition, if dissolution of the finely divided tungsten proceeded too vigorously, combustion ensued with subsequent loss of tungstic oxide by volatilization. There was no problem with the silicate binder which dissolved readily as soon as the melt became liquid.

A temperature of about 310-350 °C was maintained with a Tirrel burner placed about 3-3/4 in. from the bottom of the crucible. The flame was adjusted so that it had a blue cone length of about 3/4 in. A useful technique for temperature control during the reaction was intermittant heating of the crucible near the top with a small glass blowing torch, while at the same time a low flame from a Tirrel burner was steadily heating the bottom of the crucible.

2. This method, mentioned briefly by Hillebrand, et al.,[89] quantitatively removed any dissolved nickel from the solution. As a further check, the final ignited precipitate of tungstic oxide was tested for nickel contamination by the dimethylgloxine spot test which is sensitive to 0.015 μgram. The results were negative.

3. It was essential to thoroughly wash the filter paper to insure the absence of alkali salts. Otherwise, constant weight on ignition was difficult to achieve because of the slow volatilization of any alkali salt present.

4. Alkali salt, instead of being prejudicial, was necessary in this procedure for satisfactory flocculation of the precipitate. If only trace amounts of tungsten was present, or if the solution was too acidic when tannin was added, the precipitate did not appear until the addition of cinchonine alkaloid.

5. The usual reaction of cinchonine with tungsten (VI) is formation of the insoluble white precipitate, cinchonine tungstate. With tannin present, a flocculent cinchonine-tannin complex which acts as a collector for colloidal tungsten is formed.

6. If much chloride was present, the tannin sometimes formed a white turbidity which appeared in the filtrate. According to Schoeller and Jahn[90] this turbidity does not affect the final results and, therefore, it was ignored.

7. The wash solution was prepared by adding 250 ml of a 20% ammonium chloride solution to 20 ml of the cinchonine solution and diluting to 1 liter.

8. Thorough washing was necessary here for the same reason as mentioned in Note 3. Alkali salts present in a tungstic oxide precipitate give the precipitate a green color.

9. A stream of oxygen was passed through the muffle furnace to keep the tungstic oxide completely oxidized, and thus a green ignition product was avoided. Remy[91] describes the nonstoichiometric compound $WO_{2.98}$ which has the same crystal structure as WO_3 but is blue in color. A mixture of small amounts of $WO_{2.98}$ with WO_3 gives a green ignition product. The ignited WO_3 was a soft, lemon yellow color.

10. A temperature of 1200 °C is needed to completely dehydrate silica. Therefore, a very small error in silica analysis may have been introduced here.

BIBLIOGRAPHY

1. David Lazarus in "Solid State Physics", Vol. 10, Edited by Frederick Seitz and David Turnbull, Academic Press, New York, 1960, p. 109.
2. E. J. Rapperport and C. S. Hartley, paper presented at AIME Technical Conference on Refractory Metals, Chicago, Illinois, April 12-13, 1962.
3. Carl Wagner in "Atom Movements", ASM Seminar, Cleveland, Ohio, 1951, p. 153.
4. Pol Duwez, ibid. p. 192.
5. R. W. Christy, J. Appl. Phys. 30:760 (1959).
6. B. Ya Pines, Uspekhi Fizicheskikh Nauk 52:501 (1954).
7. Clarence Zener, J. Appl. Phys. 22:372 (1951).
8. G. J. Dienes, J. Appl. Phys. 22:848 (1951).
9. A. D. LeClaire, Acta Met. 1:438 (1953).
10. F. S. Buffington and Morris Cohen, Acta Met. 2:660 (1954).
11. S. A. Rice, J. Chem. Phys. 32:1026 (1960).
12. R. L. Andelin and L. E. Godfrey, Los Alamos Scientific Laboratory Report LAMS-2562 (1961).
13. "Mechanical Properties of Metals and Alloys", Nat. Bur. Std., Circ. C447 (1943).
14. V. P. Vasil'ev and S. G. Chernomorchenko, Zavodskaiia Lab. 22:688 (1956).
15. J. A. M. van Liempt, Rec. Trav. Chim. 64:239 (1945).
16. Walter V. Green, Trans. AIME 215:1057 (1959).
17. R. H. Schnitzel, J. Appl. Phys. 30:2011 (1959).
18. W. Danneberg, Metall. 15:977 (1961).
19. David Lazarus, op. cit. p. 110.

20. Carl T. Tomizuka in "Methods of Experimental Physics", Vol. 6, Part A, Edited by K. Lark-Horovitz and Vivian A. Johnson, Academic Press, New York, 1959, p. 364.

21. B. V. Rollin, Phys. Rev. 55:231 (1939).

22. Jui Hsin Wang in "Radioactivity Applied to Chemistry", Edited by A. C. Wahl and N. A. Bonner, John Wiley and Sons, Inc., New York, 1951, p. 66.

23. David Lazarus, op. cit. p. 95.

24. H. Letaw, Jr., L. Slifkin and W. Portnoy, Rev. Sci. Instr. 25:865 (1954).

25. Carl T. Tomizuka, op. cit. p. 368.

26. D. R. F. Cochran and J. D. Knight, Phys. Rev. 128:1281 (1962).

27. Roger H. Moore and Royal K. Zeigler, Los Alamos Scientific Laboratory Report LA-2367 (1959).

28. B. P. Bayhurst and R. J. Prestwood, Nucleonics 17:82 (1959).

29. J. D. Knight, Private Communication.

30. C. J. Gallagher, Jr., D. Strominger, and J. P. Unik, Phys. Rev. 110:725 (1958).

31. Gerhart Friedlander and Joseph W. Kennedy, "Nuclear and Radiochemistry", John Wiley and Sons, Inc., New York, 1955, p. 190.

32. M. Rich and R. Madey, University of California Report UCRL-2301 (1954).

33. G. Wilkinson and H. G. Hicks, Phys. Rev. 77:314 (1950).

34. N. R. Johnson, Bull. Am. Phys. Soc. 6:73 (1961).

35. E. Bodenstedt, E. Mathias, H. J. Korner, E. Gerdau, F. Frisius and D. Hovestadt, Nuc. Phys. 15:239 (1960).

36. W. J. Ramler, J. Wing, D. J. Henderson, and J. R. Huizenga, Phys. Rev. 114:154 (1959).

37. R. J. Prestwood, private communication from B. J. Dropesky (November 1957).

38. G. G. Eichholz, Phys. Rev. 89:525 (1953).

39. A. Fick, Ann. Phys. Lpz., 94:59 (1855).

40. Jui Hsin Wang, op. cit. p. 62.

41. J. Crank, "The Mathematics of Diffusion", Clarendon Press, Oxford, 1957, p. 3.

42. Ibid., p. 9.

43. W. Jost, "Diffusion in Solids, Liquids, Gases", Academic Press, New York, 1960, p. 16.

44. Linde Co. Report, LC-SL-Final, 6/61 - 2/62 (1962).

45. E. F. Northrop, Trans. Am. Electrochem. Soc. 25:69 (1919).

46. G. Babat and M. Losinsky, J. Appl. Phys. 11:816 (1940).

47. Paul H. Dike in "High Temperature Technology", Edited by I. E. Campbell, John Wiley and Sons, Inc., New York, 1956, p. 338.

48. L. Malter and D. B. Langmuir, Phys. Rev. 55:743 (1939).

49. W. D. Klopp, D. J. Maykuth, H. R. Ogden, and R. I. Jaffee, paper presented at AIME Meeting, Chicago, Illinois, November 2, 1959.

50. J. Paul Pemsler, J. Electrochem. Soc. 108:744 (1961).

51. A. G. Worthing, Phys. Rev. 25:846 (1925).

52. A. Taylor, N. J. Doyle and B. J. Kagle, J. Less-Common Metals 3:265 (1961).

53. T. H. Schofield, J. Inst. Metals 85:372 (1957).

54. "Metals Handbook", Vol. 1, 8th Edition, Am. Soc. for Metals, Novelty, Ohio, 1961, p. 46.

55. Carl T. Tomizuka, op. cit., p. 366.

56. Kenneth B. Lewis, "The Grinding Wheel", Rumford Press, 1951, p. 291.

57. G. A. Shirn, E. S. Wajda and H. B. Huntington, Acta. Met. 1:513 (1953).

58. W. T. Mullins and G. W. Leddicotte, "The Radiochemistry of Tungsten", NAS-NS-3042, National Academy of Sciences-National Research Council, Nuclear Science Series Report, 1961.

59. G. W. Leddicotte, "The Radiochemistry of Rhenium", NAS-NS-3028, National Academy of Sciences-National Research Council, Nuclear Science Series Report, 1961.

60. E. A. Hakkila, G. R. Waterbury and G. B. Nelson, Fifth Analytical Chemistry Conference in Nuclear Reactor Technology, Gatlinburg, Tennessee, October 10-12, 1961, TID-7629, 1962, p. 55.

61. Fritz Feigl, "Qualitative Analysis by Spot Tests", Elsevier Publishing Co., New York, 1947, p. 252.

62. Roger H. Moore and Royal K. Zeigler, op. cit., pp. 10-13.

63. M. W. Thompson, Phil. Mag. 5:278 (1960).

64. R. C. Koo, J. Less-Common Metals 3:412 (1961).

65. J. W. Pugh in "Plansee Proceedings 1958, High Melting Metals", Edited by F. Benesovsky, Pergamon Press, New York, 1959, p. 97.

66. Saul Dushman, "Scientific Foundations of Vacuum Technique", 2nd Edition, Edited by J. M. Lafferty, John Wiley and Sons, Inc., New York, 1962, p. 20.

67. "Handbook of Chemistry and Physics", 44th Edition, Editor in Chief, Charles D. Hodgman, Chemical Rubber Publishing Co., 1962-1963, p. 3097.

68. Saul Dushman, op. cit., p. 94.

69. A. G. Worthing, Phys. Rev. 10:638 (1917).

70. Colin J. Smithels, "Tungsten", Chemical Publishing Co., Inc., New York, 1953, p. 188.

71. G. A. Shirn, E. S. Wajda and H. B. Huntington, op. cit., p. 518.

72. Lyman G. Parratt, "Probability and Experimental Errors in Science", John Wiley and Sons, Inc., New York, 1961, p. 128.

73. Ibid. p. 68.

74. W. Edwards Deming, "Statistical Adjustment of Data", John Wiley and Sons, Inc., New York, 1938, p. 128.

75. A. D. LeClaire in "Progress in Metal Physics", Vol. I, Edited by B. Chalmers, Interscience Publishers, Inc., New York, 1949, p. 306.

76. N. H. Nachtrieb and G. S. Handler, Acta Met. 2:797 (1954).

77. D. R. Stull and G. C. Sinke, "Thermodynamic Properties of the Elements", American Chemical Society, Washington D. C., 1956, p. 34.

78. O. D. Sherby and M. T. Simnad, Am. Soc. Metals, Trans. Quart. 54:227 (1961).

79. Ibid. p. 236.

80. David Lazarus, op. cit., p. 72.

81. H. B. Huntington and Frederick Seitz, Phys. Rev. 61:315 (1942).

82. H. B. Huntington, ibid. p. 325.

83. W. Köster, Z. Metallk. 39:1 (1948).

84. David Lazarus, op. cit., p. 95.

85. A. D. LeClaire, Phil. Mag. 7:141 (1962).

86. W. F. Hillebrand and G. E. F. Lundell, "Applied Inorganic Analysis", John Wiley and Sons, Inc., New York, 1950, p. 551.

87. W. R. Schoeller and C. Jahn, Analyst 52:504 (1927).

88. D. A. Lambie, Analyst 64:481 (1939).

89. W. F. Hillebrand and G. E. F. Lundell, op. cit., p. 314.

90. W. R. Schoeller and C. Jahn, op. cit., p. 505.

91. H. Remy, "Treatise on Inorganic Chemistry", Vol. II, Elsevier Publishing Co., New York, 1956, p. 176.